AD-A175 421 STUDIES OF ELEMENTARY PROCESSES AND COUPLING INVOLVED IN THE D2/F2 CHEMICAL LASER(U) IOWA UNIV IOWA CITY DEPT OF CHEMISTRY D C TARDY 01 DEC 86 UI-CHEM-DCT-86 1/2

UNCLASSIFIED N00014-81-K-0207 F/G 20/5 NL

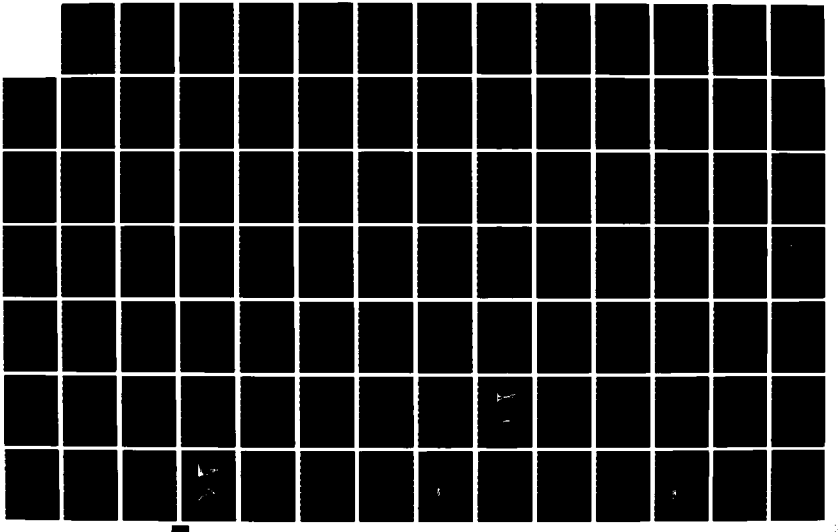

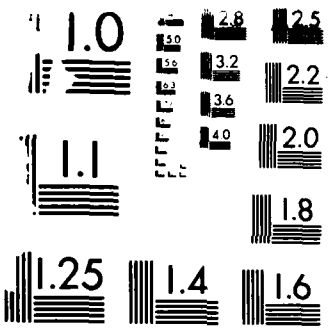
1.0
1.1
1.25
1.4
1.6
1.8
2.0
2.2
2.5
2.8
3.2
3.6
4.0

12

Report Number: UI-CHEM-DCT-86

STUDIES OF ELEMENTARY PROCESSES AND COUPLING INVOLVED IN THE D_2/F_2 CHEMICAL LASER

D.C. Tardy
Department of Chemistry
University of Iowa
Iowa City, Iowa
52242

December 1, 1986

Prepared for
Office of Naval Research
Arlington, Virginia
22217

UNCLASSIFIED

SECURITY CLASSIFICATION OF THIS PAGE (When Data Entered)

REPORT DOCUMENTATION PAGE	READ INSTRUCTIONS BEFORE COMPLETING FORM
1. REPORT NUMBER: UI-CHEM-DCT-86	2. GOVT ACCESSION NO. / 3. RECIPIENT'S CATALOG NUMBER
4. TITLE (and Subtitle): Studies of Elementary Processes and Coupling Involved in the D_2/F_2 Chemical Laser	5. TYPE OF REPORT & PERIOD COVERED: Final: 10/1/84-12/31/85
	6. PERFORMING ORG. REPORT NUMBER
7. AUTHOR(s): D.C. Tardy	8. CONTRACT OR GRANT NUMBER(s): N00014-81-K-0207
9. PERFORMING ORGANIZATION NAME AND ADDRESS: University of Iowa, Department of Chemistry, Iowa City, Iowa 52242	10. PROGRAM ELEMENT, PROJECT, TASK AREA & WORK UNIT NUMBERS
11. CONTROLLING OFFICE NAME AND ADDRESS: Office of Naval Research, Physics Division, Code 412, 800 N. Quincy St., Arlington, Virginia 22217	12. REPORT DATE: 1 December 1986 13. NUMBER OF PAGES: 110 total
14. MONITORING AGENCY NAME & ADDRESS (if different from Controlling Office)	15. SECURITY CLASS (of this report): UNCLASSIFIED 15a. DECLASSIFICATION DOWNGRADING SCHEDULE

16. DISTRIBUTION STATEMENT (of this Report)

Approved for public release; distribution unlimited

17. DISTRIBUTION STATEMENT (of the abstract entered in Block 20, if different from Report)

18. SUPPLEMENTARY NOTES

19. KEY WORDS (Continue on reverse side if necessary and identify by block number)

Energy disposal
Energy transfer
Chemical laser
Modeling

Accession For
NTIS GRA&I ☒
DTIC TAB ☐
Unannounced ☐
Justification
By
Distribution/
Availability Codes
Dist | Avail and/or Special
A-1

20. ABSTRACT (Continue on reverse side if necessary and identify by block number)

The performance of a H_2/D_2 chemical laser is a function of the nascent energy disposal parameters for the F + H_2 (D_2) and H (D) + F_2 chemical reactions and the vibrational relaxation of HF (DF). Chemiluminescence Mapping (CM) in which chemical components are observed by their spectral and time resolution is a technique which is capable of providing fundamental information on both nascent energy distributions for bimolecular exchange reactions and vibrational relaxation. Knowledge of the reactants (atoms or ions) and residence times must be known in order to interpret the data. Using a double

DD FORM 1 JAN 73 1473 EDITION OF 1 NOV 65 IS OBSOLETE

UNCLASSIFIED

SECURITY CLASSIFICATION OF THIS PAGE (When Data Entered)

floating probe the ion content flowing from a microwave discharge of hydrogen was found to be <~~1.8 10^{-6}~~ of the total flow, thus ion molecule reactions are unimportant. Using pressure profiles for the pulsed reactant it was calculated that the residence time in the reactor is approximately 50 milleseconds; for CM experiments radiational relaxation of HF is important and for arrested relaxation (steady state experiments) a background of relaxed HF may be a source for collisional relaxation.

The interpretation of CM experiments requires realistic modeling to deconvolute the experimental data. Primary processes include: initial formation of products, collisional and/or radiative relaxation, and physical removal of reactants and products from the observation volume. Using the well studied reaction, $F + H_2 \rightarrow HF(v) + H$, as a benchmark, experiments and computer simulations reveal two types of CM experiments: CM-PP in which there is a repetitive pressure pulse of the diatomic species and CM-LP in which the atomic species is formed repetitively in a constant pressure environment. The results of the CM-PP computer simulations are understood in terms of deviations from a steady state system and by the relative fluxes of the primary processes as a function of time. CM-LP experiments are easier to analyze than CM-PP experiments because of pseudo first order conditions.

Both types of CM experiments provide nascent vibrational energy distributions. In CM-PP experiments, obtaining these distributions is simplified for conditions of low flow ($F >> H_2$), observation times must be short enough to resolve the fastest relaxation process, and the reaction vessel must be evacuated between pulse sequences. The previous CM-PP experiments in which the nascent distribution for the $D + F_2$ was reported did not meet these requirements; the pulse time was reduced from 10 to 0.5 msec.

CM-LP experiments also provide total reaction rate constants and microscopic relaxation rate constants. To process the experimental data, an iterative method of extracting reaction and relaxation rate constants for vibrational levels, (v), below the maximum vibrational level populated, was developed. Input to the v-2 level from relaxation of the v level was decoupled from the reaction input to the v-1 level. It is shown that reaction and deactivation rate constants obtained by analysis of specific vibrational levels are more accurate than those obtained by analyzing total intensity-time profiles.

In addition to the $F + H_2(D_2)$ benchmark reactions, experimental results for $H(D) + F_2$, F + HBr, and $F + CH_2Cl_2$ are discussed and compared to other studies when available. Discrepancies between the previous CM results and those reported here can be resolved by the high reagent flows and long observation times used in the earlier experiments.

CONTENTS

PREFACE

This work was performed jointly by C.K. Man, T.O. Nelson and L.L. Feezel. Parts of this report have been taken from the M.S. thesis of T.O. Nelson and the Ph.D. thesis of L.L. Feezel. The author acknowledges helpful discussions with G. Hart, T. Wang and H. Pilloff. Support by the Office of Naval Research is greatly appreciated.

LIST OF FIGURES

LIST OF TABLES

I. INTRODUCTION

The D_2/F_2 chemical laser is comprised of elementary chemical reactions which include various feedback loops[1-3] so that a chain reaction is possible. The chain is propagated with the production of either deuterium or fluorine atoms. For typical DF lasers the chain length is estimated to be about 30. The overall laser efficiency is directly related to the production of DF from the elementary processes; an increase in the concentration of D or F will directly enhance the DF production.

A simplified laser model consists of DF production steps, DF relaxation steps and the stimulated emission of photons (lasing). This model is depicted by

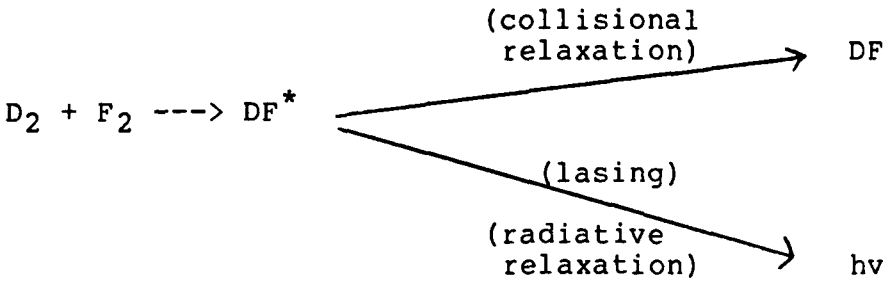

The laser output energy can be optimized by increasing the production rates and decreasing the relaxation rates. In order for this to be accomplished detailed knowledge of the important production and relaxation steps involving DF must be known.

To display the complex set of reactions with the various feedback loops a schematic representation is shown in Figure I-1. The terminology for this diagram is that the initial state is defined at the tail end of the arrow while the final state for a particular process is at the head of the arrow. This representation is analogous to that used in models demonstrating transport in biochemical systems. Although the diagram is complex, it is easily seen that any process that increases DF^* will enhance the probability of lasing. The traditional representation of these processes is listed in Table I-1. The net production of DF^* can be placed into three elementary categories:

1. initial (nascent) production (processes 1F and 1D)
2. relaxation
    a. collisional (processes 2D, 2F, $2D_2$, $2F_2$ and 2M)
    a. radiative (processes 2 and 2hv)
3. enhancements
    a. reactant translation (processes $1F^*$ and $1D^*$)
    b. reactant vibration (processes $1F^{**}$ and $1D^{**}$)
    c. chain branching (processes 3DF and $3D_2$)

The radiative relaxation processes (2 and 2hv), corresponding to spontaneous and stimulated emission, are well understood; their contributions are calculated from the well known Einstein coefficients[4]. The enhancement reactions are based on increased reactivity with reactant energy (3a and 3b) and an increase in chain carrier (3c) concentrations. These lead to thermal and population explosions,

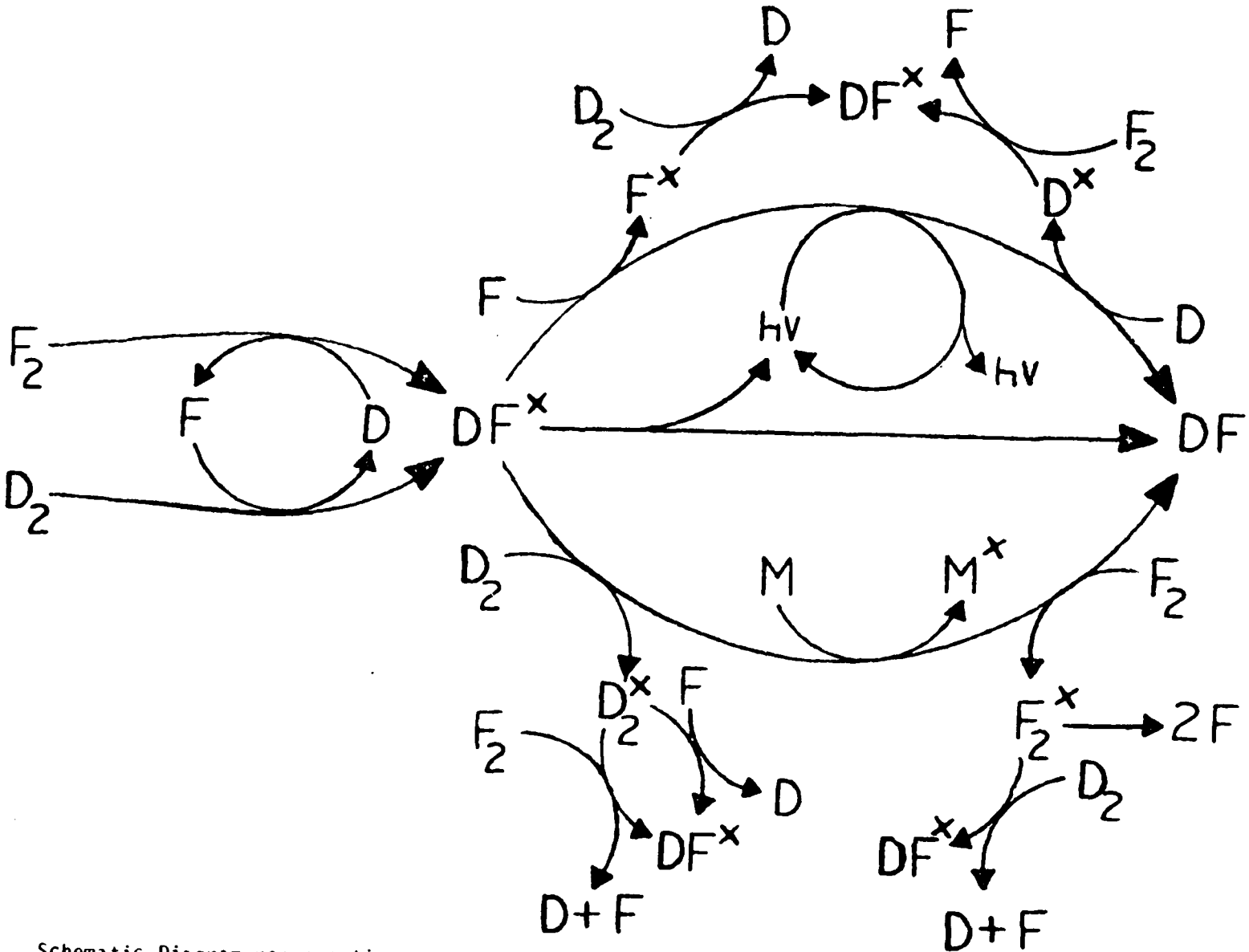

Figure I-1. Schematic Diagram representing processes for the reaction of D_2 and F_2. The first loop represents the chain reaction involving F and D as carriers. The second loop contains relaxation processes of DF^* (the upper arc represents relaxation by single particles: F, D and hv, while the lower arc is with more complex particles: F_2, D_2 or M); both paths produce DF, DF and the chain carriers. The straight line corresponds to spontaneous emission.

Table I-1

Elementary Processes Involved in the D_2/F_2 Chemical Laser

	Process	Label+
PRODUCTION (1)		
	$F + D_2 \rightarrow DF^* + D$	1F
	$D + F_2 \rightarrow DF^* + F$	1D
RELAXATION (2)		
	$DF^* + D \rightarrow DF + D^*$	2D
	$DF^* + F \rightarrow DF + F^*$	2F
	$DF^* + D_2 \rightarrow DF + D_2^*$	$2D_2$
	$DF^* + F_2 \rightarrow DF + F_2$	$2F_2$
	$DF^* + M \rightarrow DF + M^*$	2M
	$DF^* \rightarrow DF + hv$	2
	$DF^* + hv \rightarrow DF = 2hv$	2hv
ENHANCEMENTS EXCITED REACTANTS		
	$F^* + D_2 \rightarrow DF^* + D$	1F*
	$D^* + F_2 \rightarrow DF + F$	1D*
	$F + D_2^* \rightarrow DF^* + D$	1F**
	$D + F_2^* \rightarrow DF^* + F$	1D**
CHAIN BRANCHING (3)		
	$DF^* + F_2 \rightarrow DF^* + F + F$	3DF
	$D_2^* + F_2 \rightarrow DF^* + F + D$	$3D_2$
	$\rightarrow D_2 + F + F$	

+ The reaction labels are generated by the type of process (1,2,3) followed by the atomic species for reaction or the deactivator for relaxation. A single * represents translational excitation while a ** corresponds to vibrational excitation in the diatomic reactant.

respectively.

Although the above description gives an overall model for the gross features of the D_2/F_2 chemical laser system a more detailed model including particular vibrational and rotational states of DF (v & J, respectively) must be invoked to understand specifics such as laser emission wavelength, output power etc. Hart[5] has reported on the computer model for the DF chemical laser and the need for an enlarged and reliable data base for the rate constants of the elementary processes.

The partitioning of the energy released in the DF production reactions (1F and 1D) have been experimentally characterized by replacing D_2 and D with H_2[6-8] and H[9-12], respectively. Using similar techniques the energy distributions for DF resulting from reactions 1F[6-9,14] and 1D[13-14] have been reported. All of these studies were performed with the reactants in a vessel at room temperature or below. Although these studies provide fundamental information for the understanding of chemical dynamics they may not be appropriate for modeling the D_2/F_2 chemical laser. High temperatures will be achieved since reactions 1F and 1D are highly exoergic and the D_2/F_2 reactor is thermally isolated. These high temperatures will enhance the reaction rate constants and effect the vibrational energy distribution of the DF product. Thus in order to understand the overall operation of the D_2/F_2 chemical laser the reaction dynamics of the fundamental processes must be understood, an understanding that is necessary for optimizing the efficiency of these chemical lasers.

Various experimental techniques have been used to obtain the nascent vibrational-rotational energy distribution. Most of these techniques use a microwave discharge to produce the atomic species. Wang[15] has suggested that both atoms and ions (H^-, D^-, D_2^-, H_2^-, etc) are produced in the atomic source and the possiblity of negative ion-molecule reactions (NIMR) must be considered when analyzing earlier results. Similar NIMR's have been observed by Leone and coworkers[16]. Wang[15] estimates the rate constants for NIMR's to be 100-1000 times faster than the corresponding atom molecule reaction. Thus an ion "impurity" (contaminant) of 0.1% would allow NIMR's to compete favorably with the expected neutral reactions. Measurements pertaining to the ion content of gases flowing thru a microwave discharge cavity are presented in section II of this report. These results indicate that NIMR's are not important for the experimental conditions used in producing D, F or H atoms.

Measurements of the formation and relaxation rate constants and of nascent distributions have been obtained using steady state experiments and monitoring the spectrally resolved infrared emission (chemiluminescence). These steady state experiments are somewhat limited by the relative magnitudes of the rate constants for relaxation, reaction and infrared emission and the large pumping speed necessary to maintain a short lifetime for the excited molecule. Chemiluminescent Mapping (CM)[14,17], a pulsed technique, has been developed as an alternative method in obtaining formation and relaxation information for exoergic bimolecular exchange reactions. Both time and spectral resolution are obtained simultaneously.

Initial CM results for reactions 1F and 1D have been reported. Although the technique was benchmarked with the F atom reactions the F_2 results were suspicious. In addition to the possibility of NIMR's as discussed above the primary concern was with the 'unknowns' associated with a new experimental technique. Section II of this report includes diagnostics of the CM apparatus while section III presents model calculations which simulate the CM experiments. These simulations provide the means for analysis of the experiments as well as providing the optimum experimental conditions for abstracting the fundamental information from the raw experimental data. The CM experimental apparatus and data processing are described in section IV while the initial experimental results from CM experiments are presented in section V. These results provide the foundation for future studies related to the processes involved in the D_2/F_2 chemical laser.

II. DIAGNOSTICS OF CM APPARATUS

Earlier[14] we reported nascent vibrational energy distributions for the reactions

$$H(D) + F_2 \text{ ---> } HF_v\ (DF_v) + F \qquad v_{max}=<10(15) \qquad \text{II-1)}$$

$$F + H_2\ (D_2) \text{ --->} HF_v\ (DF_v) + H\ (D) \qquad v_{max}<=3\ (4) \qquad \text{II-2)}$$

using Chemiluminescence Mapping (CM) in which the diatomic reactant is pulsed into a low pressure of atomic reactants. A specially designed Evenson type microwave cavity was used to generate either F, D or H atoms. The CM product energy distribution for the F atom reactions were in agreement with those reported by other techniques, however the F_2 results indicated a higher level of vibrational excitation than that which was observed in steady state experiments.

Although the technique was benchmarked with the F atom reactions the F_2 results were suspicious. Of primary concern was the possiblity of negative ion-molecule reactions (NIMR); similar NIMR's have been observed by Leone and coworkers[16]. It has been suggested by Wang[15] that earlier chemiluminescence results in which a microwave discharge was used for producing the atomic species are due to NIMR's and not from the assumed neutral reactions. The postulated negative ions (H^-, D^-, D_2^-, H_2^-, etc) are allegedly generated by the microwave discharge source which is used to produce atomic species (H, D, F). The negative ion molecule reactions suggested are:

$$D^- + F_2 \text{ ---> } DF_v + F + e \qquad v_{max}=<12 \qquad \text{II-3)}$$

$$F + D_2^- \text{ ---> } DF_v + D^- \qquad v_{max}=<13 \qquad \text{II-4)}$$

Wang[15] estimates the rate constants for reaction II-3 to be 1000 times faster than II-2 and reaction II-4 to be 100 times faster than II-2. Thus an ion "impurity" (contaminant) of 0.1% would allow reactions II-3 and II-4 to compete favorably with II-1 and II-2. For normal experimental conditions, the reaction involving D_2^- will not be important since its lifetime is less than a microsecond[17].

Diagnostic experiments (unpublished) in our laboratory using a single probe indicated the ion concentration from a microwave discharge cavity to be < 0.0003 (0.03 %) of the atom concentration. If the NIMR's have a reaction cross section 100-1000 times greater than the neutral reaction then the NIMR products could account for up to 30% of the observed HF (DF). Since there are inherent problems with the single probe technique it appeared conceivable that NIMR may be interfering with the reactions which had been reported. Preliminary double floating probe experiments were reported[18] with a comparable upper ion concentration limit. Hence quantitative analyses of ions in the discharge region and in the reaction vessel with a double floating probe were needed. Additionally the pressure-time profile of the pulsed diatomic molecule is necessary in order to adequately model the CM results and abstract the nascent population distribution. This section includes the diagnostics of the CM apparatus; the results can be applied to any system in which atoms are formed by a microwave discharge and/or

a similarly pumped reactor (as is used in the Arrested Relaxation experiments: see reference 14 for additional citations)

ION CONTENT: Double Floating Probe Experiments

Background:

The microwave induced plasma (MIP) which is formed in the discharge region of the microwave cavity has been reviewed[19]; aside from atom production the MIP has been used successfully as a source for spectroscopic studies[20]. Although the overall mechanism involved in a plasma is not completely understood[19] it is believed to primarily involve the ionization of the gas molecules by high energy electrons; metastables producing Penning ionization may also be involved.

The use of a double floating probe technique in the CM system was needed to reduce the disturbance (withdrawal of charge) of the plasma by the probe itself (especially in the reaction vessel measurements) and to provide a reference potential (a defined space potential) which is not present in the single probe technique. The double floating probe technique has been applied successfully to MIP's by Busch and Vickers[21] and by Brassem et al[22-25]; the characteristic curve (current vs applied voltage) is used to calculate the electron concentration and temperature. Ideally the characteristic should be symmetric about the origin and exhibit saturation currents. The non-ideal characteristic is due to probe asymmetry (different surface areas or collecting efficiencies), different floating potentials resulting from a potential gradient in the plasma or a difference in contact potential between each probe and the plasma (this could be due to contamination).

Experimental Setup:

The specifics of the CM apparatus have been reported earlier[14,26]. The microwave cavity encapsulated a 12 mm OD quartz flow tube leading into a continually pumped 10 l reaction vessel (<0.0001 torr); a 1 mm restriction at the end of the tube maintained a steady pressure of 1 torr in the discharge region. A Raytheon Model PGM 10X2 microwave generator with variable output power up to 120 watts was used.

In order to assure that systematic errors were absent in these results a set of benchmark experiments were performed. These experiments probed the discharge region of the MIP and can be directly compared to results from similar MIP systems[21,23-25]. After confirming the benchmark experiments the reaction vessel was probed for ion content.

The experimental setup for the benchmark experiments is shown in Figure II-1. The probes were designed according to the limitations on probe radius and probe separation assumed in the theory as delineated by Schott[27]. Two sets of cylindrical probes were used: copper (0.10 +0.05 mm OD by 2.00 + 0.05 mm in length) and tungsten (1.00 +0.05 mm OD by 2.00 +0.05 mm in length). The copper probe has a total surface area of $6.2 * 10^{-3}$ cm^2 while that of the tungsten probe was $7.4 * 10^{-2}$ cm^2; the

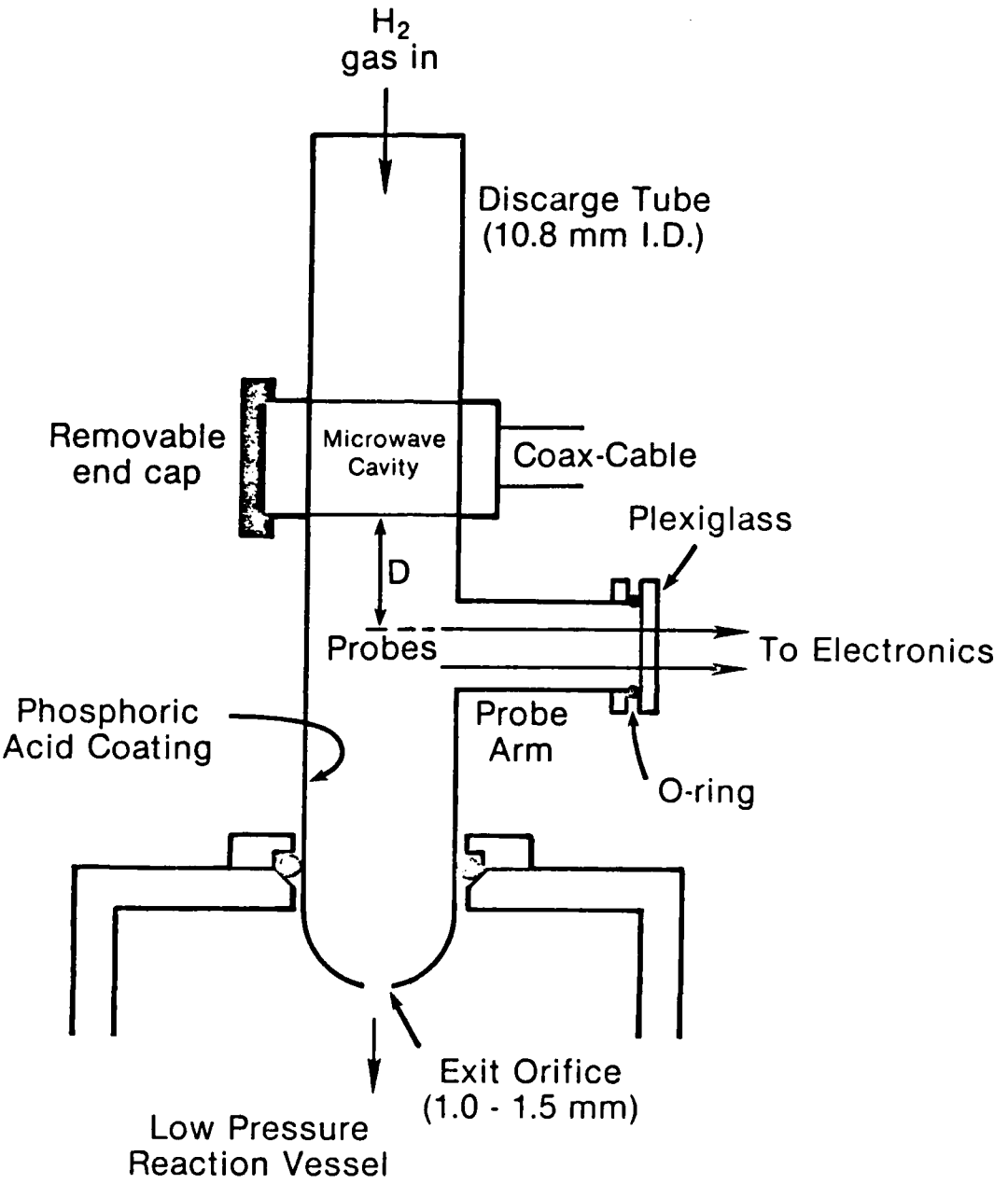

Figure II-1. Schematic Diagram for Setup of Discharge Tube Experiments.

inactive surface area was insulated with "Corona Dope" (GC Electronics), a high voltage insulating paint.

The probes were mounted on a 1/4" plate of plexiglass using high vacuum epoxy; the separation was 6.0 and 2.90 mm for the copper and tungsten probes, respectively. This plate was attached to the discharge tube with a vacuum seal comprised of a #9 glass joint and 'O' ring. The copper probes penetrated 2 mm into the discharge tube while the tungsten probe was ~1.4 mm from the edge of the discharge tube. Due to the plexiglass mounting, a high voltage degassing heater could not be used; unfortunately this enhances the chance of probe contamination. Nonetheless contamination was only observed near the probe where carrier concentrations are highest. The probe was nominally degassed with a Tesla coil prior to measurments as reported earlier[28].

An Evenson microwave cavity[29] with a removable end cap allowed for easy movement so that the distance between probes and microwave cavity could be systematically varied; this distance (D) was measured from the probe arms to the bottom of the microwave cavity; the distance from probe to the center of cavity is 0.75" larger. Alternatively, one end of the quartz discharge tube was connected to a conventional low pressure gas handling system and the other end to a 3" oil diffusion pump.

The probes were connected to a variable voltage power supply; a Keithly 417K picoammeter was connected in series with one of the probes, while a Dana digital voltmeter was connected in parallel. All of these devices were isolated from external ground as is required for the double floating probe technique.

The probes for the reaction vessel experiments were made from the inner elements of a vacuum tube. The tungsten probe had an inner total surface area of 1.24 cm^2 and a total outer area of 34.3 cm^2; probe separation was 1.78 cm. Since this asymmetric probe has a surface area ratio <300 it fulfills the requirements for a floating probe[30]. This probe was mounted on a glass rod which in turn was mounted on a vacuum feed through; this allowed the probe to be adjusted externally without breaking vacuum.

Figure II-2 is the characteristic for the tungsten probes 1.5" (D) from the cavity; this curve has high symmetry and passes through the origin. The large sloping saturation regions are typical of measurements made inside the discharge tube.

Characteristic curves were determined for the copper probes 1.5" from the cavity for 3 different levels of microwave power. Although the distance from the cavity is the same as that for the tungsten probes these characteristics show an increasing deviation from the origin as the power is increased because the potential gradient across the probe increases with power. The large saturation slopes also indicate the influence of the positive ion species at high voltage.

Characteristics obtained for the probes located in the reaction vessel at 60 and 96% power exhibit large V_{app} for I_d=0 due to the probe asymmetry. As observed for the discharge tube experiments the ion

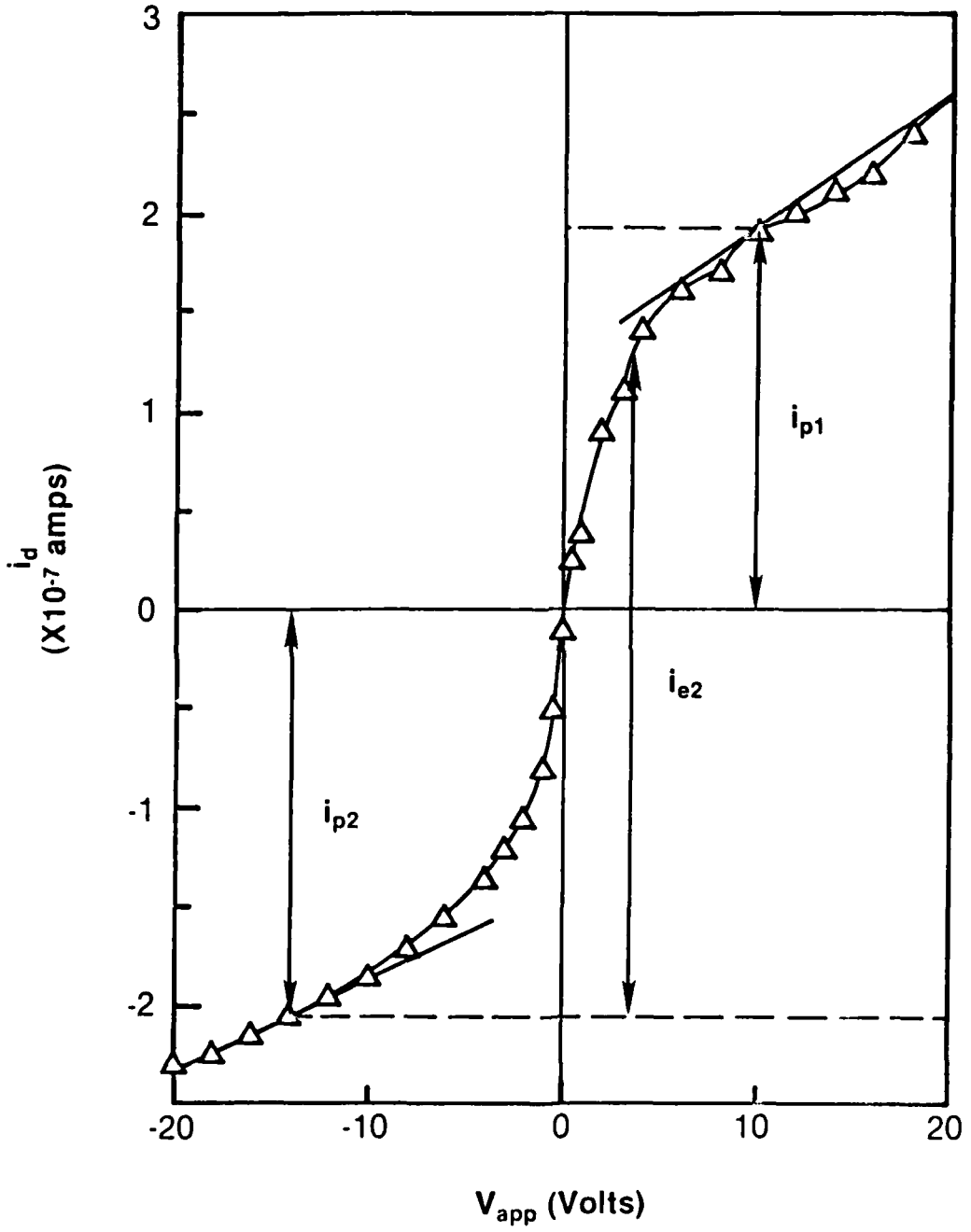

Figure II-2. Double floating probe characteristics: data taken from experiment #3-I with tungsten probes 1.5" from cavity and 60 watts microwave power. I_{p1}, I_{p2} and I_{e2} are the currents at probes 1 and 2 due to ions and electrons, respectively.

current also increases with microwave power.

The characteristic for the tungsten probes near the discharge region did not exhibit plateaus; this was a diagnostic indicating the presence of probe contamination. Characterstic curves like these were not used in calculating ion densities. The shape of these curves are similar to those of Thornton[31].

RESULTS:

Electron temperature can be determined by the logarithmic plot, equivalent resistance and intercept methods; the difference in calculated temperature between these methods is <5% [28]. The equivalent resistance and intercept methods were used in this work. The electron temperature does not depend on the probe area, contact potential or difference in plasma potential between probes. The electron concentration was calculated from the equation derived by Massey[32]:

$$i_{sat}=0.5*N_0*A*e*(kT_e/m)^{1/2}$$

where N_0 is the number of positive ions/cc, A is the surface area of the probes, T_e is the electron temperature and e is the electronic charge. This equation has been derived for spherical probes; for cylindrical probes only an order of magnitude concentration can be extracted. The results for the double floating probe experiments (complete characteristics) are tabulated in Table II-1; the discharge tube and reaction vessel results will be discussed separately.

Discharge Tube Results

Brassem[25] has measured electron densities of approximately $2 * 10^{12}$ per cc and electron temperatures of ~ 100,000 K under similar conditions to these experiments inside the microwave cavity. These values are larger than experiments #7-I and 8-I of the present work which are at lower microwave power and not in the microwave cavity (i.e. 0.75" removed). As seen in experiments #1-I and 4-I or 2-I and 5-I or 8-I,9-I and 11-I the ion densities decrease dramatically with distance. For an atmospheric argon plasma Goode and Otto[33] showed a decrease of a factor of 25 when the distance increased from 1 to 7 cm; for experiments #8-I and 11-I at a pressure of 500 microns there is a decrease of ~400 in going 1.7" (3.8 cm) from the plasma. This suggests the importance of wall collision neutralization. When a short set of copper probes were used (the tips did not penetrate into the discharge tube) a characteristic curve was not obtained; presumably the ion density was below the critical limit to form a sheath around the probes. The implication is that the restriction at the end of the discharge tube will drastically reduce the number of ions that can flow into the reaction vessel.

The ion densities increase with increasing microwave power (experiments #1-I and 2-I or 4-I, 5-I, and 6-I, or 7-I and 8-I or 10-I thru 14-I); however, the electron temperature of the hot electrons increase with power up to ~80% and then decreases as the power is increased to 100% (experiments 10-I thru 13-I and 14-I). This decrease

Table II-1

Data and Results for the Double Floating Probe Experiments

Exper. No.	Probe	Distance (inches)	Power (watts)	Ie2 (amps)	Ip (amps)	G-G^2	Ro	Te (Kelvin)	Discharge Tube Pressure (microns)	Reaction Vessel Pressure (torr)	Ion Density (ions/cm^3)
1-I	W	0.5	36	4.25×10^{-7}	6.36×10^{-7}	.222	1.90×10^{7}	31,000	500	6.6×10^{-4}	6.7×10^{7}
2-I	W	0.5	72	28.5×10^{-6}	48.5×10^{-6}	.242	4.36×10^{5}	59,000	300	3×10^{-3}	3.7×10^{7}
3-I	W	1.5	60	1.75×10^{-7}	3.25×10^{-7}	.248	1.97×10^{7}	16,000	500	1×10^{-2}	4.5×10^{7}
4-I	W	2.5	36	--	3.6×10^{-8}	--	--	49,000	300	3×10^{-3}	3.0×10^{6}
5-I	W	2.5	72	--	6.6×10^{-8}	--	--	67,000	300	3×10^{-3}	4.8×10^{6}
6-I	W	2.5	120	--	11.5×10^{-8}	--	--	51,000	300	3×10^{-3}	9.6×10^{6}
7-I	Cu	0.0	36	1.97×10^{-5}	3.4×10^{-5}	.243	7.27×10^{5}	70,000	500	1×10^{-3}	2.9×10^{10}
8-I	Cu	0.0	48	3.22×10^{-5}	5.2×10^{-5}	.235	5.63×10^{5}	80,000	500	1×10^{-3}	4.1×10^{10}
9-I	Cu	0.75	48	1.6×10^{-7}	2.6×10^{-7}	.236	6.67×10^{7}	48,000	475	2×10^{-3}	2.6×10^{8}
10-I	Cu	1.5	36	$.55\times10^{-7}$	1.05×10^{-7}	.249	13.3×10^{7}	40,000	475	8×10^{-4}	1.2×10^{8}
11-I	Cu	1.5	48	$.708\times10^{-7}$	1.28×10^{-7}	.247	18×10^{7}	66,000	475	8×10^{-4}	1.1×10^{8}
12-I	Cu	1.5	72	$.806\times10^{-7}$	1.52×10^{-7}	.249	16.3×10^{7}	72,000	475	8×10^{-4}	1.3×10^{8}
13-I	Cu	1.5	96	1.62×10^{-7}	2.62×10^{-7}	.236	12.8×10^{7}	92,000	475	8×10^{-4}	1.9×10^{8}
14-I	Cu	1.5	120	1.97×10^{-7}	3.31×10^{-7}	.241	7.8×10^{7}	73,000	475	8×10^{-4}	2.7×10^{8}
15-I[a]	VT		60	--	4.13×10^{-8}	--	--	83,000	350-800	5×10^{-6}	1.6×10^{5} (max)
16-I[b]	VT		96	--	8.81×10^{-8}	--	--	120,000	350-800	5×10^{-6}	2.8×10^{5} (max)

a) W represents tungsten, Cu represents copper and VT represents vacuum tube.
b) The difference in pressure between these experiments and the discharge tube experiments is due to both pumping speed and H_2 flow rates.

can be explained by the loss of available power to the discharge tube walls. Recently it has been reported[34] that when the plasma plume is in direct contact with the wall, the wall erodes. The energy necessary for this errosion (decomposition) is provided by the microwave generator, thus decreasing the energy available to produce hot electrons.

Lower electron temperatures and densities are the apparent effect of using larger diameter probes as was observed by replacing the smaller copper probes with the larger tungsten set. This has also been reported by Cohen[35] and Little and Waymouth[36]. Cohen[35] has shown that the ratio of the radius of the wall boundary (R_w) to the probe radius (R_p) determines the electron temperature and density. For R_w/R_p=100 the calculated temperatures are 20% less than for an infinite ratio while the densities vary by only 1-2%; R_w/R_p= 50 will produce a 50% decrease in the calculated temperature. In our experiments the tungsten probes have R_w/R_p < 50 so it is expected that the calculated temperatures could be less than 50% of the true temperature. The shorter penetration of the tungsten probe into the plasma could also account for the smaller electron density.

Reaction Vessel Results:

Our earlier work[18] indicated ion concentrations <0.03% of the atom contentration; this is based on the assumption that the density of negative ions is equal to the density of all available electrons, i.e. an upper limit for the number of negative ions is determined. By assuming 50% dissociation of the H_2 then the H atom flow through the exit orifice of the discharge tube is equal to the measured H_2 flow into the discharge tube. Having shown the agreement of the double floating probe technique in the cavity region the present work also indicates that the negative ion concentration is less than $1.8 * 10^{-4}$ % and $9.8 * 10^{-5}$ % for 96 and 60% power, respectively. Additionally, the electron temperature measured in the reaction vessel are higher than in the discharge tube; this may be due to the radius ratio of ~500 as compared to 50.

RESIDENCE TIMES: Pressure time profiles

Experimental Setup:

The diatomic reactant is pulsed using a Bosch fuel injector (previously[14] a homemade solenoid valve was used); the on/off duty cycle and cycletimes can be varied. A nude ionization gauge (NRC #538) was used for measuring the pressure-time profiles. The gauge was mounted on a glass rod so that the position inside the reaction vessel could be changed. A glass encapsulated ionization gauge was mounted on top of the reaction gauge; its conductance was limited by a 1/2" diameter entrance tube 2" long.

A standard ionization gauge power supply was used for biasing the grid and collector and to provide current to the heater for degassing. The collector was connected to an operational amplifier configured as a current to voltage converter. This output was then input to a variable gain inverting operational amplifier and subsequently fed to an oscilloscope or PARC/EG&G model 4203 signal averager. The signal

averager was used to reduce any 60 Hz noise. The signal was averaged for 25-60 pulses: 2048 data points were used to represent the time profile. The time response of the gauge and amplifiers was <0.1 msec. The data from the signal averager was then transferred to a microcomputer for data formatting and then to a Prime 750 mainframe computer for data processing and plotting.

Results and Discussion:

The pressure-time profiles were analyzed with a non-linear least squares program; the starting values for this program were estimated by a zero order linear least squares analysis. The general profile indicated three regions: a rise, a fast exponential decay and a slower exponential decay. The pumpout rate constants (i.e. the slower decay rates) were determined using data from point number 1000 to 2000. In general, the peak heights increase with flow; the response for argon is greater than that of hydrogen due to the larger ionization efficiency for argon.

Two types of experiments were done: with and without the inner can (normally in a CM experiment the inner can is cooled with liquid nitrogen to facilitate complete vibrational deactivation of the excited reaction product which collides with the wall). Experiments with argon and hydrogen were performed for various duty cycles and cycle times. The nude gauge was placed at either the center of the vessel or at the end while the encapsulated gauge was permanently located at the top (near center) of the reaction vessel. The "on" time (time the valve was opened) varied from 10 to 20 milliseconds and the cycle time (the time between pulses) was either 100 or 200 milliseconds.

Figure II-3 illustrates pressure time profiles for hydrogen <u>with</u> the inner can and "on" times of 10, 15 and 20 msecs (the total flow rate remained constant). The starting trigger times are the same; the delay between the energiziation of the injector and the detection of the pressure pulse is due to the mechanical delay of the injector. The peak times are equal to the time of the energization. When the cycle time is increased to 200 msec (see Figure II-4) the baseline approaches zero, indicating that the vessel has been completely pumped out. With the inner can in placea double exponential for the decay portion of the profile is observed. This is somewhat masked when the can is removed as shown in Figure II-4 for both argon and hydrogen.

When the cycle time is decreased to 100 msec the baseline increases and a decay between the trigger and before the next pressure increase is observed. When the nude gauge is placed at the end of the vessel the pressure profile exhibits a rounded top; due to the longer transit time the peak is broadened at the top. When the encapsulated gauge (which has an inherently small pumping conductance) is used. Presumably the time constant of this gauge has been substantially increased and the gauge container is acting as a ballast. The experimental conditions and calculated results for all of the pressure profile experiments are tabulated in Table II-2.

In general the pumpout out rate for H_2 (20 sec^{-1}) is larger than that for argon (~16 sec^{-1}). The differences between the pump out rate

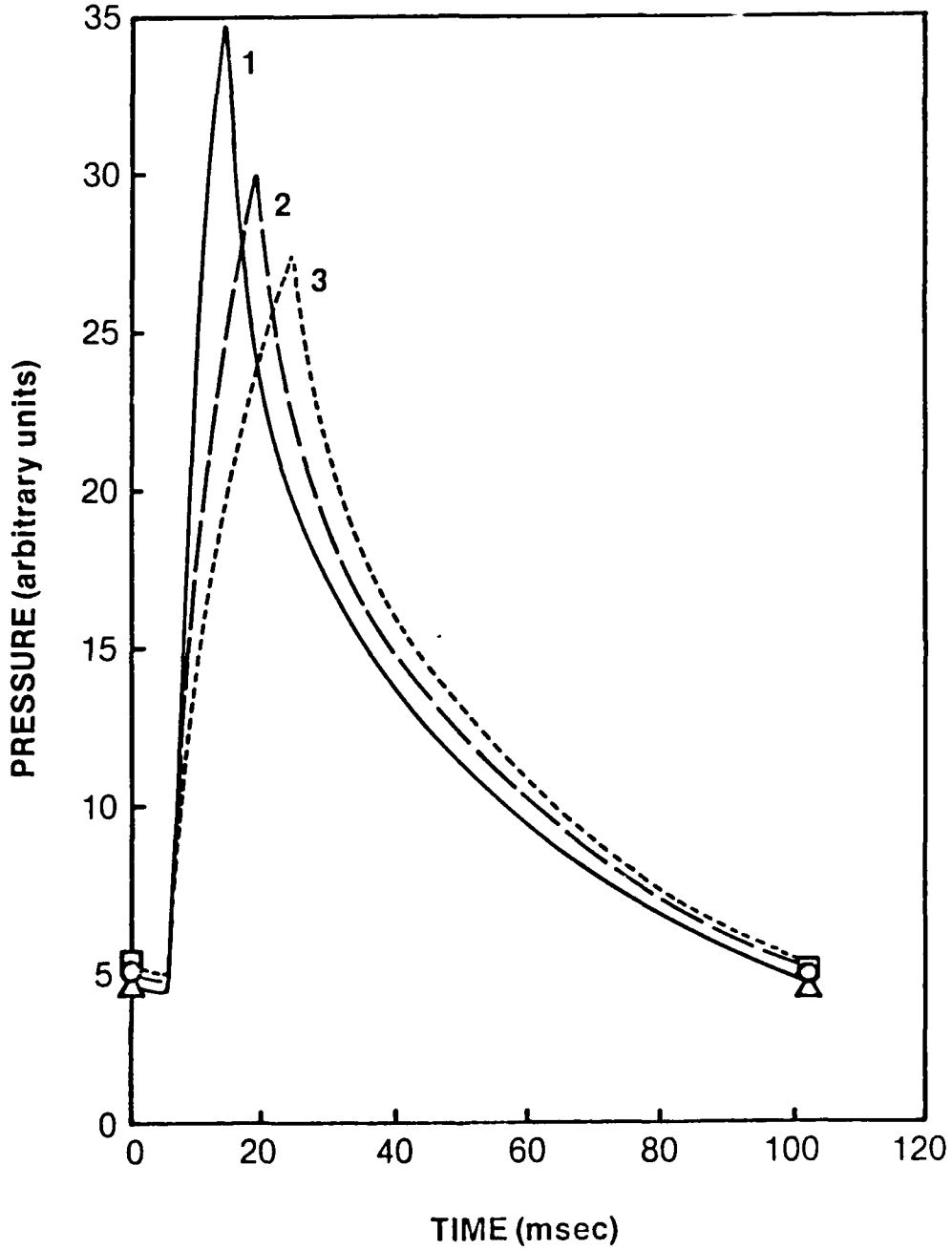

Figure II-3. Pressure-time profiles with nude gauge located below pulser for hydrogen with the inner can and a cycle time of 100 msec. The "on" times are: 10 msec (curve 1, experiment #1-P), 15 msec (curve 2, experiment #2P), 20 msec (curve 3, experiment #3-P).

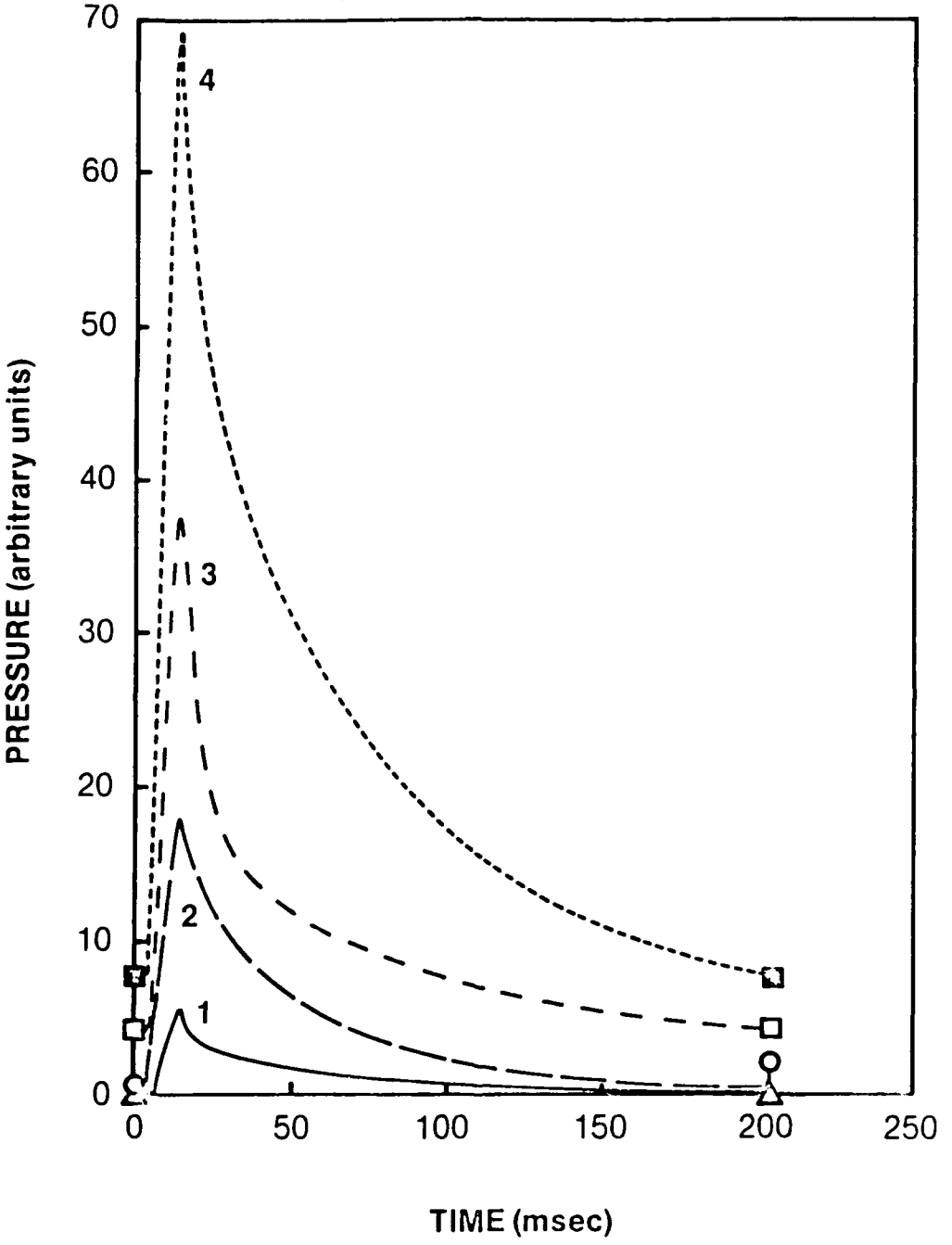

Figure II-4. Pressure time profiles with nude gauge located below pulser with a cycle time of 200 msec and "on" times of 10 msec.
curve 1: hydrogen with inner can, experiment #4-P
curve 2: hydrogen without inner can, experiment #5-P
curve 3: argon with inner can, experiment #6-P
curve 4: argon without inner can, experiment #7-P

Table II-2

Conditions and Results for the Pressure Profile Experiments

Exper. #	t_{on} (msec)	t_{cyc} (msec)	Gas	Config.	Probe Location	Reaction Vessel Pressure (torr)	Molar Flow Rate (moles/sec)	Calculated Pumpout Rate Constant (sec^{-1})
1-P	10	100	H_2	can	center	1.0×10^{-5}	$<6.1\times10^{-6}$	20.1
2-P	15	100	H_2	can	center	1.0×10^{-5}	$<6.1\times10^{-6}$	18.8
3-P	20	100	H_2	can	center	1.0×10^{-5}	$<6.1\times10^{-6}$	19.8
4-P	10	200	H_2	can	center	1.0×10^{-5}	$<6.1\times10^{-6}$	21.3
5-P	10	200	H_2	no can	center	1.3×10^{-5}	7.4×10^{-6}	21.0
6-P	10	200	Argon	can	center	9.0×10^{-5}	4.8×10^{-6}	12.7
7-P	10	200	Argon	no can	center	3.0×10^{-5}	6.1×10^{-6}	15.1
8-P	10	100	H_2	can	center	1.0×10^{-5}	$<6.1\times10^{-6}$	20.1
9-P	10	100	H_2	no can	center	1.3×10^{-5}	7.4×10^{-6}	25.3
10-P	10	100	Argon	can	center	1.0×10^{-5}	4.8×10^{-6}	16.0
11-P	10	100	Argon	no can	center	4.2×10^{-5}	6.1×10^{-6}	15.1
12-P	10	100	H_2	can	end	1.0×10^{-5}	7.5×10^{-6}	20.7
13-P	10	100	H_2	no can	end	1.3×10^{-5}	7.4×10^{-6}	24.7
14-P	10	100	Argon	can	end	1.0×10^{-4}	4.8×10^{-6}	16.0
15-P	10	100	Argon	no can	end	4.2×10^{-5}	6.1×10^{-6}	15.4
16-P	10	100	H_2	can	top	1.0×10^{-5}	7.5×10^{-6}	NA
17-P	10	100	H_2	no can	top	1.3×10^{-5}	7.5×10^{-6}	NA
18-P	10	100	Argon	can	top	1.0×10^{-5}	4.8×10^{-6}	NA
19-P	10	100	Argon	no can	top	4.2×10^{-5}	6.1×10^{-6}	NA

constants with and without the inner can are small and within experimental error, thus they are not considered distinguishable. However the double exponential decay is more apparent with the inner can. Presumably this double exponential decay can be attributed to the possibility that molecules which leave the inner can return before eventually exiting through the diffusion pump.

CONCLUSIONS

These diagnostic experiments indicate that the ions produced from a microwave discharge and entering a reaction vessel through a restriction are not at a sufficiently large concentration to allow NIMR's to interfere with atomic reactions. The relative flows of ions was determined to be less than $1.8\ 10^{-6}$ times the flow of atoms, so that even with a factor of 1000 increase in reaction cross section NIMR's will not be competitive with the atom-diatomic reactions.

The pressure profiles indicate that the pumping speed for this system is $\sim 20\ sec^{-1}$, giving a residence time of 50 msec. For the CM experiments radiative relaxation for HF is important on this time scale; for steady state experiments a background 'soup' comprised of products and reactants will build up so that secondary reactions and collisional relaxation will be important. although these diagnostics were performed for a specific CM experimental apparatus the results are applicable to other experiments in which atoms are formed in a microwave dischare and/or reactants are pulsed in a low pressure environment.

III. CM MODELING

INTRODUCTION

Chemiluminescent Mapping (CM) has been developed as an alternative method in obtaining formation and relaxation information for exoergic bimolecular exchange reactions. Both time and spectral resolution are obtained simultaneously. Conventionally steady state experiments have been performed (Arrested and Measured Relaxation and Fast Flow experiments) in which constant flows of the atomic and molecular reactants are maintained and the chemiluminescence is recorded. A typical reaction is

$$F + H_2 \longrightarrow HF_{v,J} + H \quad k_{v,J} \quad (v=1\text{-}3)$$

Two disadvantages of the steady state experiments are: i) that for slow reactions the gas flows must be increased to obtain a useable emission intensity which in turn requires larger pumping speeds to maintain the required low pressure, and ii) that the observed luminescence signal is a composite of blackbody background and the desired chemiluminescence emission. For reactions that have large exoergicities the scanned spectral region is sufficiently large so that the change in blackbody background can be greater than or comparable to the emission signal for the reaction. However, compensation for the background can be made by internally modulating the signal, i.e. by pulsing either one of the reactants. Variations of the pulse rate and duty cycle allow collection of different types of information. A slow pulse rate and a long reaction "on" time is equivalent to two experiments. With the reactant "on" the signal plus background is detected, while with the reactant "off" only the background is detected. The numerical difference between these signals is that which is due solely to the emission produced by the reaction. Extensive signal averaging beyond that of phase sensitive detection is easily implemented for CM experiments.

A single CM pulse cycle consists of two stages: input (reactant injection) and output (relaxation of reactants and or products). Two limiting regions can be considered for the input cycle: i) instantaneous input in which the formation time is substantially less than relaxation processes (i.e. reaction) and ii) slow input in which the formation time is slow relative to reaction times. Further simplifications can be made by requiring that one of the reactants is in excess (this reduces second order kinetics to first order kinetics). Thus during a CM cycle one of the reactants is depleted via reaction while the excited product is depleted via radiative or collisional relaxation, physical removal by pump out or deactivated by wall collisions to its ground state. The relative importance of each of the above processes is related to the initial conditions and reactant preparation time.

A CM experiment can be performed by pulsing either the atomic or diatomic (molecular) species; both techniques have specific advantages. Our earlier CM experiments were based on pulsing the diatomic molecule. In this case there is an initial increase in pressure followed by a decrease for each cyle. In this report we denote this CM Pressure Pulse experiment as CM-PP. Alternatively in a CM-LP (Laser Pulse) experiment the atomic reactant is pulsed; using laser excitation the atom is formed

nearly instantaneously under approximate isobaric conditions.

Four different time scales must be considered in a CM experiment: reactant formation, reaction, relaxation, and sampling (observation). It is more difficult to obtain information about a specific process if the time scales are comparable than it is if the time scales are well seperated. It is also important that the sampling interval time is short enough to resolve the fastest process otherwise significant time averaging will result. If sufficient relaxation occurs during a single CM cycle, the relative composition of the reaction mixture can change dramatically. This can then cause a change in the relative importance of the different relaxation processes. Computer modeling aids in the understanding of which processes are dominant in the different time regions of a CM cycle. This knowledge can be used to optimize the experimental conditions necessary to obtain specific information (nascent energy distribution, total reaction rate constants, deactivation rate constants).

It is also important that the ensemble of species which is being observed is homogeneous. This corresponds to a uniform concentration over the observation volume. The homogeneity can be obtained if reaction takes place in a small volume. The observed emission signal which is directly proportional to the observation volume is degraded resulting in a lower signal to noise ratio. Thus a trade off between small observation volume and emission intensity must be made. The calculations presented here assume a homogeneous mixture so that spatial averaging is not necessary.

The first generation CM experiments[14,18,26a] were based on pulsing the molecular reagent (CM-PP). Initially, we modeled these experiments and the simulation results indicated that experimental modifications were needed. Simulations that incorporated these modifications into the CM-PP model were then performed. Additional model computer simulations were then performed for both CM-PP and CM-LP experiments; these results were then used to fine tune the experiments so that nascent energy distributions, total rate constants and relaxation rate constants could be extracted from the experimental data. The results of these CM-PP and CM-LP model calculations are discussed separately in this section. The 'new' experiments are reported in section V

CM-PP MODEL CALCULATIONS

The CM-PP experiments consist of F atoms (produced in a microwave discharge of CF_4) with a flow rate F_{in} into a low pressure reaction vessel with liquid nitrogen cooled walls. The reaction vessel is connected to a diffusion pump with a first order pumping rate constant, k_p. Hydrogen is pulsed into the reaction vessel at a rate, $H2_{in}$, with an "on" time of t_{on} and a total cycle time of t_{cyc}. The F atoms can react with H_2 to form HF(v) (for simplicity the rotational quantum number, J, has been dropped), diffuse to the walls of the vessel to form F_2, or be physically removed from the reaction vessel (i.e. pumped out). Likewise H_2 can react with F atoms to form HF(v), deactivate HF(v), or be pumped out of the vessel. The excited product, HF(v) can be depleted by radiative or collisional relaxation, deactivated by wall collisions to its ground state, or be pumped out of the vessel. The following

reaction scheme is used to model the CM-PP experiments:

$$F + H_2 \xrightarrow{k_i} HF(i) + H$$

$$F \xrightarrow{k_p}$$

$$H_2 \xrightarrow{k_p}$$

$$HF(i) \xrightarrow{k_p}$$

$$F \xrightarrow{k_w} F_2$$

$$HF(i) \xrightarrow{k_w} HF(0)$$

$$HF(i) + H_2 \xrightarrow{k_{j,i}(H_2)} HF(j) + H_2$$

$$HF(i) + HF(0) \xrightarrow{k_{j,i}(HF_0)} HF(j) + HF(k)$$

$$HF(i) \xrightarrow{A_{j,i}} HF(j)$$

This reaction scheme can be described by the following set of differential equations in which it is assumed that i = j +/- 1 (only nearest neighbor transitions are allowed).

$$d[F]/dt = F_{in} - k_{tot}[H_2][F] - k_p[F] - k_w[F]$$

$$d[H_2]/dt = H2_{in} - k_{tot}[H_2][F] - k_p[H_2]$$

$$d[HF(i)]/dt = k_i[H_2][F] + A_{i,j}[HF(j)] + k_{i,j}(H_2)[H_2][HF(j)] - A_{j,i}[HF(i)] - k_{j,i}(H_2)[H_2][HF(i)] - k_p[HF(i)] - k_w[HF(i)] + k_{i,j}(HF_0)[HF(j)][HF(0)] - k_{j,i}(HF_0)[HF(i)][HF(0)]$$

k_i = microscopic reaction rate constant for state i

$k_{tot} = k_i$

$A_{i,j}$ = Einstein coefficient for emission from state j to state i

$k_{i,j}(H_2)$ = HF-H_2 bimolecular collisional energy transfer rate constant from state j to i

$k_{i,j}(HF_0)$ = HF-HF(0) bimolecular collisional energy transfer rate constant from state j to i

k_p = pump out rate constant

k_w = wall collision rate constant

These differential equations are numerically integrated to obtain $[H_2]$, [F], and [HF(v)] as a function of time for various experimental conditions and rate constants. An IMSL (International Mathematical and Statistical Libraries) subroutine (Runge-Kutta-Verner 5th and 6th order Method) is used for the numerical integration; the convergence tolerance was set for 0.001 while the time interval ranged from 5×10^{-6} to 1×10^{-4} sec depending on the cycle time.

Two experimental variables are F_{in} and $H2_{in}$. The absolute [F] is unknown, but will be less than four times the CF_4 flow rate divided by $k_p + k_w$. Hydrogen pressure profiles have been measured[26b] and are characterized by a fast rise, initial fast exponential decay, and a second slower exponential decay. A pump out rate constant, k_p, was determined by a linear least squares fit of the slower exponential decay[26b]. To be noted is that there are equal pressures of H_2 during the input ("up") and output ("down") stage. Differences in the HF(v) emission intensity at these equivalent pressure points can be attributed to changes in the relative composition of the environment.

The H_2 pressure-time profile was simulated using a double exponential function with t_{on} = 10 msec and t_{cyc} = 100 msec. A linear least squares fit of the slow exponential decay was used to obtain a k_p and the "best" simulated H_2 pressure-time profile was chosen to be the one in which the k_p obtained was equivalent to the experimental k_p. Either the experimental or parameterized H_2 pressure-time profiles were used in solving the above differential equations with no meaningful difference in the results.

Typical HF emission intensity-time profiles obtained from diagnostic CM experiments[39] are shown in Figure III-1. These profiles are for moderate (10 umoles/sec) and high (40 umoles/sec) flows of H_2 with a t_{on} = 10 msec and t_{cyc} = 100 msec. At moderate flows, the HF follows the hydrogen profile, peaking when the H_2 is turned off. At high flows of H_2, the HF intensity-time profiles exhibit a double maxima. The first maximum and decay occurs while the H_2 is "on". After the H_2 is turned off, there is another increase and final decay.

In Figure III-2, the data from Figure III-1 is plotted as a function of the experimentally measured H_2 pressure. This type of graph indicates how HF(v) varies with the H_2 environment. Because there are equivalent H_2 pressures during the input and pump out stages, it is expected that the "up" and "down" branches of this plot will be superimposable for equivalent amounts of available H_2. However, the experimentally observed time dependence of H_2 is experimentally measured without the presence of F so that the experimental H_2 profile is for the total H_2 input to the system and not the amount of available H_2. For small percent reaction, the difference between these quantities is negligible. However, this difference will account for a slight displacement of the "up" and "down" branches (in general, the "down" branch is displaced to the right of the "up" branch). In the plots of Figure III-2 both a displacement between the "up" and "down" branches and a change of curvature are to be noted.

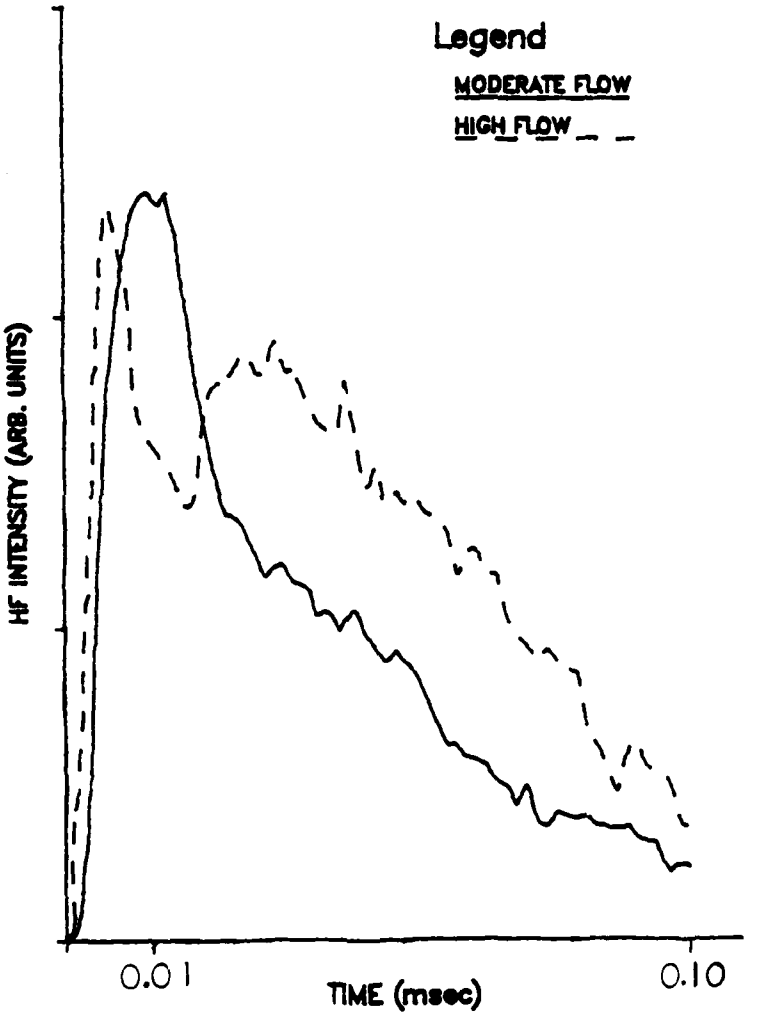

Figure III-1. Experimental HF(v) Emission Intensity Versus Time, t_{on} = 10 msec, t_{cyc} = 100 msec

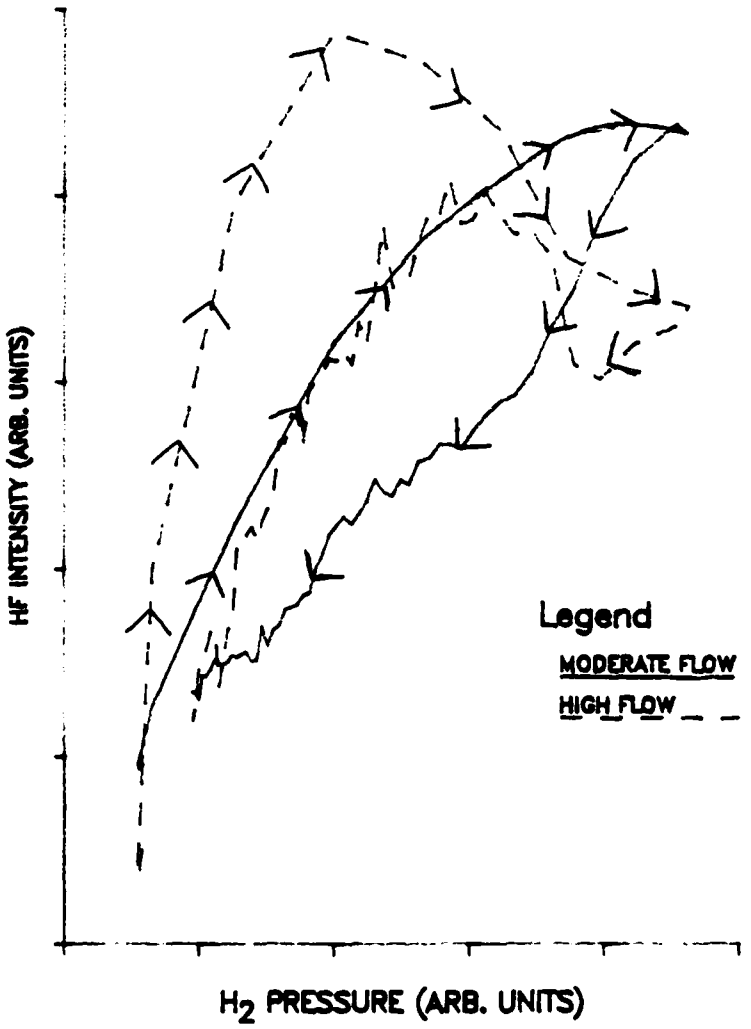

Figure III-2. Experimental HF(v) Emission Intensity Versus H_2 Pressure, t_{on} = 10 msec, t_{cyc} = 100 msec

Parameters in the simulation were varied in order to qualitatively reproduce the features of these experimentally observed profiles. The parameters used were $A_{0,1_1} = 180\ sec^{-1}$, $A_{1,2} = 320\ sec^{-1}$, $A_{2,3} = 400\ sec^{-1}$, $k_{tot} = 1 \times 10^6\ torr^{-1}\ sec^{-1}$, $k_3/k_2 = 0.5$, $k_1/k_{2_1} = 0.3$, $k_{i,j}(H_2) = 2 \times 10^5\ torr^{-1}\ sec^{-1}$, $k_p = 40\ sec^{-1}$, $k_{wall} = 500\ sec^{-1}$, $k_{1,2}(HF_0) = 5.0 \times 10^5\ torr^{-1}\ sec^{-1}$, $k_{2,3}(HF_0) = 9.0 \times 10^5\ torr^{-1}\ sec^{-1}$. The Einstein coefficients are from reference 4, k_{tot} from reference 40, k_3/k_2 and k_1/k_2 from reference 7, and $k_{i,j}(HF_0)$ from reference 41.

Simulation Results And Discussion

Simulations of the first generation CM-PP experiments (t_{on} = 10 msec) and the modified CM-PP experiments (t_{on} = 0.5msec) are discussed in this section. The discussion is divided into four parts. Each part is identified by a number: "1" (low reagent flow) or "2" (high reagent flow) or a letter: "a" (t_{on} = 10 msec) or "b" (t_{on} = 0.5 msec)

1a. Low Flow ($F/H_2 > 30$), t_{on} = 10 msec

In Figure III-3, the time dependence of the partial pressures of F and H_2 is displayed. The F atoms are 17% depleted and H_2 is the limiting reagent. The H_2 partial pressure initially increases while that for F decreases. When the H_2 is turned off, the H_2 decays while the F increases back to its non-reactive steady state value. The H_2 is depleted by reaction and pumping and this depletion increases with time.

The HF(v) pressure-time profiles are shown in Figure III-4 and mimic the H_2 pressure time profiles. Also, for this cycle time, significant background is present (the curves do not relax to zero pressure) indicating that the reaction vessel is not completely pumped out before the next H_2 pulse.

A comparision between equivalent steady state experiments and a single CM-PP experiment can be made for the time dependence of [F] or the dependence of [F] with H_2 pressure. The deviation between the "up" and "down" branches of the steady state calculations is due to the fact that the total H_2 pressure is used and not the instantaneous H_2 pressure which takes into account the H_2 that has reacted. If there is a small percent reaction, the deviation between the two branches is reduced. The deviation for the real time dependence of F with H_2 pressure is larger than that observed for the steady state curves. The finite time for reaction and relaxation accounts for this difference. Similar dependences for the HF(v) partial pressures are plotted in Figure III-5 for HF(v=3).

Molecular and atomic fluxes are the individual rate terms in the differential equations for H_2, F and HF(i) and their magnitudes indicate which processes are dominant at given times during a CM cycle. Tables III-1 thru III-3 summarize these fluxes for HF(v) at low and high flow conditions. For low flows, the input (production) terms dominate so that the net flux is positive until the H_2 is turned off, then the output (depletion) terms (net flux negative) cause the HF to decay. The dominant processes are reaction, collisions with the vessel walls, and

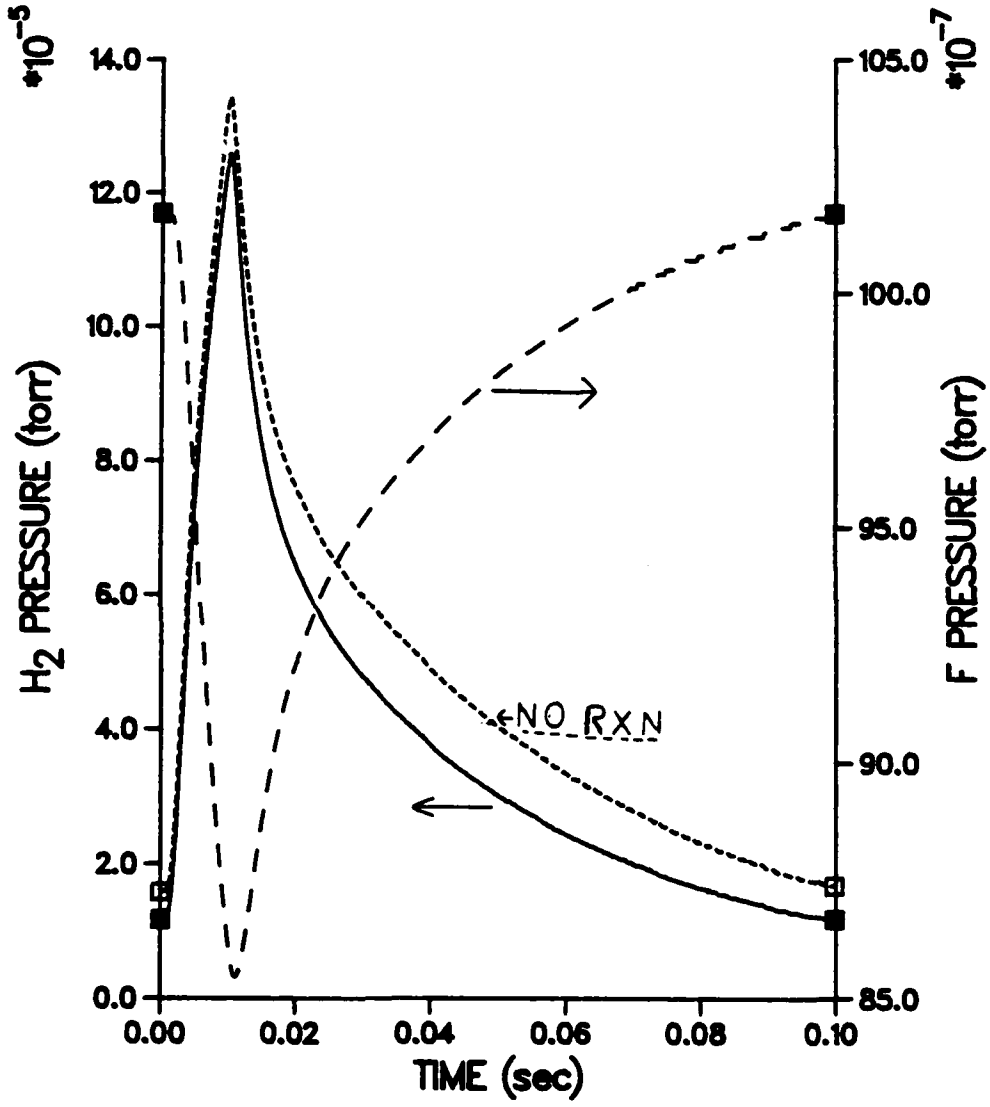

Figure III-3. F and H_2 Partial Pressure Versus Time, CM-PP Simulations: Low Flow, t_{on} = 10 msec, t_{cyc} = 100 msec

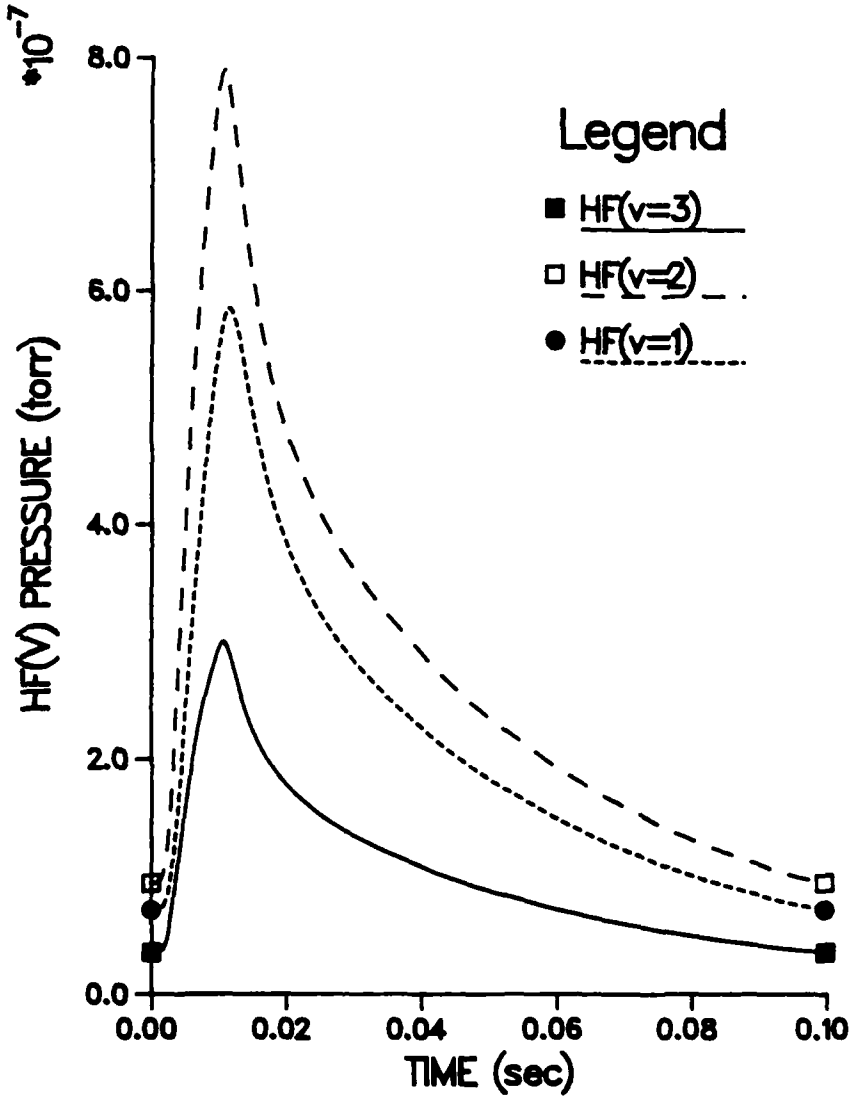

Figure III-4. HF(v) Partial Pressure Versus Time, CM-PP Simulations: Low Flow, t_{on} = 10 msec, t_{cyc} = 100 msec

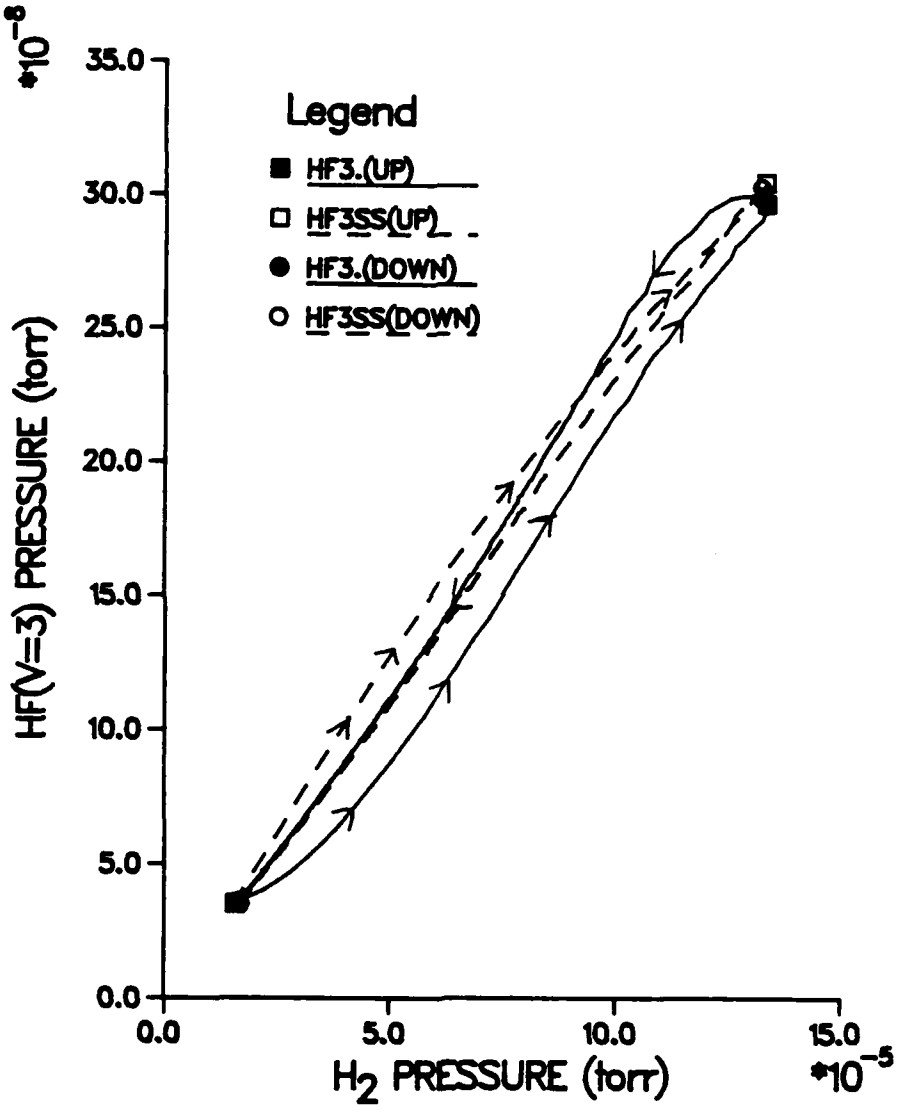

Figure III-5. HF(v=3) Pressure Versus H_2 Pressure, CM-PP Simulations: Low Flow, t_{on} = 10 msec, t_{cyc} = 100 msec

Table III-1

HF(v=3) Fluxes (x 10^{-4} torr/sec)
t_{on} = 10 msec, t_{cyc} = 100 msec

Time (msec)	Pump	Rxn	Wall	$H_2(2,3)$	$HF_0(2,3)$	Rad(2,3)	In	Out	Net
Low Flow									
2.0	-0.0172	0.5762	-0.2151	-0.0018	-0.0018	-0.1721	0.5762	-0.4079	0.1683
6.0	-0.0790	2.255	-0.9879	-0.0344	-0.0091	-0.7903	2.255	-1.900	0.354
10.0	-0.1174	3.006	-1.468	-0.0737	-0.0190	-1.174	3.008	-2.852	0.154
12.0	-0.1124	2.507	-1.405	-0.0591	-0.0213	-1.124	2.507	-2.721	-0.214
14.0	-0.0960	2.147	-1.200	-0.0423	-0.0204	-0.9600	2.147	-2.318	-0.172
40.0	-0.0432	1.009	-0.5404	-0.0081	-0.0107	-0.4323	1.009	-1.035	-0.026
70.0	-0.0238	0.5501	-0.2969	-0.0024	-0.0041	-0.2376	0.5501	-0.5647	-0.0146
High Flow									
1.0	-0.2893	8.442	-3.616	-0.8883	-0.0525	-2.893	8.442	- 8.211	0.230
2.0	-0.3249	11.60	-4.061	-1.504	-0.5875	-3.249	11.60	- 9.726	1.87
4.0	-0.4030	14.36	-5.037	-4.826	-0.7433	-4.030	14.36	-15.039	-0.68
6.0	-0.3370	14.06	-4.213	-6.132	-0.8486	-3.370	14.05	-14.700	-0.65
10.0	-0.2789	14.26	-3.486	-7.359	-0.5763	-2.789	14.26	-14.466	-0.23
12.0	-0.2795	13.68	-3.494	-6.300	-0.5919	-0.2795	13.68	-13.460	0.22
36.0	-0.3401	12.23	-4.252	-3.436	-0.7884	-3.401	12.23	-12.217	0.02
40.0	-0.3414	11.98	-4.268	-3.164	-0.7915	-3.414	11.98	-11.979	-0.00
70.0	-0.3293	10.04	-4.116	-1.660	-0.7094	-3.293	10.04	-10.107	-0.07

Table III-2

HF(v=2) Fluxes (x 10 ^ torr/sec)
t_{on} = 10 msec, t_{cyc} = 100 msec

Low Flow

Time (msec)	Pump	Rxn	Wall	$H_2(1,2)$	$H_2(2,3)$	$HF_\theta(1,2)$	$HF_\theta(2,3)$	Rad(1,2)	Rad(2,3)	In	Out	Net
2.0	-0.0443	1.152	-0.5536	-0.0045	0.0018	-0.0025	0.0018	-0.3543	0.1721	1.328	-0.9593	0.369
6.0	-0.1988	4.509	-2.485	-0.0868	0.0344	-0.0127	0.0091	-1.591	0.7903	5.343	-4.374	0.969
10.0	-0.3075	6.013	-3.843	-0.1931	0.0737	-0.0276	0.0190	-2.460	1.174	7.280	-6.831	0.449
12.0	-0.3022	5.013	-3.778	-0.1568	0.0591	-0.0318	0.0213	-2.418	1.124	6.217	-6.688	-0.471
14.0	-0.2619	4.294	-3.273	-0.1153	0.0423	-0.0309	0.0204	-2.095	0.9600	5.316	-5.776	-0.460
40.0	-0.1163	2.018	-1.453	-0.0218	0.0081	-0.0159	0.0107	-0.9300	0.4323	2.469	-2.537	-0.069
70.0	-0.0636	1.100	-0.7956	-0.0083	0.0024	-0.0061	0.0041	-0.5092	0.2376	1.344	-1.3582	-0.037

High Flow

1.0	-0.8087	16.88	-10.11	- 2.483	0.8883	-0.8160	0.5254	-6.470	2.893	21.19	-20.69	0.50
2.0	-0.8897	23.19	-11.12	- 4.118	1.504	-0.8938	0.5875	-7.117	3.249	28.53	-24.14	4.39
4.0	-1.135	28.72	-14.19	-13.60	4.626	-1.163	0.7433	-9.081	4.030	38.32	-39.16	-0.84
6.0	-0.9834	28.11	-12.29	-17.89	6.132	-1.051	0.6486	-7.867	3.370	38.26	-40.09	-1.83
10.0	-0.8138	28.53	-10.17	-21.47	7.369	-0.9342	0.5763	-6.509	2.789	39.25	-39.90	-0.65
12.0	-0.8076	27.37	-10.10	-18.20	6.300	-0.9501	0.5919	-6.461	2.795	37.05	-36.52	0.53
36.0	-0.9748	24.47	-12.18	- 9.846	3.436	-1.255	0.7884	-7.798	3.401	32.09	-32.05	0.04
40.0	-0.9774	23.95	-12.22	- 9.058	3.164	-1.259	0.7915	-7.819	3.414	31.32	-31.33	-0.01
70.0	-0.9340	20.07	-11.68	- 4.708	1.660	-1.118	0.7094	-7.472	3.293	25.73	-25.91	-0.18

Table III-3

HF(v=1) Fluxes (x 10^{-4} torr/sec)
t_{on} = 10 msec, t_{cyc} = 100 msec

Time (msec)	Pump	Rxn	Wall	$H_2(0,1)$	$H_2(1,2)$	$HF_0(1,2)$	$HF_0(1,3)$	Rad(0,1)	Rad(1,2)	In	Out	Net
Low Flow												
2.0	-0.0310	0.3457	-0.3875	-0.0032	0.0045	0.0051	0.0018	-0.1395	0.3543	0.7114	-0.5612	0.1502
6.0	-0.1254	1.353	-1.567	-0.0546	0.0866	0.0254	0.0091	-0.5642	1.591	3.064	-2.312	0.753
10.0	-0.2201	1.804	-2.752	-0.1382	0.1931	0.0552	0.0190	-0.9906	2.460	4.531	-4.100	0.430
12.0	-0.2323	1.504	-2.903	-0.1221	0.1586	0.0637	0.0213	-1.045	2.416	4.165	-4.303	-0.137
14.0	-0.2113	1.288	-2.642	-0.0930	0.1153	0.0618	0.0204	-0.9509	2.095	3.581	-3.897	-0.316
40.0	-0.0908	0.6052	-1.135	-0.0049	0.0218	0.0318	0.0107	-0.4085	0.9300	1.600	-1.651	-0.052
70.0	-0.0490	0.3300	-0.6128	-0.0049	0.0063	0.0122	0.0041	-0.2205	0.5092	0.8617	-0.8869	-0.025
High Flow												
1.0	-0.7580	5.065	- 9.475	- 2.328	2.483	1.632	0.5254	-3.411	6.470	16.175	-16.972	0.203
2.0	-0.7991	6.956	- 9.988	- 3.699	4.118	1.788	0.5875	-3.596	7.117	20.569	-18.082	2.487
4.0	-1.083	8.615	-13.53	-12.97	13.60	2.326	0.7433	-4.872	9.081	34.36	-32.46	1.90
6.0	-1.060	8.433	-13.24	-19.28	17.89	2.103	0.6486	-4.768	7.867	36.94	-38.35	-1.41
10.0	-0.8930	8.558	-11.16	-23.57	21.47	1.868	0.5763	-4.019	6.509	38.98	-39.64	-0.66
12.0	-0.8669	8.209	-10.84	-19.54	18.20	1.900	0.5919	-3.901	6.461	35.37	-35.14	0.23
36.0	-1.006	7.340	-12.57	-10.16	9.846	2.510	0.7884	-4.526	7.796	28.281	-28.27	0.01
40.0	-1.005	7.185	-12.56	- 9.312	9.058	2.518	0.7915	-4.522	7.819	27.371	-27.40	-0.03
70.0	-0.9241	6.021	-11.55	- 4.858	4.708	2.236	0.7094	-4.158	7.472	21.146	-21.29	-0.15

radiative relaxation. Collisions with H_2 and HF(v=0) are negligible for low flow conditions.

Fluorine atoms were found to be depleted mainly by recombination on the walls of the vessel followed by reaction and pump out from the vessel. Wall collisions account for ~54% of HF(v=3) depletion followed by radiative relaxation (~42%). Because the Einstein coefficients become smaller with decreasing vibrational level, the fraction of depletion due to radiative relaxation decreases as the vibrational energy is decreased. Wall collisions account for ~58% of the depletion of HF(v=2) while ~37% is due to radiative emission. For HF(v=1), ~69% of the depletion is by collisions with the walls and ~25% is due to radiative relaxation.

Reaction is the only input to HF(v=3) and is the dominant input (80%) to HF(v=2). Radiative relaxation from HF(v=3) accounts for only 20% of the input to HF(v=2). Initially radiative relaxation from HF(v=2) into HF(v=1) is dominant, between 2 and 5 msec reaction becomes more important, and finally radiative relaxation is again dominant. If the cycle time is increased, reaction is the dominant input to HF(v=1) until 5 msec when radiative relaxation from HF(v=2) takes over. These results, again, illustrate that the reaction vessel is not completely evacuated between pulses for t_{cyc} = 100 msec. For radiative relaxation to be the initial dominant input, residual HF(v=2) must be present. However, even when the cycle time is increased, radiative relaxation is a dominant input to HF(v=1) after 5 msec in contrast to HF(v=2) where reaction is dominant for all times. This is due to the fact that the microscopic reaction rate constant for HF(v=2) is larger than for HF(v=1) or HF(v=3) (k_2/k_1 = 3.3, k_2/k_3 = 2).

Figure III-6 shows plots of HF(v)/HF(v=2) as a function of time for both t_{cyc} = 100 msec and 200 msec. For a cycle time of 200 msec, the HF(v) and H_2 decay to zero and the ratio plots are linear out to 2 msec. An extrapolation of the linear portion of these curves to zero time gives the nascent distributions (k_3/k_2 = 0.5, k_1/k_2 = 0.3). The slopes of the curves depend on the relaxation processes; k_3/k_2 has a negative slope and k_1/k_2 has a positive slope. Unfortunately, only data for 20% of t_{on} can be used for the extrapolation so that the majority of the data does not provide direct information on the nascent distributions. These initial points will have the lowest intensity and the smallest signal/noise ratio so that the extrapolated distribution would have very large errors associated with it. The ratio plots obtained for a cycle time of 100 msec indicate that if the vessel is not completely evacuated between pulses, nascent distributions are not easily obtained.

2a. High Flows (F/H2 < 0.75), t_{on} = 10 msec

The time dependence of the partial pressures of F and H_2 illustrate that F atoms are the limiting reagent (~80% depletion). Reaction is now the dominant depletion process of F at the expense of wall recombination. The difference between the H_2 profiles with and without reaction is small due to the small percent reaction. Figure IV-7 shows the time dependence of the HF(v). Double maxima are observed; the first appears before the H_2 is turned off and the second after.

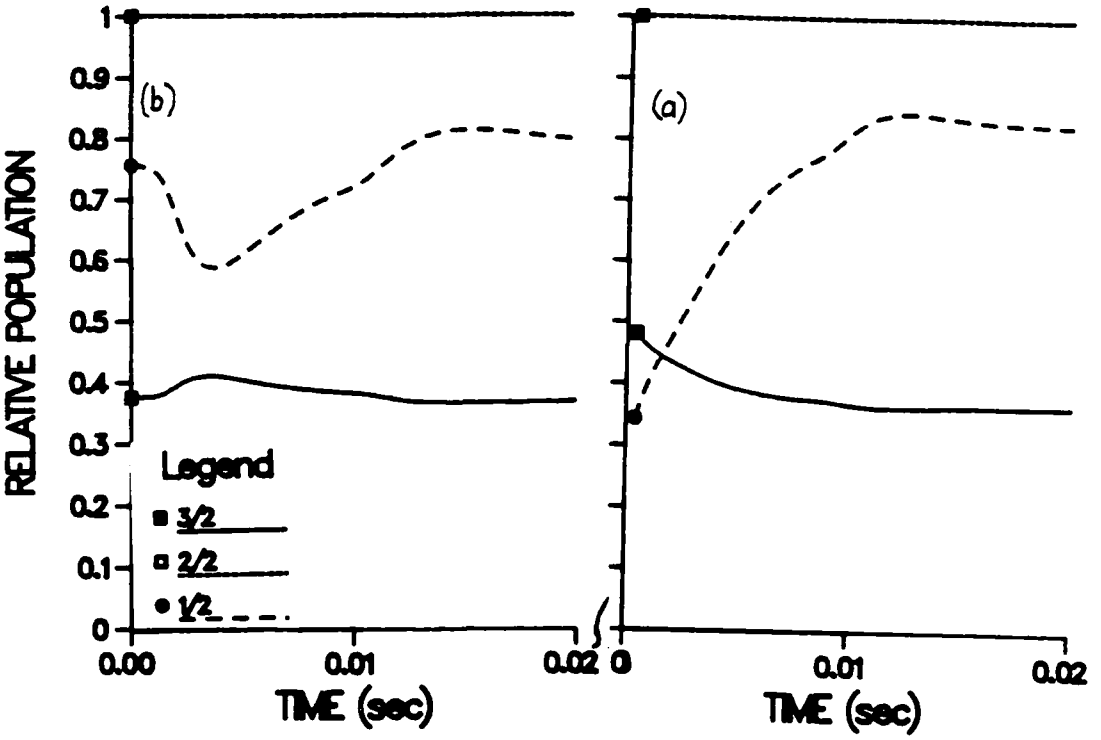

Figure III-6. HF(v) Relative Population Versus Time, CM-PP Simulations: Low Flow,
(a) t_{on} = 10 msec, t_{cyc} = 200 msec
(b) t_{on} = 10 msec, t_{cyc} = 100 msec

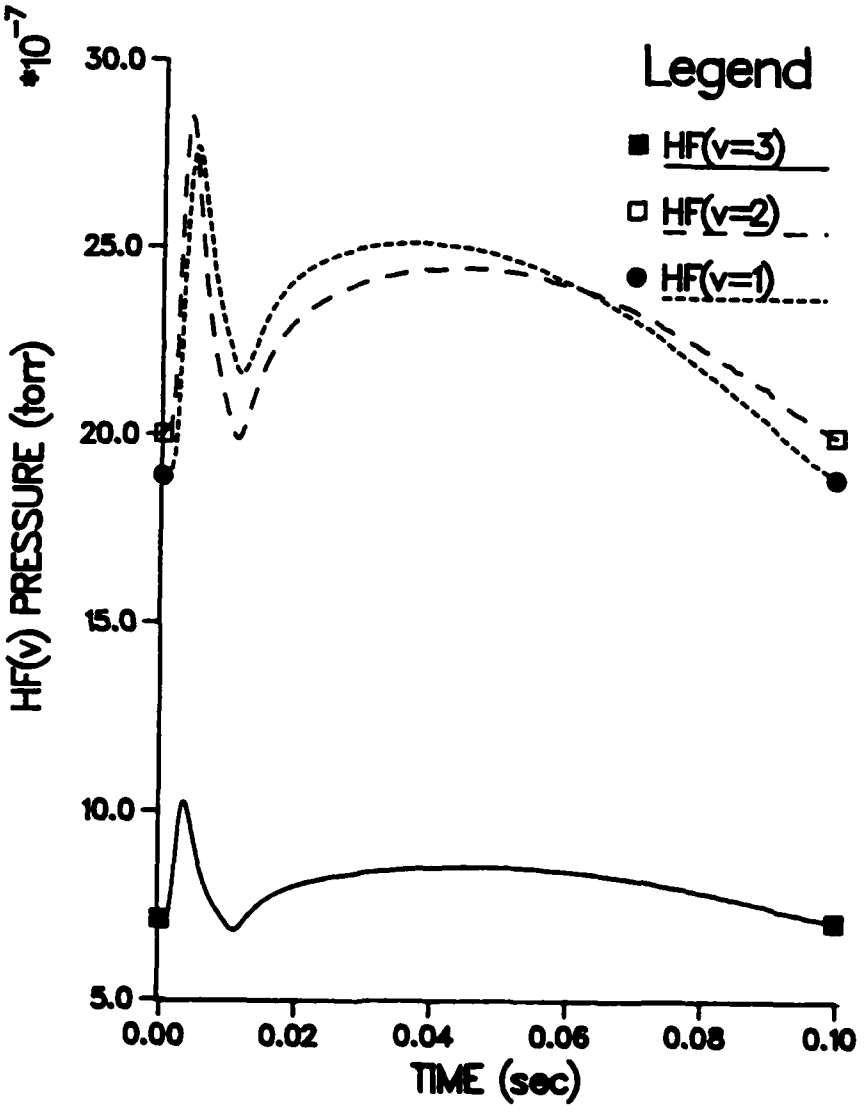

Figure III-7. HF(v) Partial Pressure Versus Time, CM-PP Simulations: High Flow, t_{on} = 10 msec, t_{cyc} = 100 msec

The [F] variation with H_2 pressure is similar to that observed for low flows. The deviation between the "up" and "down" curves for the steady state calculations of [F] is smaller because of less percent reaction. Figure IV-8 shows the HF(v=3)-H_2 profile which is also similar to the behavior of HF(v=1) and HF(v=2). Steady state calculations exhibit a maximum before and after the H_2 is turned off. This behavior can be understood by considering the steady state equation for HF(v=3):

$$HF^{ss}(v=3) = \{(k_3[H_2])/(k_{2,3}[H_2] + k_r)\}\{F_{in}/(k_{tot}[H_2] + k_p)\} \quad \text{III-1)}$$

where k_r is the sum of all depletion processes that are independent of H_2. Because $[H_2]$ varies with time, the importance of H_2 collisional deactivation ($k_{2,3}[H_2]$) and F atom depletion ($k_{tot}[H_2]$) will also vary with time. For small $[H_2]$ (early times), $k_{2,3}[H_2] << k_r$ (absence of H_2 collisional deactivation) and $k_{tot}[H_2] << k_p$ (minimal F atom depletion), so that the increase of $HF^{ss}(v=3)$ is proportional to $[H_2]$. For large $[H_2]$, $k_{2,3}[H_2] >> k_r$ and $k_{tot}[H_2] >> k_p$ so that $HF^{ss}(v=3)$ is proportional to $1/[H_2]$. Since $[H_2]$ is large and increasing for times < t_{on}, the $HF^{ss}(v=3)$ decreases. The maximum in Figure III-8 occurs when the denominator is proportional to $[H_2]$; two possibilities are either $k_{2,3}[H_2] >> k_r$ or $k_{tot}[H_2] >> k_p$ so that $HF^{ss}(v=3)$ is independent of $[H_2]$. The behavior of the "down" branch in Figure III-8 is similar to the "up" branch since there are equivalent H_2 pressures during the input and pump out stages. The "real" HF(v) builds up to values greater than those for a steady state due to insufficient time for the F atom concentration to be depleted and collisional relaxation of HF(v).

Collisional deactivation of HF(v) by H_2 is of comparable magnitude to radiative relaxation and collisions with the walls (see Tables III-4 thru III-6). Initially collisions of HF(v=3) with the wall dominate over depletion by radiative or collisional relaxation as observed for low flows. While the H_2 is "on" collisional deactivation of HF(v) by H_2 becomes dominant and accounts for up to 50% of the relaxation. Similar results for the depletion of HF(v=1) and HF(v=2) are observed.

Input to HF(v=2) is dominated by reaction (~80%) at all times as it was for the low flow conditions; input due to H_2 collisional relaxation from HF(v=3) is only ~20%. As in the low flow case, the effect of residual HF(v) is illustrated by the fact that radiative relaxation from HF(v=2) is the initial input to HF(v=1). If the cycle time is increased, reaction is the initial dominant input. The main input to HF(v=1) after approximately 3 msec is collisional relaxation from HF(v=2).

The HF(v)/HF(v=2) ratio as a function of time is shown in Figure III-9. As was observed for low flow conditions, the ratio plots for t_{cyc} = 100 msec cannot be used to obtain nascent distributions because of the presence of residual HF(v). If the cycle time is increased to 200 msec, the plots show linear behavior during the time when relaxation processes are of less importance than reaction (16% of t_{on}). Again the major portion of the data does not provide information that can be readily interpreted.

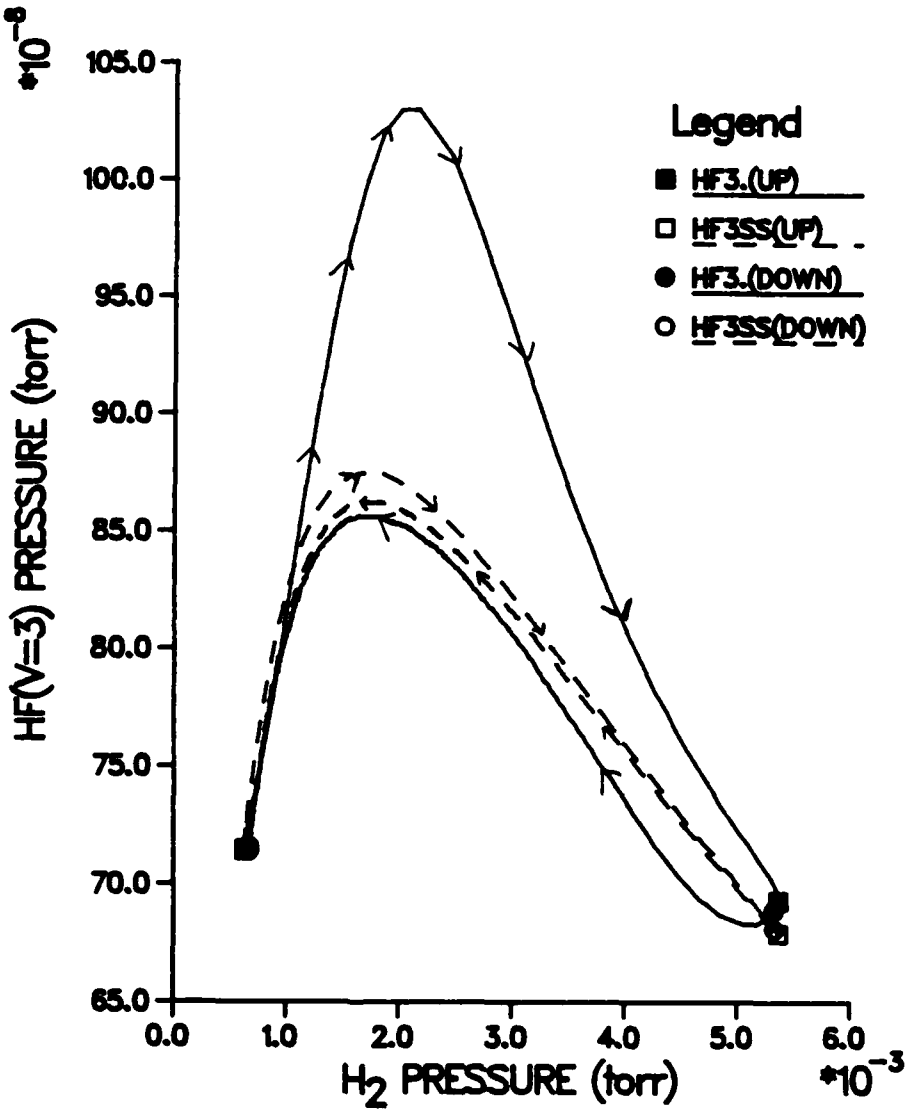

Figure III-8. HF(v=3) Pressure Versus H_2 Pressure, CM-PP Simulations: High Flow, t_{on} = 10 msec, t_{cyc} = 100 msec

Table III-4

HF(v=3) Fluxes (x 10^{-3} torr/sec)
t_{on} = 0.5 msec, t_{cyc} = 10 msec

Time (msec)	Pump	Rxn	$H_2(2,3)$	$HF_0(2,3)$	Rad(2,3)	In	Out	Net
Low Flow								
0.20	-0.0672	0.7093	-0.0003	-0.0000	-0.0207	0.7093	-0.0905	0.6188
0.50	-0.3756	1.240	-0.0282	-0.0000	-0.1156	1.240	-0.5194	0.720
0.70	-0.4711	0.7866	-0.0239	-0.0000	-0.1450	0.7866	-0.6399	0.1467
0.90	-0.4646	0.6363	-0.0206	-0.0000	-0.1491	0.6363	-0.6542	-0.0179
1.00	-0.4780	0.5815	-0.0188	-0.0000	-0.1471	0.5815	-0.6439	-0.6234
1.30	-0.4457	0.4939	-0.0152	-0.0000	-0.1371	0.4939	-0.5981	-0.1042
1.50	-0.4173	0.4473	-0.0131	-0.0000	-0.1284	0.4473	-0.5508	-0.1115
7.00	-0.0631	0.0688	-0.0003	-0.0000	-0.0194	0.0688	-0.0828	-0.0140
High Flow								
0.10	-0.3696	8.698	-0.1952	-0.0000	-0.1137	8.698	-0.6786	8.219
0.20	-1.717	13.46	-2.648	-0.0001	-0.5285	13.46	-4.894	8.59
0.26	-2.140	9.337	-4.299	-0.0004	-0.6584	9.337	-7.097	2.239
0.30	-2.163	6.618	-4.918	-0.0008	-0.6657	6.618	-7.748	-1.130
0.50	-1.198	1.695	-3.611	-0.0017	-0.3686	1.695	-5.179	-3.484
1.20	-0.5120	1.407	-0.7409	-0.0010	-0.1575	1.407	-1.4114	-0.005
1.30	-0.5134	1.409	-0.7116	-0.0010	-0.1580	1.409	-1.3840	0.025
1.70	-0.5382	1.396	-0.6336	-0.0008	-0.1656	1.396	-1.3382	0.058
5.30	-0.6932	1.134	-0.2214	-0.0003	-0.2133	1.134	-1.1282	0.006
5.40	-0.6929	1.109	-0.2109	-0.0003	-0.2132	1.109	-1.1172	-0.008

Table III-5

HF(v=2) Fluxes (x 10^{-3} torr/sec)
t_{on} = 0.5 msec, t_{cyc} = 10 msec

Time (msec)	Pump	Rxn	$H_2(1,2)$	$H_2(2,3)$	$HF_0(1,2)$	$HF_0(2,3)$	Rad(1,2)	Rad(2,3)	In	Out	Net
Low Flow											
0.20	-0.1365	1.419	-0.0053	0.0026	-0.0000	0.0000	-0.0336	0.0207	1.442	-0.1753	1.267
0.50	-0.7874	2.479	-0.0592	0.0282	-0.0000	0.0000	-0.1938	0.1158	2.623	-1.0405	1.583
0.70	-1.015	1.573	-0.0514	0.0239	-0.0000	0.0000	-0.2499	0.1450	1.742	-1.317	0.425
0.90	-1.072	1.273	-0.0456	0.0206	-0.0000	0.0000	-0.2639	0.1491	1.442	-1.382	0.061
1.00	-1.073	1.179	-0.0427	0.0191	-0.0000	0.0000	-0.2642	0.1476	1.346	-1.380	-0.035
1.30	-1.027	0.9877	-0.0351	0.0152	-0.0000	0.0000	-0.2526	0.1371	1.140	-1.315	-0.175
1.50	-0.9761	0.8945	-0.0305	0.0131	-0.0000	0.0000	-0.2403	0.1284	1.0360	-1.2469	-0.2109
7.00	-0.1535	0.1375	-0.0006	0.0003	-0.0000	0.0000	-0.0378	0.0194	0.1572	-0.1919	-0.0347
High Flow											
0.10	-0.7478	17.80	- 0.3950	0.1952	-0.0000	0.0000	-0.1841	0.1137	18.11	- 1.3269	16.78
0.20	-3.635	26.97	- 5.604	2.648	-0.0001	0.0001	-0.8947	0.5285	30.15	-10.133	20.01
0.30	-4.982	13.24	-11.33	4.918	-0.0010	0.0007	-1.226	0.6657	18.82	-17.53	1.29
0.40	-4.473	5.807	-12.64	4.906	-0.0021	0.0015	-1.101	0.5340	11.048	-18.22	- 7.17
0.50	-3.464	3.390	-10.44	3.611	-0.0027	0.0017	-0.8526	0.3666	7.371	-14.76	- 7.39
1.40	-1.439	2.808	- 1.906	0.6860	-0.0014	0.0009	-0.3541	0.1593	3.654	- 3.700	- 0.046
1.50	-1.437	2.803	- 1.825	0.6652	-0.0014	0.0009	-0.3537	0.1611	3.630	- 3.617	0.013
2.40	-1.546	2.720	- 1.389	0.5306	-0.0009	0.0006	-0.3805	0.1817	3.433	- 3.317	0.117
5.00	-1.733	2.348	- 0.6190	0.2473	-0.0004	0.0003	-0.4267	0.2131	2.809	- 2.780	0.029
5.20	-1.732	2.253	- 0.5639	0.2259	-0.0004	0.0003	-0.4262	0.2134	2.693	- 2.722	- 0.029

Table III-6

HF(v=1) Fluxes (x 10^{-3} torr/sec)
t_{on} = 0.5 msec, t_{cyc} = 10 msec

Time (msec)	Pump	Rxn	$H_2(0,1)$	$H_2(1,2)$	$HF_0(1,2)$	$HF_0(1,3)$	Rad(0,1)	Rad(1,2)	In	Out	Net
Low Flow											
0.20	-0.0433	0.4256	-0.0017	0.0053	0.0000	0.0000	-0.0060	0.0338	0.4844	-0.0509	0.4135
0.50	-0.2809	0.7438	-0.0211	0.0592	0.0000	0.0000	-0.0389	0.1938	0.9988	-0.3409	0.6580
0.70	-0.3988	0.4720	-0.0201	0.0514	0.0000	0.0000	-0.0549	0.2499	0.7733	-0.4718	0.3015
0.90	-0.4544	0.3818	-0.0193	0.0455	0.0000	0.0000	-0.0629	0.2839	0.6912	-0.5386	0.1548
1.00	-0.4712	0.3537	-0.0188	0.0427	0.0000	0.0000	-0.0652	0.2642	0.6807	-0.5552	0.1055
1.30	-0.4913	0.2963	-0.0188	0.0351	0.0000	0.0000	-0.0680	0.2528	0.5843	-0.5761	0.0082
1.50	-0.4879	0.2684	-0.0153	0.0305	0.0000	0.0000	-0.0676	0.2403	0.5392	-0.5707	-0.0315
7.00	-0.0881	0.0413	-0.0004	0.0006	0.0000	0.0000	-0.0122	0.0378	0.0797	-0.1007	-0.0210
High Flow											
0.10	-0.2362	5.339	- 0.1248	0.3950	0.0000	0.0000	-0.0327	0.1841	5.918	- 0.3937	5.524
0.20	-1.412	8.091	- 2.176	5.604	0.0003	0.0001	-0.1955	0.8947	14.589	- 3.783	10.806
0.30	-2.651	3.971	- 6.027	11.33	0.0019	0.0007	-0.3671	1.226	16.53	- 9.046	7.48
0.50	-3.329	1.017	-10.04	10.44	0.0055	0.0017	-0.4610	0.8526	12.32	-13.83	- 1.51
0.80	-3.025	0.8274	- 7.138	6.348	0.0055	0.0016	-0.4188	0.6621	7.845	-10.582	- 2.737
2.40	-1.273	0.8160	- 1.144	1.389	0.0019	0.0006	-0.1782	0.3805	2.588	- 2.593	- 0.004
2.50	-1.272	0.8130	- 1.103	1.353	0.0018	0.0006	-0.1782	0.3841	2.553	- 2.552	0.001
2.54	-1.272	0.8101	- 1.086	1.337	0.0018	0.0006	-0.1782	0.3855	2.535	- 2.534	0.001
2.60	-1.272	0.8052	- 1.058	1.309	0.0017	0.0006	-0.1781	0.3875	2.504	- 2.506	- 0.002

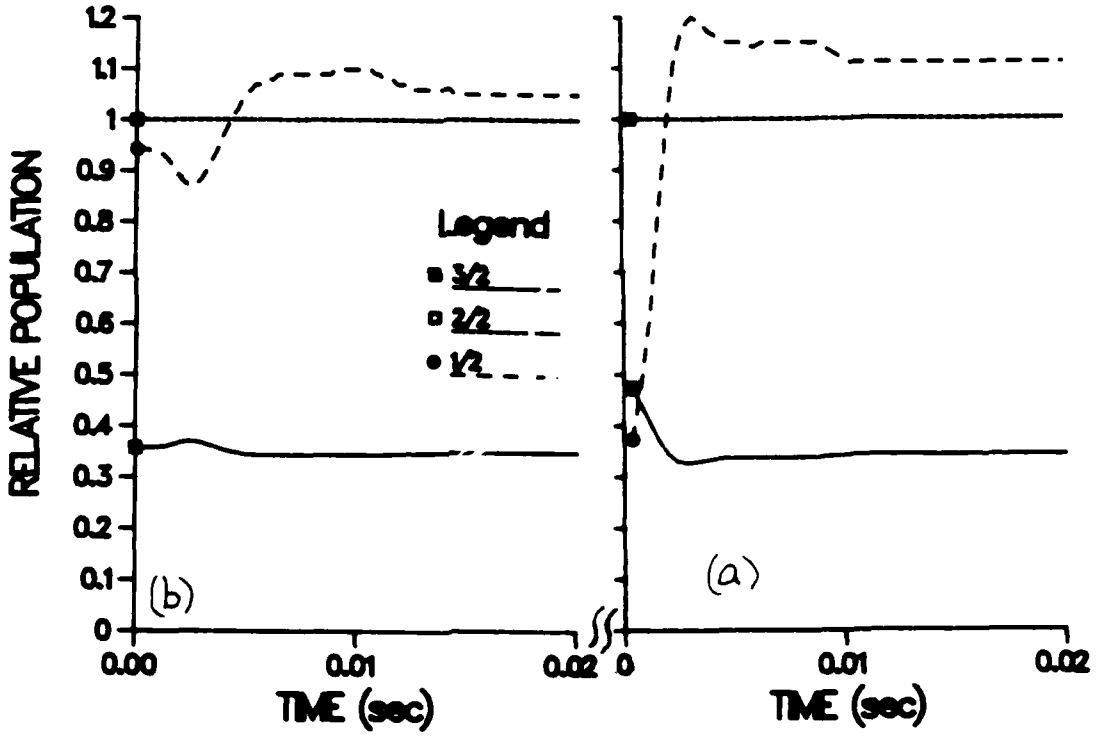

Figure III-9. HF(v) Relative Population Versus Time, CM-PP Simulations: High Flow,
(a) t_{on} = 10 msec, t_{cyc} = 200 msec
(b) t_{on} = 10 msec, t_{cyc} = 100 msec

The results of the above two sets of simulations indicate that in order to obtain nascent distibutions, the cycle time must be long enough to ensure that there is no residual HF(v) present and that relaxation processes must be minimized during the observation time. The latter suggests that a shorter pressure pulse and usable data for a given observation time is maximized. Therefore, the "old" CM-PP experimental system needed to be modified; a second set of simulations were done to show that the "new" experiments would be an improvement. The "new" changes in the model are that the H_2 is pulsed into the reaction vessel with a t_{on} = 0.5 msec and a t_{cyc} = 10 msec. In addition, the observation volume was reduced so that HF(v) is homogeneously produced in this volume; reagents flow out of this volume with a rate constant, k_p. Because of the smaller observation time and the reduced observation volume, HF(v) does not have time to collide with the vessel walls and return to the observation region; the k_w term was omitted. The value of k_p used for HF(v) flow from the observation volume was 1.3×10^3 sec^{-1} while all other parameters remained the same.

1b. Low Flows ($F/H_2 > 30$), t_{on} = 0.5 msec

The H_2 pressure increases with time and at 0.5 msec starts to decrease. There is less percent reaction than was observed for the same flow conditions and t_{on} = 10 msec. The F atoms decay (25% depletion) but do not reach a minimum until <u>after</u> the hydrogen is turned off. Depletion of F atoms is due mainly to wall recombination followed by reaction and pump out of the reaction vessel. The HF(v) partial pressure - time profiles show a single maximum that does not occur until after the H_2 is turned off.

The HF(v)-H_2 and F-H_2 pressure profiles show a greater deviation from the steady state calculations than was observed for the t_{on} = 10 msec case. This is to be expected since there is less time for reaction and relaxation to establish a steady state before the next incremental H_2 pressure change. The $HF^{SS}(v)$ increase and decay is proportional to H_2 which indicates that there is minimal F atom depletion and that collisional relaxation is not important (see equation III-1). The decay of the $HF^{SS}(v)$ begins when the H_2 is turned off. For $t < t_{on}$, the "real" F is much greater than F^{SS} (less reaction than ocurrs for steady state) and therefore the "real" HF(v) is greater than $HF^{SS}(v)$. When the H_2 is turned off, the "real" F still decays (reaction) and tries to approach a steady state. Because the H_2 is changing more slowly during its pump out stage, the F eventually reaches a steady state and at this time starts to increase. Likewise, since the F is still reacting after the H_2 is turned off, the "real" HF(v) is still being formed and approaches its steady state value at which time it decays. Therefore, because the "real" CM-PP system deviates from a steady system, the HF(v) pressure-time profiles do not decay until after the H_2 is turned off.

Fluxes are listed in Tables III-4 thru III-6 for low and high flow conditions. For low flows, the net flux shows a single sign change, that occurs after the H_2 is turned off, indicative of the single maximum observed in the HF(v) pressure-time profiles. Depletion of HF(v) is predominantly due to flow from the observation volume followed by

radiative relaxation. Collisional relaxation is not important.

Approximately 80% of HF(v) depletion is due to flow from the observation volume, while depletion due to radiative relaxation is ~25% for HF(v=3), ~20% for HF(v=2), and ~12% for HF(v=1).

Reaction is the dominant input for all vibrational levels. Radiative relaxation of HF(v=3) accounts for <10% of the input to HF(v=2). For HF(v=1), radiative relaxation from HF(v=2) becomes of comparable importance as input only after 2 msec.

The HF(v)/HF(v=2)-time plots (Figure III-10) show linear behavior to 0.5 msec. One hundred percent of the t_{on} data can be used to extrapolate to zero time and obtain nascent distributions.

2b. High Flows ($F/H_2 > 0.75$), t_{on} = 0.5 msec

The time dependence of the partial pressures of F and H_2 are similar to that for t_{on} = 10 msec and t_{cyc} = 100 msec. The F atoms are the limiting reagent and are ~80% depleted within 0.5 msec. This depletion is due predominately to reaction. The HF(v) pressure-time profiles exhibits a double maxima; the first occuring before the H_2 is turned off.

The $HF^{ss}(v)$-H_2 pressure profiles show similar behavior as the profiles in Figure III-8 and this behavior is explained in the same way as for the t_{on} = 10 msec case by considering equation III-1. The "real" F and HF(v) show larger deviations from steady state for $t < t_{on}$ than was observed for a t_{on} = 10 msec. However, because F is depleted during t_{on}, at times $> t_{on}$, the "real" F is approximately equal to F^{ss}. Thus, the behavior of the HF(v) pressure-time profiles for t_{on} = 0.5 msec and t_{on} = 10 msec is essentially the same.

Tables III-4 thru III-6 show the fluxes for high flow conditions. H_2 collisional relaxation accounts for up to 70% of the depletion of HF(v) while radiative relaxation is less than 10%.

Reaction is the dominant input to HF(v=2). For HF(v=1), reaction is dominant to 0.1 msec after which collisional relaxation from HF(v=2) accounts for 85% of the input. Radiative relaxation from HF(v=2) accounts for 10% of the input until after 2 msec when it increases to ~30%.

The HF(v)/HF(v=2)-time plots are shown in Figure III-11. These plots are linear out to 0.1 msec (where relaxation processes are minimal) and when extrapolated to zero time give the correct nascent distributions. In this case 24% of the t_{on} data can be used for the extrapolation; for t_{on} = 10 msec only 16% of the t_{on} data could be used.

Qualitative Comparison With CM-PP Experiment

Figure III-12 shows experimental HF(v) population-time profiles and ratio plots for the F + H_2 reaction using a t_{on} = 0.5 msec and t_{cyc} = 25 msec. These HF(v) population-time profiles show broad maxima that occur

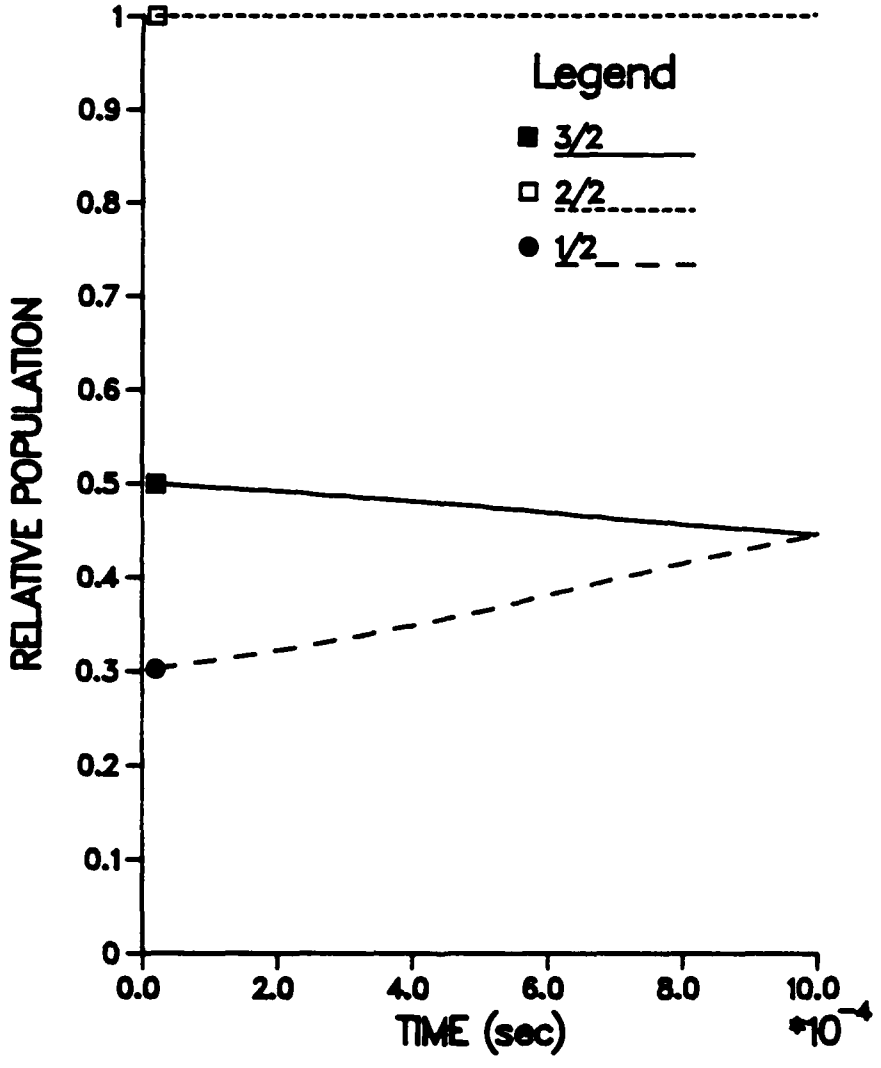

Figure III-10. HF(v) Relative Population Versus Time, CM-PP Simulations: Low Flow, t_{on} = 0.5 msec, t_{cyc} = 10 msec

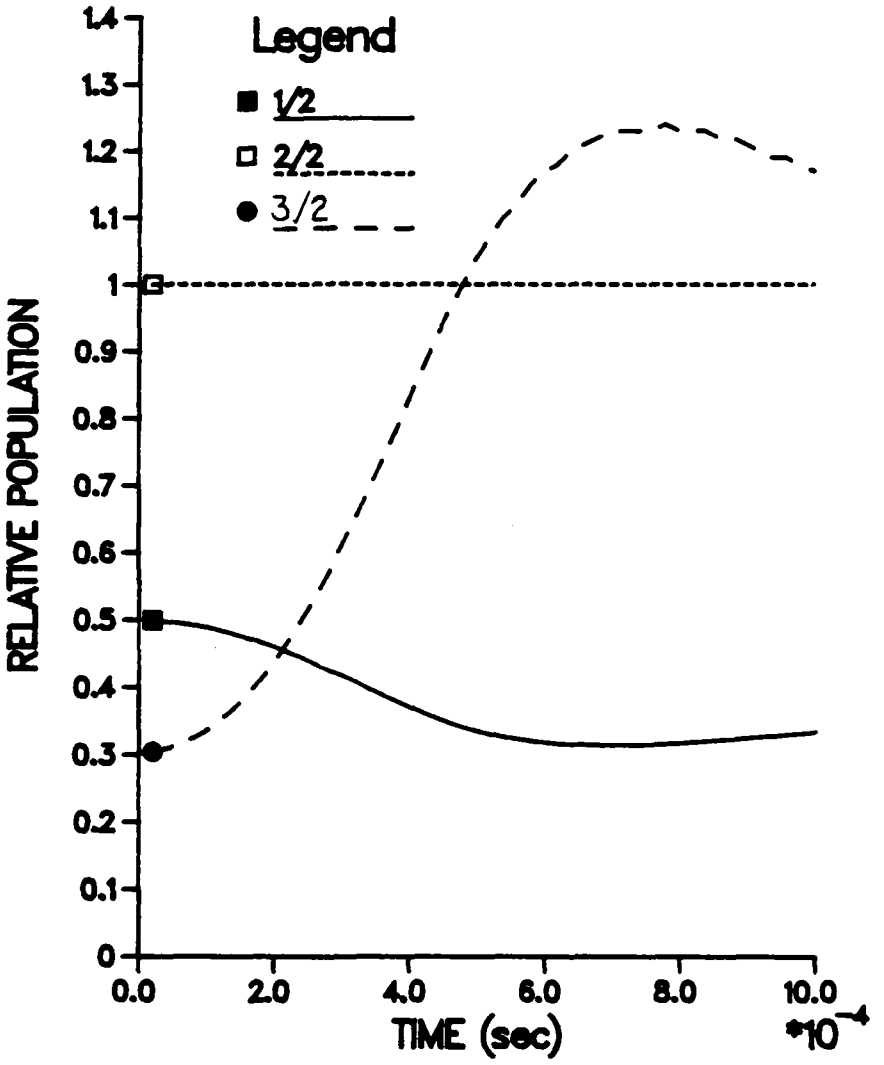

Figure III-11. HF(v) Relative Population Versus Time, CM-PP Simulations: High Flow, t_{on} = 0.5 msec, t_{cyc} = 10 msec

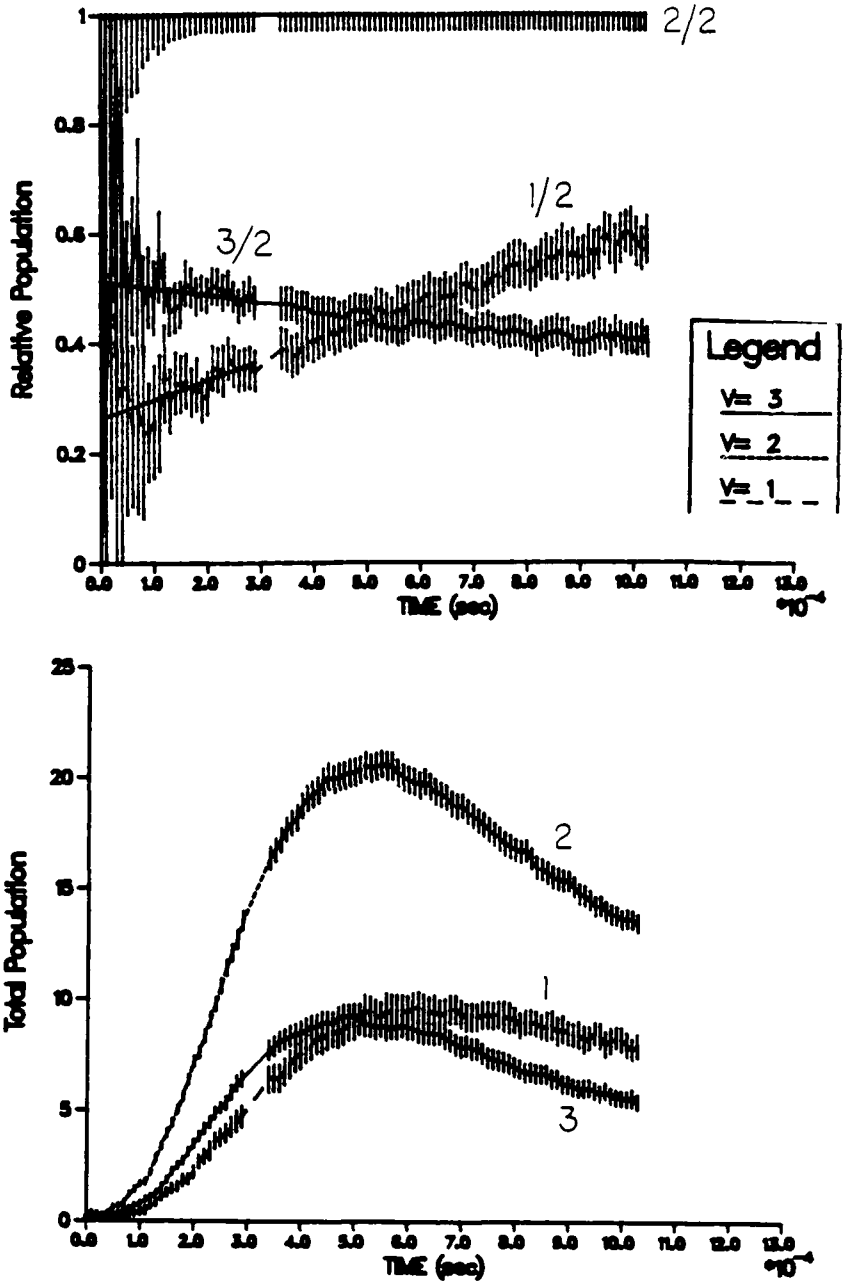

Figure III-12. Experimental HF(v) Total Population and Relative Population Versus Time, t_{on} = 0.5 msec, t_{cyc} = 25 msec

at times closer to when the H_2 is turned off than do the simulations. The ratio plots show linear behavior and when extrapolated to zero time give nascent distributions in agreement with literature values.

Parameters in the model were varied in order to qualitatively reproduce the experimental results. It was found that by increasing the flows of F and/or H_2 (increased [F] and/or [H_2]) that the HF(v) maxima moved closer to the time when the H_2 was turned off. By increasing the flows of reactants, percent reaction is increased. The [F] and HF(v) reach their steady state values at earlier times, but still after the H_2 is turned off. Increasing the k_p rate constant for flow of HF(v) from the observation volume also caused the HF(v) maxima to move closer to the times when the H_2 is turned off. By increasing this rate constant, the depletion flux becomes dominant at an earlier time. As long as the [F] was in excess of [H_2], the ratio plots showed behavior similar to that of Figure III-10, otherwise relaxation processes became important and the ratio plots resembled those of Figure III-11.

The difference between the experimental and simulated profiles may be some combination of larger [F] and/or [H_2] and faster flow from the observation volume. The behavior of the experimental profiles could also indicate that the HF(v) reenters the observation zone after being partially relaxed by either the vessel walls or by gas phase collisions. As pointed out earlier, this path is not included in the simulation. However, if this process occured it would be expected that the product energy distributions obtained would be relaxed.

CM-PP Conclusions

There are two limiting cases of experimental conditions: low and high flow of H_2. The experiments performed under low flow conditions are characterized by a small amount of F depletion and a single maximum in the HF(v) pressure-time profiles. Collisions with H_2 are not a dominant process under these conditions. Plots of the pressure ratios of HF(v)/HF(v=2) as a function of time show linear behavior at times when relaxation processes are minimal and extrapolation to zero time gives the nascent product energy distributions. By decreasing the observation time, a larger portion of the data (out to the time when the H_2 is turned off) can be used in the extrapolation. This is an important experimental consideration because the earliest data will have the lowest intensity and thus the lowest signal/noise ratio. It was also shown that in order to obtain nascent distributions, the cycle time must be long enough to ensure that the reaction vessel is evacuated before the next pulse.

Double maxima are observed in the HF(v) pressure-time profiles for high flow conditions. The double maxima are due to F atom depletion and H_2 collisional relaxation. The times at which the ratio plots exhibit linear behavior are much shorter than for low flow conditions even when the observation time is reduced. This is because H_2 collisional relaxation changes the relative composition of the reaction mixture before the H_2 is turned off. Although the nascent distributions can be obtained from the simulated data, experimentally it would be more difficult because of the small signal/noise ratio of these initial

points.

The "best" CM-PP experiment is then one in which: the observation time is shorter than the fastest relaxation process, the cycle time is long enough to evacuate the observation volume, a low flow of H_2 (minimal F depletion), so that the HF(v) profile exhibits a single maximum.

CM-LP MODEL CALCULATIONS

The CM-LP experiments consist of flowing mixtures of SF_6 in Ar, HR (HR is a generic chemical entity attached to H) in Ar, Ar, and a deactivator, M, into a reaction vessel. Fluorine atoms are formed on a microsecond time scale by the multiphoton dissociation of SF_6[42]. The F atoms react with HR to produce HF(v) which can be collisionally deactivated, undergo radiative emission, or flow out of the observation volume. The CM-LP experiments are further simplified by having [F] << [HR] (pseudo first order conditions). For the experiments described in this report M = HR although essentially any deactivator could be used.

The following reaction scheme is used to model the experiments:

$$SF_6 \xrightarrow{nh\nu} F$$

$$F + H_2 \xrightarrow{k_i} HF(i) + H$$

$$HF(i) + H_2 \xrightarrow{k_{j,i}(H_2)} HF(j) + H_2$$

$$HF(i) + HF(0) \xrightarrow{k_{j,i}(HF_0)} HF(j) + HF(k)$$

$$HF(i) + Ar \xrightarrow{k_{j,i}(Ar)} HF(j) + Ar$$

$$HF(i) \xrightarrow{A_{j,i}} HF(j) + h$$

$$HF(i) \xrightarrow{k_p}$$

An equilibrium (Boltzmann) rotational distribution is assumed, justifiably, since these experiments are done at total pressures of approximately 4 torr.

The reaction scheme can be described by a set of coupled differential equations in which it is assumed that i = j +/- 1 (only nearest neighbor transitions are allowed):

$$d[F]/dt = -k_{tot}[H_2][F]$$

$$d[HF(i)]/dt = k_i[H_2][F] + k_{i,j}(H_2)[HF(j)][H_2] - k_{j,i}(H_2)[HF(i)][H_2] - A_{j,i}[HF(i)] + A_{i,j}[HF(j)] - k_{j,i}(Ar)[HF(i)][Ar]$$

$$+ k_{i,j}(Ar)[HF(j)][Ar]$$

$$- k_{j,i}(HF_0)[HF(i)][HF(0)]$$

$$+ k_{i,j}(HF_0)[HF(j)][HF(0)] - k_p[HF(i)]$$

These equations are numerically integrated using an IMSL subroutine (Runge-Kutta-Verner 5th and 6th order method) to obtain the time dependence of E and HF(v). A tolerance of 0.001 and time interval of 5.0×10^{-7} sec was used for the numerical integration. The parameters used were the same as for the CM-PP model except for the following:

$[H_2]$ = 20-60 mtorr

$[F]_0$ = 0.1 mtorr

[Ar] = 4.0 torr

$k_{i,j}(Ar) = 30\ torr^{-1}\ sec^{-1}$ (reference 43)

$k_p = 60\ sec^{-1}$

Analysis of Rate Constants

For the highest vibrational level populated, vmax, the input is due solely to reaction and the analytical solution for the time dependence of HF(vmax) is the sum of two exponentials[44]:

$$HF(v=vmax) = Aexp(-k_{tot}t) + Bexp(-k_{r,vmax}t) \qquad III-2)$$

$$k_{tot} = k_{tot}[H_2]$$

$$k_{r,vmax} = k_{i,j}(H_2)[H_2] + k_p + A_{i,j} + k_{i,j}(Ar)[Ar] + k_{i,j}(HF_0)[HF(0)]$$

$$A = -B = (k_{vmax}[H_2][F]_0)/(k_{r,vmax}-k_{tot})$$

The analytical solutions for the lower vibrational levels are complicated by additional input due to vibrational relaxation of the higher levels. In general, for each vibrational level below vmax an additional exponential term appears in the analytical solution[44].

The pseudo first order rate constants are obtained from a non-linear least squares fit of the data to these analytical solutions. The non-linear least squares fit was done using the CURFIT subroutine by Bevington[45] which minimizes $\chi^2 = \sum_i [HF^{calc}(t) - HF^{exp}(t)]^2 / \sigma_{HF(t)}^2$ with respect to the parameters (pseudo first order rate constants). If the pseudo first order rate constants for relaxation are then plotted as a function of H_2 pressure, the slope is the H_2 collisional deactivation rate constant, $k_{i,j}(H_2)$ and the intercept is the sum of the remainder of the rate constants for depletion of HF(v). Similarily, a plot of the

pseudo first order reaction rate constants versus H_2 pressure has a slope equal to the total reaction rate constant, k_{tot}.

Using the double exponential function, the rate constants obtained for HF(v=3) were in agreement with the ones used in the model. The rate constants obtained for HF(v=2) and HF(v=1) using the multiexponential function were low by 25%. For HF(v=3), only 4 parameters must be fit by the non-linear least squares, while fitting HF(v=2) and HF(v=1) data involves 6 and 8 parameters respectively.

An alternative method to obtain the rate constants is to decouple the HF(v) differential equation into components: relaxation from the upper levels into v and input to v due to reaction, thereby the lower levels have an analytical solution equivalent to equation III-2. Figure III-13 shows a two level system (using the F + H_2 reaction (vmax = 3) as an example) from which the algorithm for this method is illustrated. For HF(v=3), input is due only to reaction while output is the sum of all the depletion processes. This can be fit to the analytical solution in equation III-2. For HF(v=2), input is due to reaction and some fraction, X_3, of the population from HF(v=3) that is relaxed into v=2. The HF(v=2) population formed by reaction can undergo relaxation processes with a pseudo first order rate constant ($k_{r,2}$) while the HF(v=2) population formed by relaxation from HF(v=3) can also undergo relaxation processes, $k'_{r,2}$. The terms $k_{r,2}$ and $k'_{r,2}$ are equivalent, however the prime denotes the source. From this model, a set of differential equations can be written:

$$dHF(3)/dt = k_3[H_2][F] - k_{r,3}[HF(3)] \qquad \text{III-3)}$$

$$dHF(2)/dt = \{k_2[H_2][F] - k_{r,2}[HF(2)]\} + \{X_3 k_{r,3}[HF(3)] - k'_{r,2}[HF(2)]'\} \qquad \text{III-4)}$$

$$dHF(2)^{tot}/dt = dHF(2)^{rxn}/dt + dHF(2)'/dt \qquad \text{III-5)}$$

where the { } terms in equation III-4 are replaced by the respective dHF(2)/dt terms in equation III-5. Integration of equation III-5 for the time dependence of HF(2) gives:

$$HF(2)^{tot} = HF(2)^{rxn} + HF(2)' \qquad \text{III-6)}$$

Equation III-6 can be rearranged to give:

$$HF(2)^{rxn} = HF(2)^{tot} - HF(2)' \qquad \text{III-7)}$$

Thus after subtracting the contribution due to HF(v=3) relaxation from $HF(2)^{tot}$, the resulting $HF(2)^{rxn}$ has the analytical solution of equation III-2. An iterative method is defined in which a $k'_{r,2}$ is estimated, dHF(2)'/dt is numerically integrated to give HF(2)', and $HF(2)^{rxn}$ is determined from equation III-7. The time dependence of $HF(2)^{rxn}$ is determined by a non-linear least squares fit to equation III-2 and a new $k_{r,2}$ is obtained. Convergence occurs when $k_{r,2}$ is within 1% of the estimated $k'_{r,2}$. This procedure is performed for $0<X_3<1$. The "best" fit for a particular X_3 is chosen to be the one with the minimum chi square statistic. In addition, k_{tot} can be used as a check of self

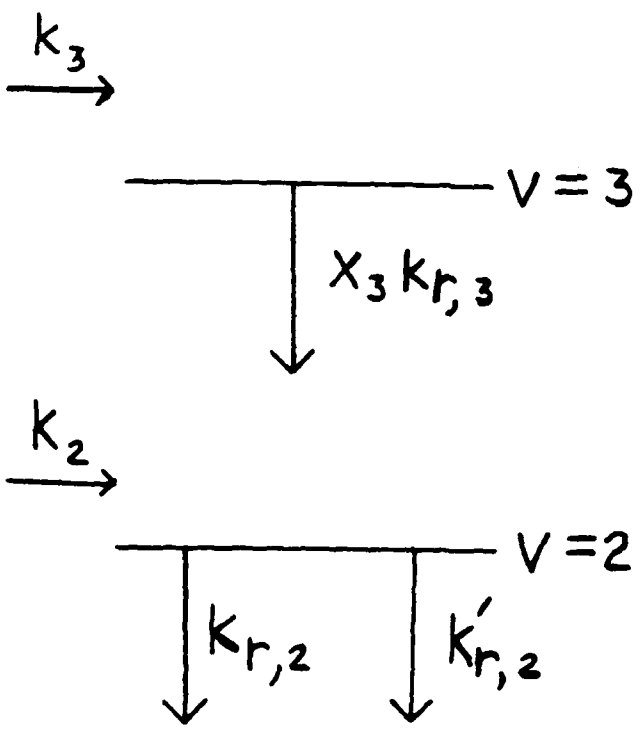

Figure III-13. Diagram of Two Level System for the Determination of Rate Constants for v < vmax

consistency, since it is constrained to be the same for all vibrational levels. The iterative procedure can then be repeated for each lower vibrational level.

The pseudo first order rate constants for reaction and relaxation obtained are then plotted as a function of H_2 pressure. The slopes of these plots give the total reaction rate constant and deactivation rate constants. Depending on the relative magnitudes of k_{tot} and $k_{i,j}(M)$, the pseudo first order rate constant obtained from the rise of the HF(v) time profile can be either due to reaction or relaxation. The same is true for the pseudo first order rate constant obtained from the fall of the HF(v) time profile. Simulations showed that when $k_{i,j}(H_2) < k_{tot}$, the pseudo first order rate constant obtained from the rise of the HF(v) time profile is equal to $k_{tot}[H_2]$ and that from the fall is due to $k_{i,j}(H_2)[H_2]$ and all other deactivation terms that are independent of H_2. When $k_{i,j}(H_2) > k_{tot}$, the reverse is true. This distinction must be made in experiments where the "correct" process is not known apriori; additional diagnostic experiments must be performed.

CM-LP Results and Discussion

The F atoms decay exponentially with a pseudo first order rate constant, $k_{tot}[H_2]$. Figure III-14 shows the HF(v) pressure-time dependence which are observed in the new CM-LP experiments. The HF(v) pressure-time profiles show an initial rise followed by a slower decay. The decay is due to collisional and radiative relaxation and appears to decrease for the lower vibrational levels because of the input they are receiving from the upper levels. The HF(v=0) shows a much slower decay which is due solely to the k_p term. The total emission intensity, which has been observed in earlier experiments, is a composite of the HF(v=1-3) populations of Figure III-14 weighted by their respective Einstein coefficients. To be emphasized is that the total intensity-time profile exhibits a non-exponential decay.

The time dependence for the population ratios (relative to HF(v=2) is shown in Figure III-15. The ratio plots behave linearly out to 0.3 msec and when extrapolated to zero time give the nascent distributions.

Table III-7 summarizes the rate constants obtained by analyzing the simulated HF(v) populations-time profiles. The reaction rate constant obtained from the simulated total intensity fit is approximately 20% lower than that input to the model, while the deactivation rate constant is approximately 35% too low. Thus within the normal error of these experiments, the total intensity should not be used to calculate these rate constants. The v=3 fit produce reaction and deactivation rate constants equivalent to that input to the model as does the fit to HF(v=2) when $X_v = 1.0$. The dependence of the reduced chi-square statistic on X_2 is significant for the simulated data; its ability to differentiate different values of X_2 will decrease for data that includes random experimental error. For experimental data both chi-square and k_{tot} can be used as a test for the goodnes of fit. A limitation of the iterative procedure is that when the amount to be subtracted in equation III-6 is > 70% of the total amount present, the algorithm either does not converge (2500 iterations are performed) or it produces incorrect rate constants. This was observed for HF(v=1)

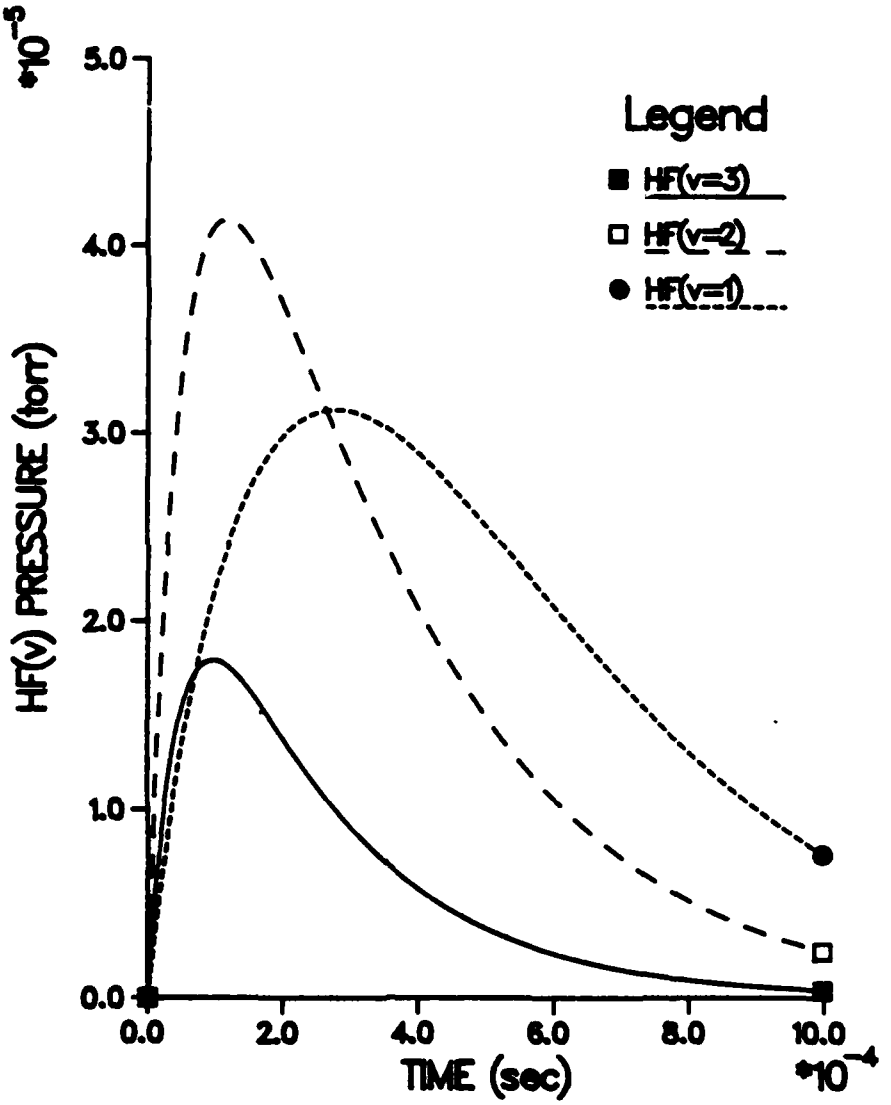

Figure III-14. HF(v) Partial Pressure Versus Time, CM-LP Simulations

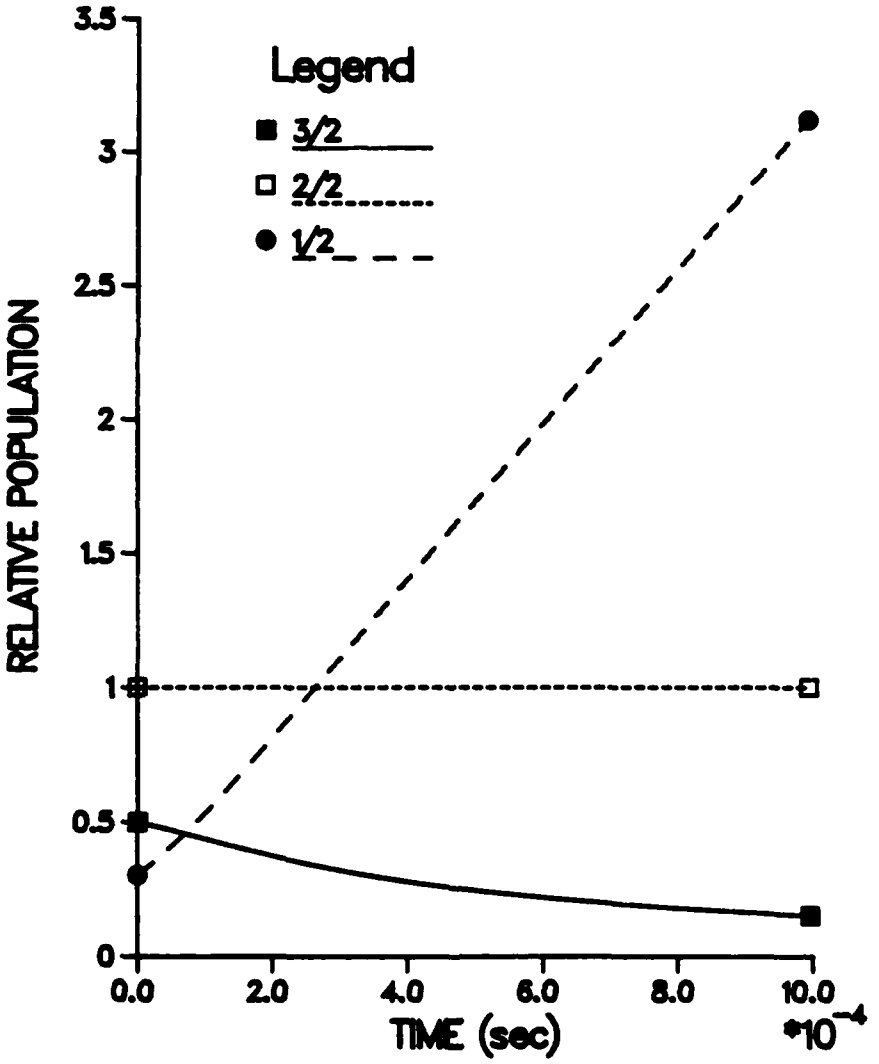

Figure III-15. HF(v) Relative Population Versus Time, CM-LP Simulations

Table III-7

Rate Constants for Simulated Data
($\times 10^6$ torr^{-1} sec^{-1})

Vibrational Level	k_{tot}	X_v	$k_{v-1,v}(H_2)$	$\chi^{2(a)}$
3	1.00	---	0.201	
2	0.838	0.0	0.149	7.46×10^{1}
2	0.915	0.5	0.175	2.22×10^{1}
2	1.01	1.0	0.195	3.08×10^{-1}
Total Intensity	0.800	---	0.130	

[a]Based on seven significant figures for single precision on the Prime computer.

simulated data where the contribution from HF(v=2) relaxation is large. Another possible method for analysis is to perform a simultaneous least squares fit of the data for HF(v=3), HF(v=2) and HF(v=1) and calculate all of the rate constants.

CM-LP Conclusions

CM-LP experiments can provide nascent distributions, total reaction rate constants, and microscopic deactivation rate constants. The analysis of these experiments are more direct than the CM-PP experiments because of the pseudo first order conditions.

Nascent distributions are obtained by extrapolating time dependent HF(v) population ratios to zero time. Pseudo first order reaction rate constants and deactivation rate constants are obtained by performing experiments at various H_2 pressures and fitting the time dependent HF(v) populations to the sum of two exponentials. For lower vibrational levels (< vmax) the contribution from relaxation of upper vibrational levels destroys the double exponential function. It was shown that the rate constants can be calculated by an iterative procedure when the relaxation contribution to the input is < 70% of the total population of the specific vibrational level. The pseudo first order rate constants are then plotted as a function of H_2 pressure and the slopes of these plots give the respective total reaction rate constant and microscopic deactivation rate constant.

It was also shown that fitting total intensity-time profiles to the sum of two exponentials produces rate constants that are consistently low and outside of the normal error range for this type of experiment.

IV. EXPERIMENTAL APPARATUS and DATA PROCESSING

EXPERIMENTAL APPARATUS

Modeling of the first generation CM-PP experiments[14,26a] (see section III) provided information for the following design improvements:

1. Replacement of diatomic reactant injector with a piezoelectric valve thereby reducing the pulse length from 10 msec to 0.5 msec

2. Replacement of a six channel signal averager (10 sec/channel) with a 2048 channel signal averager (0.5 microseconds/channel)

3. The White cell is replaced with a focusing lens and rear mirror

4. The 1500 cc reaction vessel was replaced with a 10 cc reaction vessel

Figure IV-1 displays the modified CM-PP apparatus while Figure IV-2 shows the CM-LP apparatus.

A CM experiment provides both spectral and temporal resolution. Infrared emission from the products formed by reaction of an atomic species and hydrogen donor molecule is focused by a lens onto the slit of a monochromator and dispersed by a grating (300 lines/mm); total intensity is measured using a mirror in place of the grating. A microcomputer controls the stepping motor that moves the grating through the wavelength region of interest (2.5-5.0 microns). At each wavelength, an emission intensity-time profile is measured. The infrared emission is detected by a liquid nitrogen cooled InSb detector, amplified, collected by either a transient recorder or signal averager and stored on a floppy disk from which it is transferred to a mainframe computing system for further data analysis. The individual parts of the CM-PP and CM-LP experimental apparatus will be discussed separately in the following sections.

CM-PP Experimental Apparatus

Flow System

Tank gases were used from cylinders with regulators attached while CH_2Cl_2 was stored in a 130 cc glass bulb with stopcock and was degassed by the freeze-pump-thaw method prior to use. Copper lines attached to the cylinder regulators or to the CH_2Cl_2 glass bulb allow the gases to flow into a glass high vacuum system which leads to the reaction vessel. Separate flow lines with Helicoid pressure gauges and greaseless stopcocks were used for the atomic precursor and hydrogen (deuterium) donor reagent. Fluorine and hydrogen bromide were handled in passivated copper lines attached directly to the reaction vessel. These gases were stored and handled in a well ventilated hood. All reagent (except fluorine) flows were controlled by MKS electronic flowmeters (model 258) with MKS control valves (type 248A) and an MKS control system (series 260). Fluorine flows were controlled by a needle valve and monitored

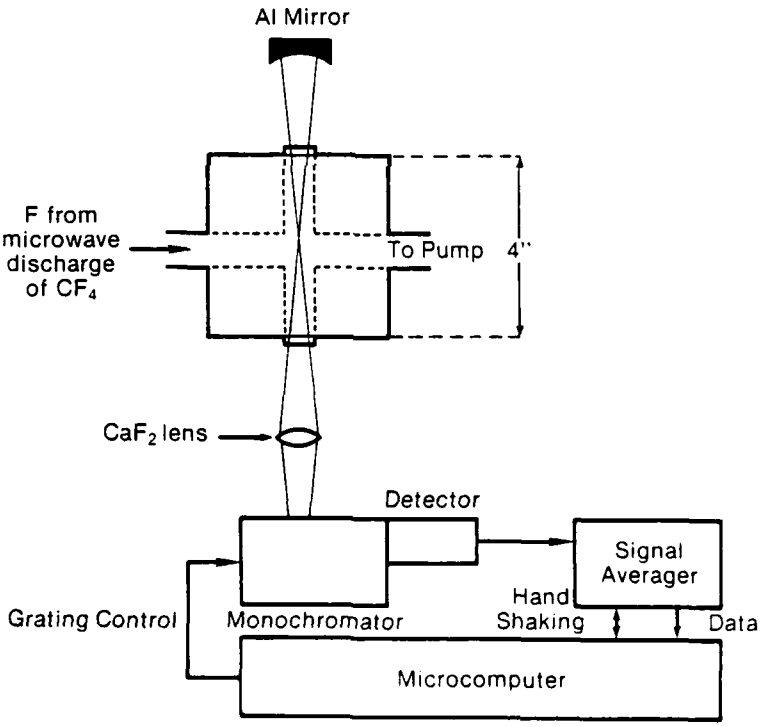

Figure IV-1. **Diagram of CM-PP Experimental Apparatus**

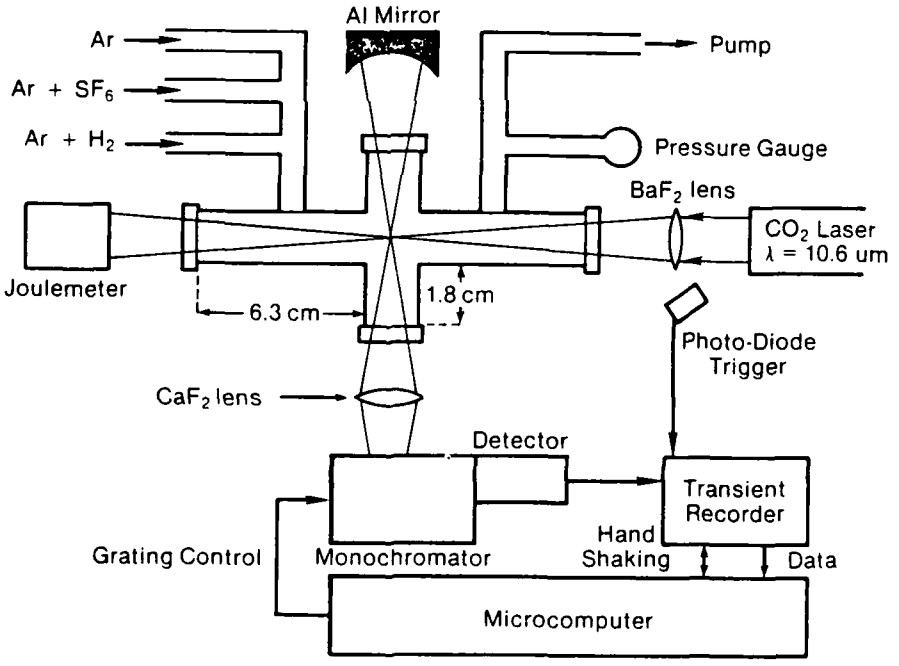

Figure IV-2. **Diagram of CM-LP Experimental Apparatus**

with the Helicoid pressure gauge.

A Cooke cold cathode vacuum gauge was used to measure the pressure near the pumpout of the reaction vessel. A Cooke thermocouple guage measured pressure along the discharge tube. Mechanical Welch Duo Seal vacuum pumps were used to evacuate the flow lines. The reaction vessel, a 4" aluminum cube with 1" holes drilled thru the center of each face, was pumped out by a Welch Duo Seal pump in series with a 6" liquid nitrogen trapped oil diffusion pump (NRC VHS-6). A 6" slide valve separates the oil diffusion pump from the cold nitrogen trap attached to the reaction vessel. Effluent from the reaction vessel was vented to the hood.

Reagent Injection

A Lasertechnics Model LPV piezoelectric valve was used to inject the hydrogen donor reactant into the reaction vessel. A Lasertechnics Model 203 LPV valve driver provides electrical pulses to control the piezoelectric valve. For the reported experiments, the valve was operated with a pulse width of 0.5 msec and a cycle time between 25 and 30 msec (pulse rate of 33-40 Hz). A nozzle with a 1.0 mm cylindrical orifice was used to minimize cluster formation. The valve driver triggers the signal averager to start data collection. The pulse width and delay between pulses is determined and checked during the experiment by connecting the trigger output from the valve driver to a Tektronix 533A oscilloscope. The cycle time is varied, depending on the experiment, to ensure that the vessel is completely pumped out (no emission observed) before the next pulse.

Atom Generator

The microwave discharge of CF_4 gas generated F atoms while hydrogen or deuterium gas was used to produce H and D atoms respectively. The microwave power was supplied by a 115 watt 2450 MHz Raytheon model PGM 10X2 microwave generator coupled to a Raytheon Model E14C Evenson type microwave cavity. The atomic precursor flows through a 12 mm o.d. Vycor discharge tube located along the axis of the cavity; the exit orifice is 1 mm in diameter. The discharge tube was inserted into the reaction vessel (approximately 0.5 cm from the center of the vessel) using a Cajon Ultra torr O-ring seal and fitting. Air flowing through the cavity efficiently cools the discharge region. When CF_4 was the atomic precursor, a clean Vycor discharge tube was used which needed to be replaced after approximately 8 hours of CF_4 flow due to etching by F atoms. The inside surface of the discharge tube, when used with hydrogen or deuterium, was treated[46] prior to use in order to decrease atom recombination on the walls. As in reference 46, the tube was filled with a 10 M NaOH solution for approximately 18 hours followed by several washings with distilled water. The tube was then filled with a 10 M HNO_3 solution for approximately 18 hours, washed several times with distilled water and dried.

Detection System

Infrared radiation from the reaction products is focused by a CaF_2

focusing lens (diameter of 2" and focal length of 6") onto the slit of a 1/4 meter near Littrow monochromator (Perkin Elmer model 99G) which is coupled to a liquid nitrogen cooled InSb detector (Infrared Laboratories) by a pair of off axis ellipsoidal mirrors. A NEP (noise equivalent power) of 1 x 10^{-13} watt/$(Hz)^{1/2}$ at 2 microns or 4 x 10^{-14} watt/$(Hz)^{1/2}$ at 5 microns was measured[39,47]. The detector response was < 1 microsecond when using a 10K feedback resistor. The wavelength sensitivity of the monochromator-detector system was calibrated with a blackbody radiation source (Infrared Industries model 463) and temperature controller (model 101B).

In the previous CM experiments, a 2.5-5.5 micron spectral bandpass filter was positioned between the InSb detector and an external KRS-5 vacuum window attached to the dewar housing. Both the filter and detector were cooled to liquid nitrogen temperatures, thereby reducing the background radiation and thermal noise viewed by the detector. Blackbody measurements using this configuration showed the presence of an absorption between 2.9 and 3.3 microns that became enhanced (larger and wider) over a 2 hour time period. In this work, a room temperature filter (2.5-5.5 microns) positioned between the exit slit of the monochromator and the KRS-5 vacuum window replaced the cold filter. Blackbody measurements indicated that the absorption was eliminated but with a reduction in signal/noise. Blackbody measurements also showed absorptions between 2.6 and 2.9 microns and between 4.2 and 4.4 microns which were due to H_2O (2.7 microns[48]) and CO_2 (4.3 microns[48]) respectively. These absorptions were eliminated when the optical path was enclosed by a cylinder through which dry air or nitrogen (for the D + F_2 experiments) was purged for approximately 8 hours prior to performing the experiment.

The signal from the detector was ac coupled to an EG&G model 113 preamplifier. For the CM-PP experiments, the high frequency rolloff was set at 30KHz which was the optimum setting to eliminate high frequency noise without distortion of the experimental signal.

An EG&G model 4203 signal averager was used for data collection. When the signal averager was triggered by the pulsed valve driver, it started data aquisition. The signal averager stores 2048 data points with a time resolution of 5 microseconds. The experimental signal is transferred via a customized parallel interface to a Z80A based microcomputer for further data analysis. The microcomputer stores 128 data points on a floppy disk, each of which is the average of two of the data points from the signal averager. Due to the inherent mechanical delay between the driver and valve, the first 10 data points stored represent the baseline and are necessary to determine the baseline for the data analysis.

A typical CM experiment consists of stepping through the wavelength region of interest, the number of steps being between 200 and 350 depending on the experiment, with step sizes ranging from 3 to 5 cm^{-1}. The spectral resolution is between 11 and 22 cm^{-1} and is determined by the monochromator slit width used (1.0 - 2.0 mm) in order to obtain sufficient measurable intensity. Total HF(v) intensity is measured before and after each experiment to ensure that flows remained constant. The microcomputer controls the stepping motor that rotates the grating

of the monochromator and also controls transfer of data from the signal averager.

CM-LP Experimental Apparatus

Flow System And Reagent Mixtures

Mixtures of atomic precursor (SF_6) or HR reactant in Ar were made and stored in 12 liter glass bulbs with stopcocks and a MKS capacitance manometer (model 222, 1000 torr) was used to measure pressures. Mixtures were made by filling the 12 liter storage vessel first with 70-100 torr of HR or SF_6. These gases were used directly from their cylinders with attached regulators. Methylene chloride was used from a 130 cc glass bulb with a stopcock and was purified by the freeze-pump-thaw method prior to use. The 12 liter storage vessel was then filled with Ar to a total pressure of approximately 700 torr. Argon was used from its cylinder with attached regulator and flowed through a liquid nitrogen cooled molecular sieve (Union Carbide type AW-500 pore diameter 5 A) trap to remove any H_2O. Typically 10% mixtures of HR in Ar and 20% mixtures of SF_6 in Ar were used approximately 24 hours after their preparation. The 12 liter glass bulbs were connected to the glass high vacuum system by O-ring seals, #9 glass joints and Cajon stainless steel flexible tubing. Argon was used from a cylinder with a gas pressure regulator attached to copper lines leading to the glass high vacuum system. The mixture flows were measured with Matheson #610A flowmeters and controlled with needle valves. Argon flows were measured with a Fischer & Porter flowmeter and controlled with a needle valve. The two mixtures and Ar flow into the reaction vessel with the Ar first flowing through a liquid nitrogen cooled molecular sieve trap to remove any H_2O. Reagent flows ensured that the reaction vessel was completely flushed twice between laser pulses and that pseudo-first order experimental conditions ($F << H_2$) are maintained. Welch Duo Seal mechanical pumps were used to pump out the system.

Reaction Vessel

The reaction vessel for these experiments was a cross shaped glass tube. Sodium chloride windows (1" in diameter and 0.25" thick) were attached to each of the four ends of the tube via #25 glass joints and clamps. The vessel was attached to the high vacuum system and pumping system via ball and socket joints. The reagent mixtures entered through an inlet attached to one arm of the vessel and was pumped through an outlet attached to the opposite arm. A CO_2 laser was focused on the center of the vessel by a BaF_2 lens (focal length of 4" and 1.5" in diameter). Ninety degrees from the laser beam an aluminum coated mirror was placed and opposite the mirror was a CaF_2 focusing lens (diameter of 2" and focal length of 6") and detection system. The vessel and optical path was enclosed in an aluminum box through which dry air was flowed to eliminate absorption of the 2.7 micron HF emission by H_2O in the air. A MKS capacitance manometer (model 222, 10 torr) was attached to the top of the vessel to measure the pressure.

Atom Generator

A pulsed (1 Hz) CO_2 Tachisto TEA laser (model 400XR) at 10.59 microns (001-100 P(20) transition) was used to generate F atoms by the multiphoton dissociation of SF_6. A Gentec joulemeter (model ED500) was used to measure the pulse energy; the output is observed on a Tektronix 533A oscilloscope. Typical pulse energy was 0.5 joules. Within 5%, the pulse energy and profile were reproducible from pulse to pulse.

Detection System

The detection system for the CM-LP experiments is the same as described for the CM-PP experiments except for the following changes. The high frequency rolloff and gain of the preamplifier were 100 kHz and 10 Hz respectively. The EG&G 4203 signal averager was replaced with a Biomation model 805 waveform recorder with time resolution of 0.5 microsecond and the capability of pretriggering. The trigger pulse to the Biomation was provided by a photodiode directed at the laser cavity. Pretriggering allows the collection of baseline points prior to collection of the signal; baseline correction of the experimental signal is necessary for correct data analysis. The signal (2048 data points) is transferred to the microcomputer via a custom parallel interface. Every 16 data points from the transient recorder are averaged to give 1 data point; thus a total of 128 data points are stored temporarily by the microcomputer. Five hundred of these data sets are coadded, providing a factor of $(500)^{1/2}$ improvement in signal/noise, and finally stored on a floppy disk.

Total HF(v) emission intensity was recorded before and after each experiment. It was found that the total intensity decreased by 10% during an experiment because of the finite volume of gas mixtures used. A linear correction based on these total intensity measurements was made to the experimental data. Laser noise affected only the first data point of the spectrally resolved emission intensity-time profile and it was excluded from the data analysis. Laser noise was insignificant in the total intensity-time profiles due to the larger measured intensity compared to the spectrally resolved intensity.

DATA ANALYSIS

In CM experiments, the intensity of individual vibration-rotation states is measured as a function of both wavelength and time. Typical CM-PP and CM-LP experimental intensity-frequency-time surfaces are shown in Figures III-3 and III-4. Generally, individual vibrational-rotational transitions are not completely resolved. Therefore, in order to obtain useful information (product energy distributions, rate constants) from these spectra, vibrational-rotational population distributions must be extracted. The following equation[49] relates the observed intensity to the populations of the individual vibration-rotation levels:

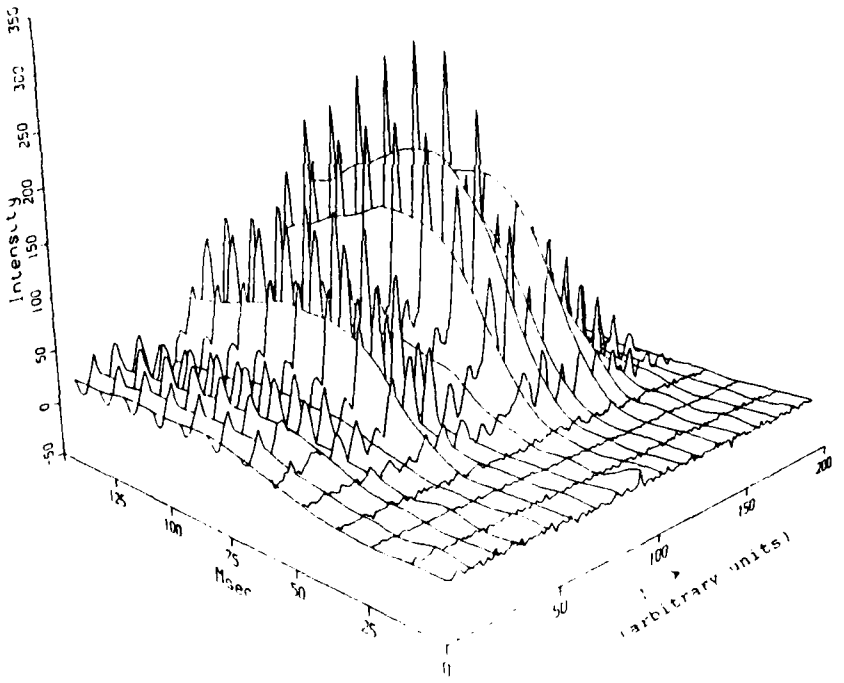

Figure IV-3. CM-PP Experimental Intensity-Frequency-Time Surface

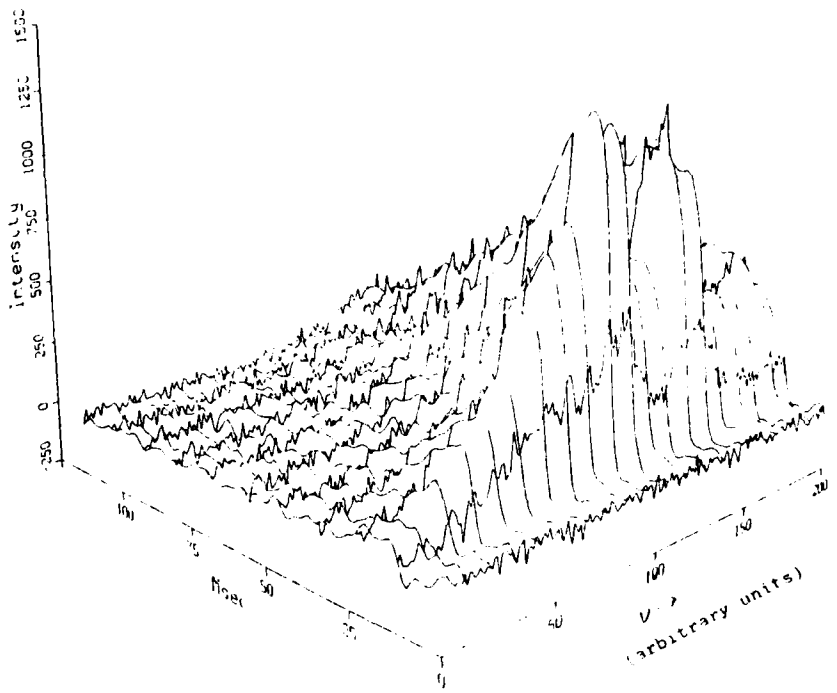

Figure IV-4. CM-LP Experimental Intensity-Frequency-Time Surface

$$I(\lambda) = A_{v,J} S_{v,J}(\lambda) T(\lambda) P_{v,J} \qquad \text{IV-1)}$$

$A_{v,J}$ = Einstein coefficient[50] for emission from vibrational level v and rotational level J in units of sec^{-1}

$S_{v,J}(\lambda)$ = Instrumental response function for a particular v,J transition

$T(\lambda)$ = Detector sensitivity

$P_{v,J}$ = Populations of vibration-rotation levels v,J respectively

$I(\lambda)$ = experimental intensity of a given wavelength in units of photons/second

The instrumental response function (monochromator slit function) is represented as a triangle function:

$$S_{v,J}(\lambda) = 1-(\lambda - \lambda(v,J))/\Delta$$

for $(\lambda - \lambda(v,J)) < \Delta$ and

$$S_{v,J}(\lambda) = 0$$

for $(\lambda - \lambda(v,J)) > \Delta$

Δ = monochromator resolution

Using equation IV-1, an iterative linear least squares is performed for each experimentally measured time. In the least squares method,

$$\chi^2 = \sum_{\lambda} (I(\lambda)^{calc} - I(\lambda)^{exp})^2 / \sigma^2_{I(\lambda)}$$

is minimized with respect to the vibrational-rotational populations (parameters of the fit). If negative populations were obtained in the fitting process, these levels were subsequently removed from the analysis and another iteration performed.

Since the errors in the emission intensities were determined to be independent of wavelength and time, equal weighting was used in the least squares technique. From the vibrational-rotational populations obtained, a calculated spectrum was constructed; the difference between the observed and calculated spectrum was used as an estimate of the final error in the vibration-rotation populations. The rotational populations obtained from the least squares fit exhibited similar distributions (Boltzmann) for each vibrational level and were used as a useful indicator that peak assignments were correct. The total population of a given vibrational level was obtained by summing the rotational populations of that level.

Since the rotational distributions were found to be Boltzmann, an alternative method of obtaining total vibrational populations is to perform a nonlinear least squares fit of the data. The function used for this fit assumes a Boltzmann rotational distribution:

$$I(\lambda) = \sum_{v} P_v A_v \sum_{J} S_{v,J}(\lambda) T(\lambda) (2J+1) \exp(-E_J/kT) \qquad \text{IV-2)}$$

The nonlinear least squares analysis was done with the subroutine CURFIT by Bevington[45] in which

$$\chi^2 = \sum_{\lambda} (I(\lambda)^{calc} - I(\lambda)^{exp})^2 / \sigma_{I(\lambda)}^2$$

is minimized with respect to the vibrational populations and the temperature, T (the parameters of the fit).

To obtain nascent product energy distributions, ratios of experimental vibrational populations as a function of time were extrapolated to zero time. A weighted linear least squares fit was used for the extrapolation where the weights used were obtained from the intensity-population conversion. Only data out to the maximum population (peak) was used in the extrapolation and the zero of time was determined from the initial rise of the total intensity-time plots.

The analysis of HF(v) population-time profiles for extracting reaction and deactivation rate constants has been described in section III. The data points at long times (close to baseline noise) were excluded from the nonlinear least squares fitting process. This was done because in the intensity to population conversion, the procedure of removing negative populations causes these populations to have only positive contributions (no negative noise).

V. CM EXPERIMENTAL RESULTS

RESULTS and DISCUSSION

Computer simulations provided the optimum experimental conditions needed to obtain nascent product vibrational energy distributions and rate constants.

The results for each chemical system are described separately below. Typical pressures in the CM-PP experiments measured at the pump out end of the reaction vessel were 6×10^{-5} - 1.4×10^{-4} torr. These experiments were done with a t_{on} = 0.5 msec and cycle times of 25-30 msec. The total pressure measured in the reaction vessel for the CM-LP experiments was approximately 4 torr. The following partial pressures were used in the CM-LP experiments: SF_6 = 60 mtorr, HR = 10-60 mtorr, Ar = 3.5 torr. Errors are reported at the 95% confidence level.

$F + H_2$

This system has been well studied[6,7,18,26a,51-54] and was used in this work as benchmark verification of both the CM-PP and CM-LP experimental techniques. The total energy available to the HF products is 35 kcal/mole[55]. The third vibrational level lies 32.5 kcal/mole[4] above the zero point energy of the products and is the maximum level that can be populated. In the CM-PP experiments, CF_4 flow rates ranged from 2.6-46 mole/sec and H_2 flows ranged from 2.0-46 mole/sec. In the CM-LP experiments, the pressures used were: SF_6 = 60 mtorr, H_2 = 20-60 mtorr, Ar = 3.5 torr.

Typical HF(v) total population-time profiles and HF(v) ratio-time profiles obtained from the CM-PP and CM-LP experiments are shown in Figures V-1 and V-2. The CM-PP HF(v) total population-time profiles show a single maximum indicating the absence of collisional relaxation and minimal fluorine atom depletion. When comparable CF_4 and H_2 flows (i.e. 46 moles/sec for both reagents) were used, the total population-time profiles peaked before the H_2 was turned off and showed the start of a second peak after the H_2 was turned off indicating high flow conditions. These experiments were not included in the determination of the reported initial distributions. The HF(v) ratio plots from both experimental methods show linear behavior and when extrapolated to zero time give nascent product energy distributions in agreement with previously reported distributions.

Reaction and deactivation rate constants (Table V-1) were obtained from the CM-LP experimental data. Figures V-3 thru V-7 show typical nonlinear least squares fit of the total intensity, and of the HF(v=3) and HF(v=2) time profiles to the sum of two exponentials. Also, shown in these figures are the residuals (HF^{calc} - HF^{exp}) of these fits.

The total reaction rate constant obtained from the analysis of the total intensity-time profile, 0.96 +/- 0.03 x 10^6 $torr^{-1}$ sec^{-1}, is in agreement with other published work in which total intensity measurements are used (see Table V-1). From the HF(v=3) population-time profiles, a reaction rate constant of 1.4 +/- 0.3 x 10^6 $torr^{-1}$ sec^{-1} is

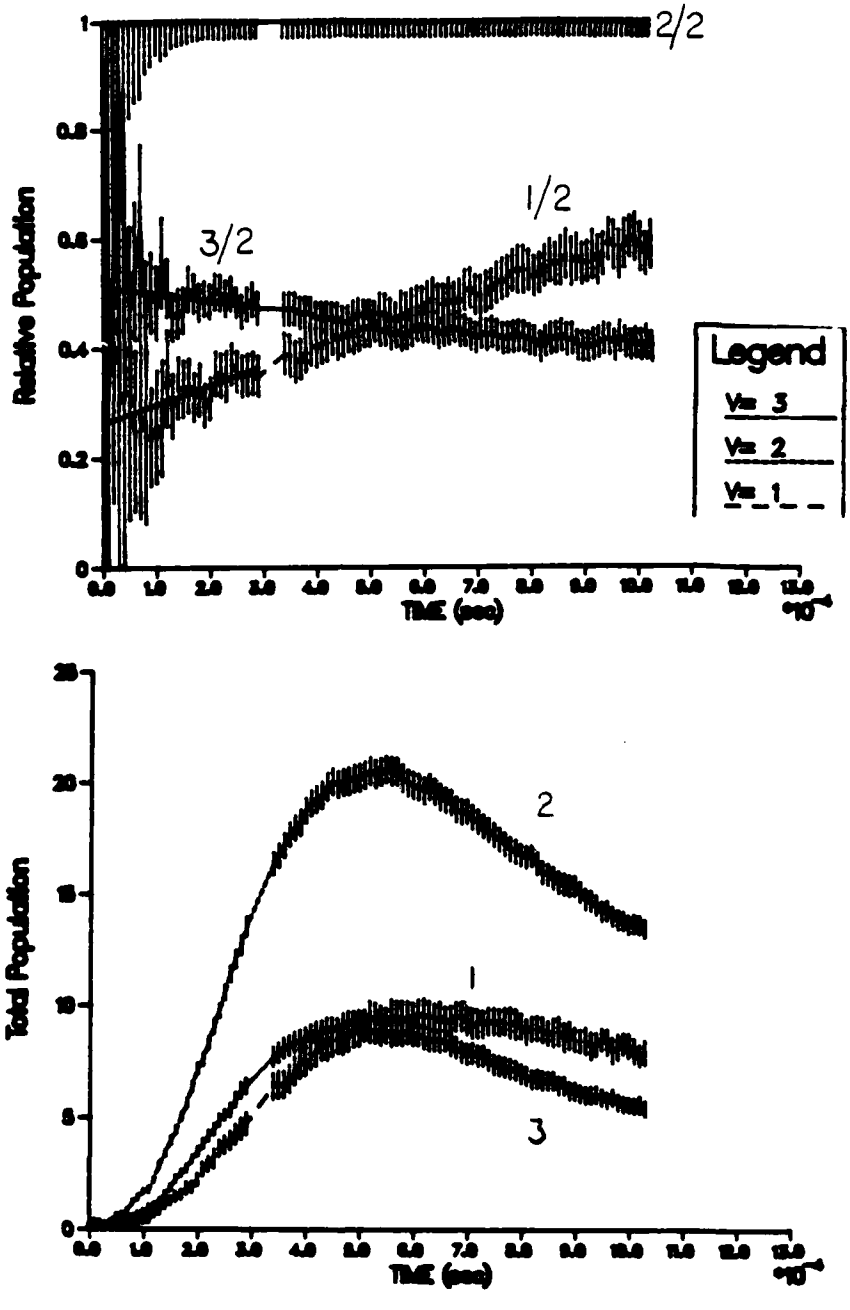

Figure V-1. HF(v) Total Population and Relative Population Versus Time, F + H_2 CM-PP Experiment

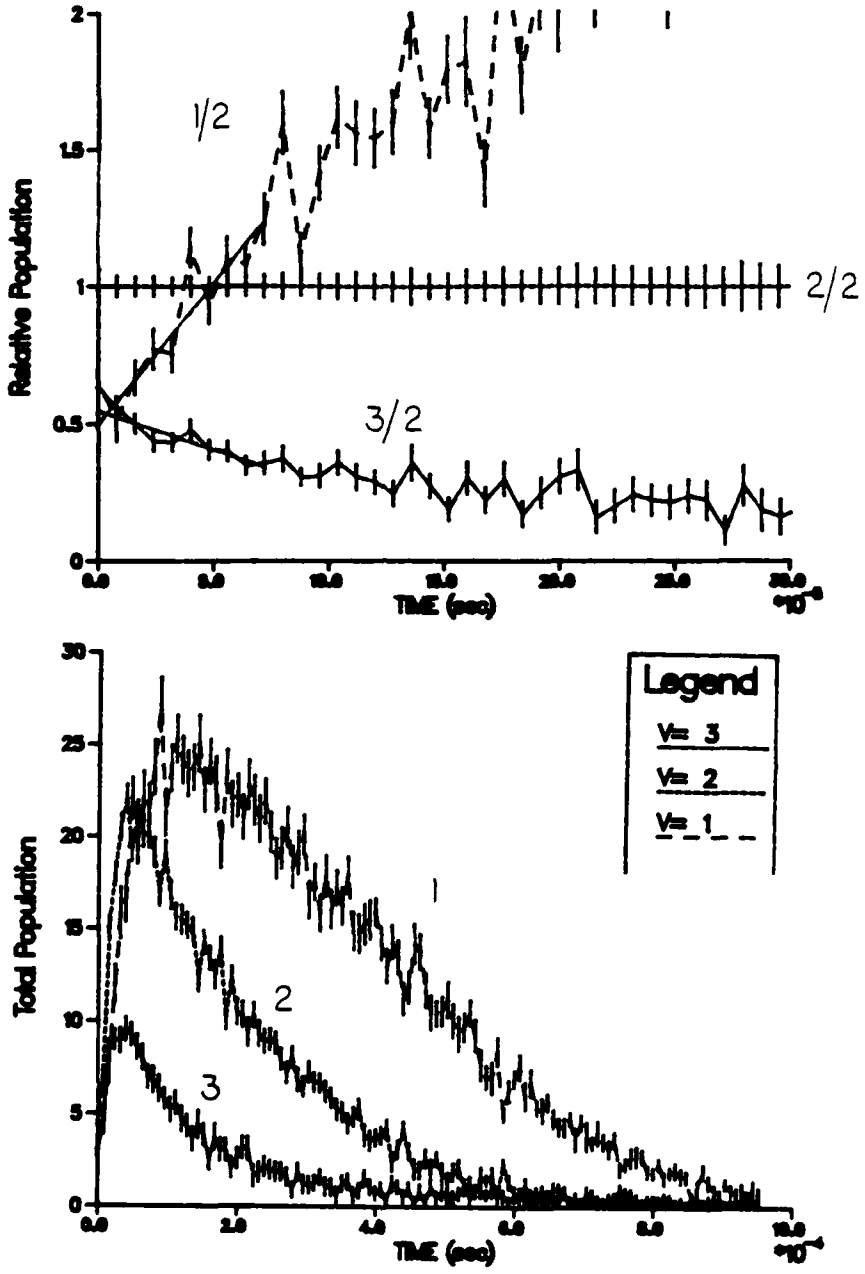

Figure V-2. HF(v) Total Population And Relative Population Versus Time, F + H_2 CM-LP Experiment

Table V-1

Reaction[a] and Deactivation Rate Constants for the Reaction $F + H_2 \rightarrow HF(v) + H$

$k_{tot} \times 10^6$ torr^{-1} sec^{-1}	Method
0.97	F from discharge F_2 HF Mass Spec.
2.0	WF_6 Photolysis in H_2 HF(total intensity)
0.81	F from discharge CF_4 HF Mass Spec.
0.54	F from Thermal F_2 F by ESR
0.75	F from Discharge SF_6 HF(total intensity)
0 54	F from Discharge CF_4 F by ESR
0.86-1.2	F from SF_6 Photolysis HF (total intensity)
1.1	F from SF_6 Photolysis HF (total intensity)
0.98	F from SF_6 Photolysis HF (total intensity)
0.96 +/- 0.03[b]	F from SF_6 Photolysis HF (total intensity)
1.4 +/- 0.3[b]	F from SF_6 Photolysis HF(v=3)
1.4 +/- 0.1[b]	F from SF_6 Photolysis HF(v=2)

Deactivation Rate Constants $k_v \times 10^4$ torr^{-1} sec^{-1}		
v= 1	2	3
1.43 +/- 0.15[c]	1.23 +/- 0.10[c]	1.13 +/- 0.10[c]
		1.2 +/- 0.8[d]
		0.99 +/- 0.19[e]
	2.5 +/- 2.0[b]	15 +/- 6[b]

[a] All values in this table are from reference 11 unless otherwise indicated.

[b] This work.

[c] From reference 68.

[d] From reference 69.

[e] From reference 70.

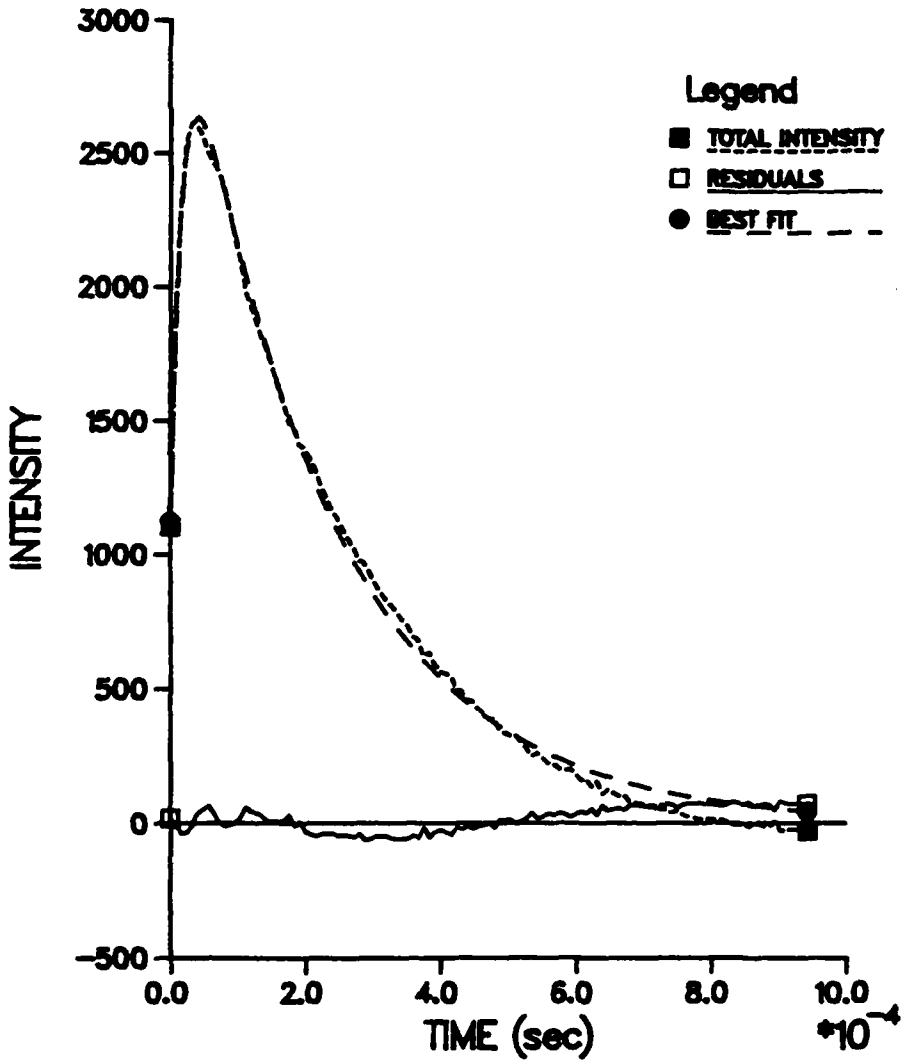

Figure V-3. Least Squares Fit of Experimental HF Total Emission Intensity Versus Time, F + H_2 Reaction

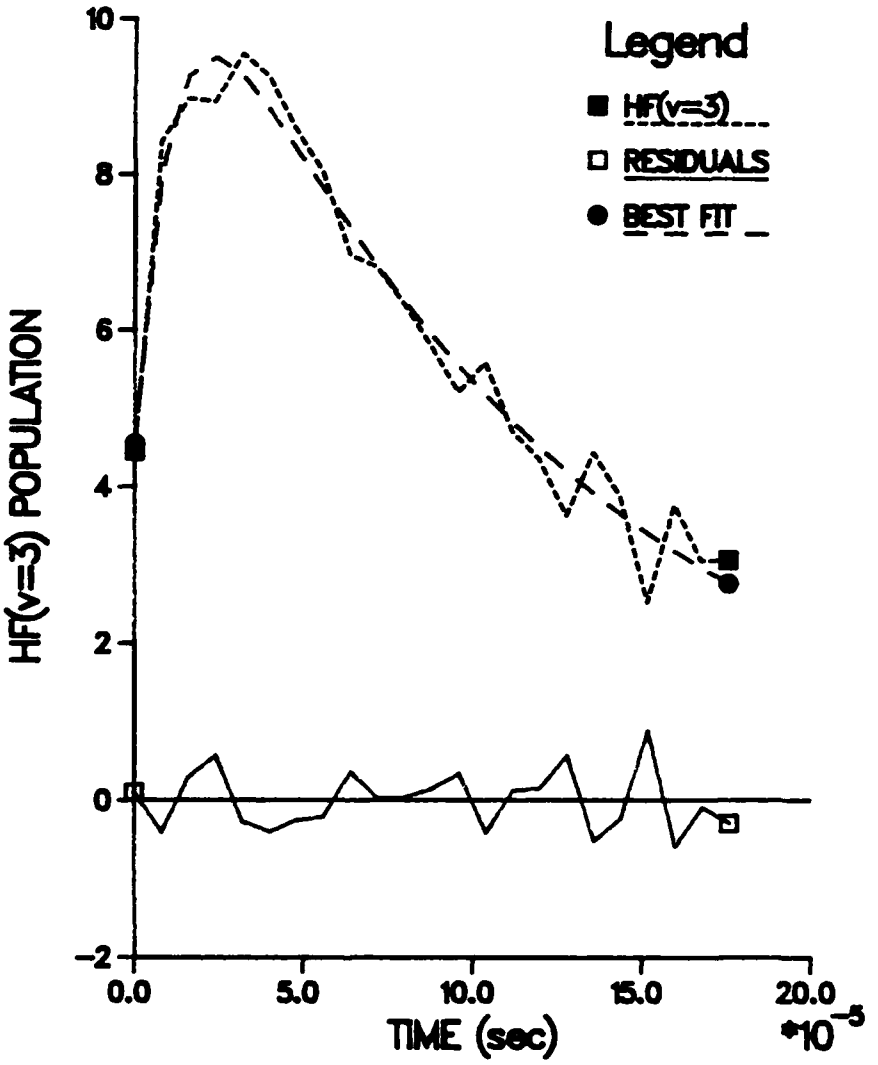

Figure V-4. Least Squares Fit of Experimental HF(v=3) Population Versus Time, F + H_2 Reaction

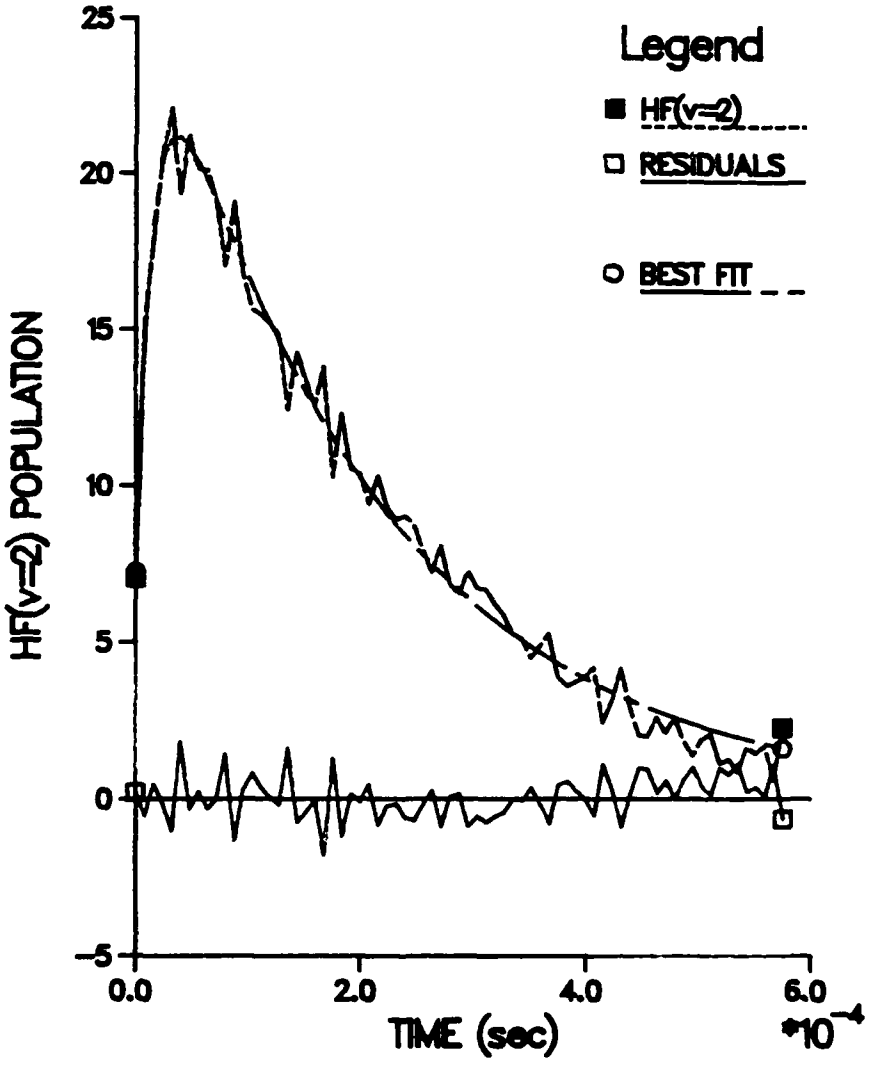

Figure V-5. Least Squares Fit of Experimental HF(v=2) Population Versus Time, (X_3 = 0.0), F + H_2 Reaction

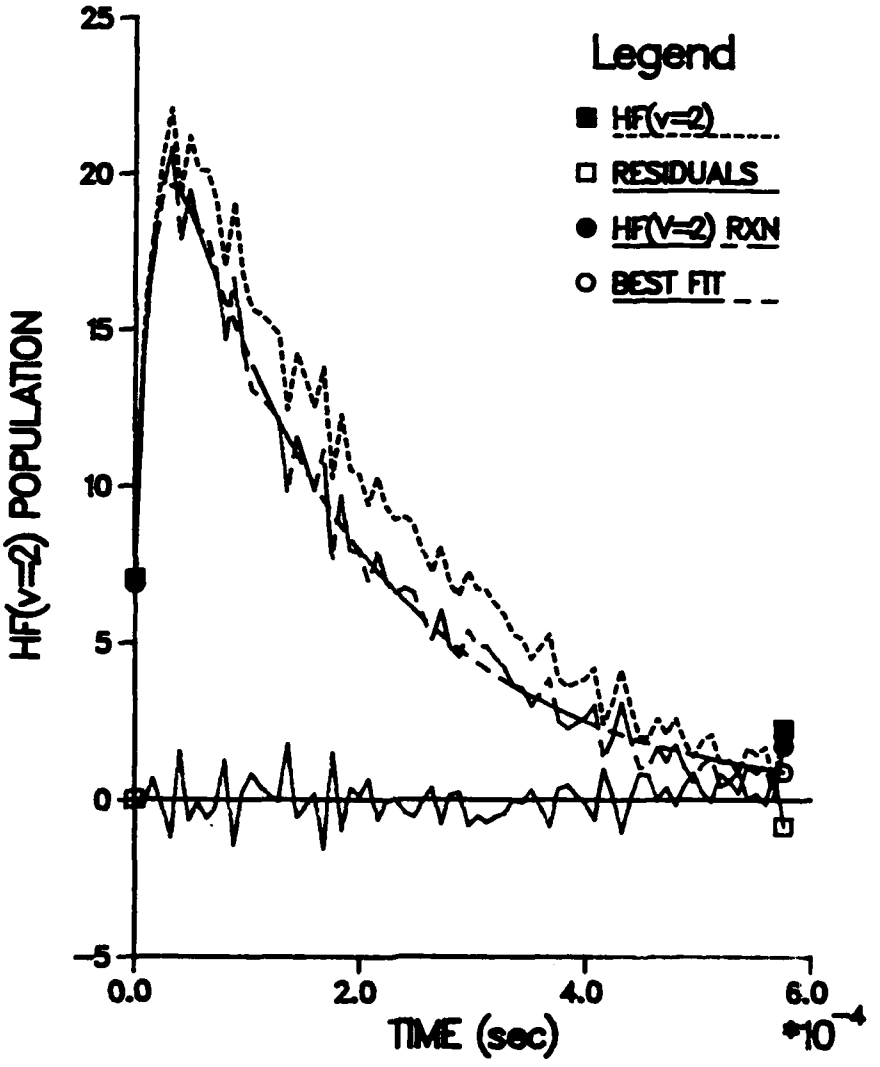

Figure V-6. Least Squares Fit of Experimental HF(v=2) Population Versus Time, (X_3 = 0.5), F + H_2 Reaction

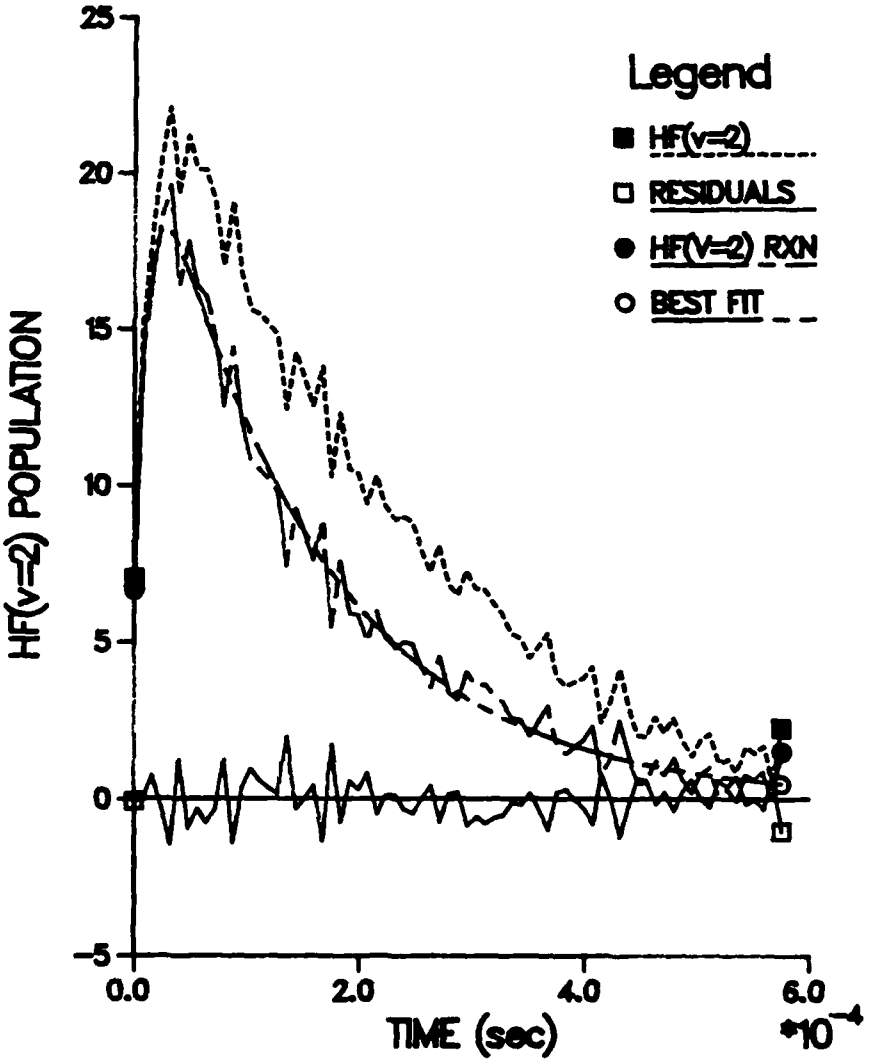

Figure V-7. Least Squares Fit of Experimental HF(v=2) Population Versus Time, (X_3 = 1.0), F + H_2 Reaction

obtained. As has been shown by modeling in this work, analysis of the total intensity-time profiles give consistently small values of the rate constants when forced to fit the sum of two exponentials, therefore the result from the fit of HF(v=3) is preferred.

The reaction rate constant obtained from the HF(v=2) population-time profiles is 1.4 +/- 0.1 x 10^6 $torr^{-1}$ sec^{-1} and is in agreement with that obtained from HF(v=3) as expected. The quoted error is propagated from the error in the populations. Since error can also be introduced by the iterative method used to obtain this rate constant, a more realistic estimate of the error would be a factor of two larger. Likewise, the errors reported for the rate constants obtained from analysis of the total intensity are propagated from errors in the emission intensity and do not include the potential error from using the wrong function. Plots of pseudo first order reaction rate constants versus H_2 pressure for total intensity, HF(v=3) and HF(v=2) gave intercepts of zero indicating that other sources of F atom depletion were absent.

The rate constant for deactivation of HF(v=3) by H_2 found in this work is 1.5 +/- 0.6 x 10^5 $torr^{-1}$ sec^{-1} which is considerably larger than previously reported measurements (Table V-1). A larger rate constant suggests the presence of deactivators other than H_2. In initial diagnostic experiments of this system plots of pseudo first order deactivation rate constants versus H_2 pressure gave varying slopes and intercepts, the largest of which were 4 x 10^5 $torr^{-1}$ sec^{-1} and 7000 sec^{-1} respectively. The intercept of these plots is the sum of all relaxation processes that are independent of H_2 pressure and include radiative relaxation, deactivation by Ar and HF(v=0), and flow out of the observation volume. When Ar was passed through a liquid nitrogen cooled molecular sieve trap, the rate constant and intercept was reduced to 1.5 x 10^5 $torr^{-1}$ sec^{-1} and 1200 sec^{-1} respectively. These diagnostic experiments showed that H_2O was present in the Argon and although this source of H_2O was eliminated, it is possible that other sources (flow lines, vacuum system, and reaction vessel) still remain and are responsible for the efficient deactivation.

$$F + D_2$$

The energy available to the DF product is 35.2 kcal/mole[6] allowing up to the 4th vibrational level (31.69 kcal/mole[55] above zero point energy) to be populated. This reaction is useful for observing isotope effects and also provides an additional verification of the CM-PP experimental method. The reaction forming DF has been reported to be a factor of 2 slower than the reaction forming HF[55] and the Einstein coefficients[4] for DF emission are smaller (x4) than for HF emission. Thus, higher reagent flows than were used in the F + H_2 system were necessary in order to study this reaction. The flow of CF_4 was 3.7 mole/sec and D_2 flows were 3.7-10.0 mole/sec.

The DF(v) total population-time plots and ratio-time plots obtained from CM-PP experiments are shown in Figure V-8. The nascent distribution (Table V-2) obtained is in agreement with previous results, peaking at the third vibrational level. Rotational population plots for each vibrational level are Boltzmann with T = 300 K. The isotopic

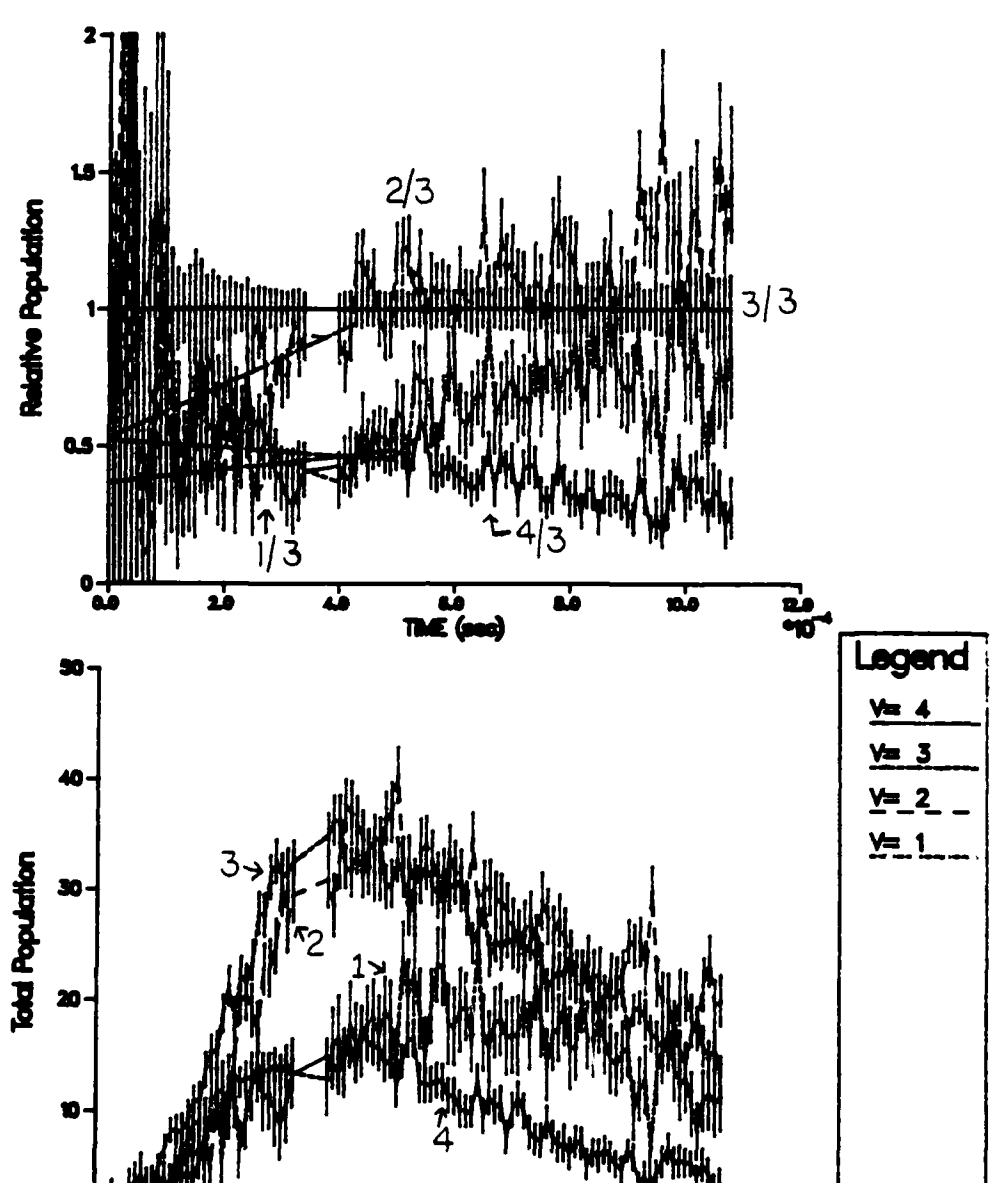

Figure V-8. DF(v) Total Population and Relative Population Versus Time, F + D_2 CM-PP Experiment

Table V-2

Relative Vibration Distributions for the Reaction $F + D_2 \longrightarrow DF(v) + D$

v	AR[a]	AR[b]	CM[c]	CM-PP[d]
1	(0.28)	0.15	0.31	0.30 +/- 0.10
2	0.65	0.52	0.58	0.57 +/- 0.16
3	1.00	1.00	1.00	1.00
4	0.71	0.59	0.80	0.54 +/- 0.22
$\langle f_v \rangle$[e]	0.66	0.665	0.65	0.63
$\langle f_r \rangle$	0.08	0.076		
$\langle f_t \rangle$	0.26	0.259		

[a]From reference 7, value in parenthesis estimated.

[b]From reference 6.

[c]From reference 26a.

[d]This work.

[e]Average fraction of the total energy that goes to vibration.

invariance of the F + H_2 and F + D_2 reaction is indicated by the similar average fraction of energy channeled into product vibration, $\langle f_v \rangle$, which from the CM-PP results was determined to be 0.67 and 0.63 for HF and DF respectively. This efficient conversion of energy into product vibration is due to mixed energy release on a repulsive surface[56].

H + F_2

The total energy available to the HF product from this reaction is 101.9 kcal/mole[55] allowing up to vibrational level 11 (99.1 kcal/mole[4] above zero point energy) to be populated. In the previous CM-PP[14,18,26a] (10 msec F_2 "on" time and 100 msec cycle time) experiments, an apparent F_2 flow dependence was observed. When low flows of F_2 (18 moles/sec) were used, the distribution peaked at v=6 in agreement with other studies[11,12,57,58] of this reaction. However, a population "hole" at v=4 and large populations in the low vibrational levels was also reported which had not been observed before. For high F_2 flows (44 moles/sec), a bimodal distribution peaking at v=2 and v=6 was reported. Vibrational levels 4 and 5 were highly depleted. CM-PP computer simulations show that for high flow conditions, double maxima in the HF(v) population-time profiles should be observed and that collisional relaxation is important. The double maxima were probably masked in the previous CM experiments since a 6 channel signal averager with a time resolution of 5 msec was used. Collisional relaxation would account for the large populations observed in these experiments for the low vibrational levels. The apparent depletion of vibrational levels 4 and 5 was found to be due to a cooled 2.5-5.5 micron spectral bandpass filter positioned between the InSb detector and a KRS-5 vacuum window attached to the detector housing as discussed in section IV of this report. To conclude whether the previous CM results were influenced by the above mentioned factors, the H + F_2 reaction was restudied.

The results reported here are from a CM-PP experiment in which a H_2 flow of 3.7 moles/sec and a F_2 flow of 14 moles/sec was used. The vibration-rotation populations were obtained by using equation IV-2 in which a Boltzmann rotational distribution is assumed. The rotational temperature was a variable parameter in the fitting process and was approximately 400 K. The assumption of a Boltzmann rotational distribution is justified because the H + F_2 reaction rate is 17 times slower[58] than the F + H_2 reaction rate and the reagent flows were higher than used in the F + H_2 experiment where Boltzmann rotational distributions were observed.

The HF(v) total population-time profiles and HF(v) ratio-time plots are shown in Figures V-9 and V-10. To avoid congestion in these plots, every other vibrational level is plotted. With the exception of the earlier reported CM results, the nascent product energy distribution is in agreement with previously determined distributions (Table V-3). For the reasons given above, the new distribution obtained from the CM-PP experiments is preferred over the previous CM results.

The $\langle f_v \rangle$ for the H + F_2 reaction is less than for the F + H_2 reaction while the $\langle f_t \rangle$[11] is larger. This behavior is described by the light atom anomaly[56] in which the H atom comes to within normal bonding

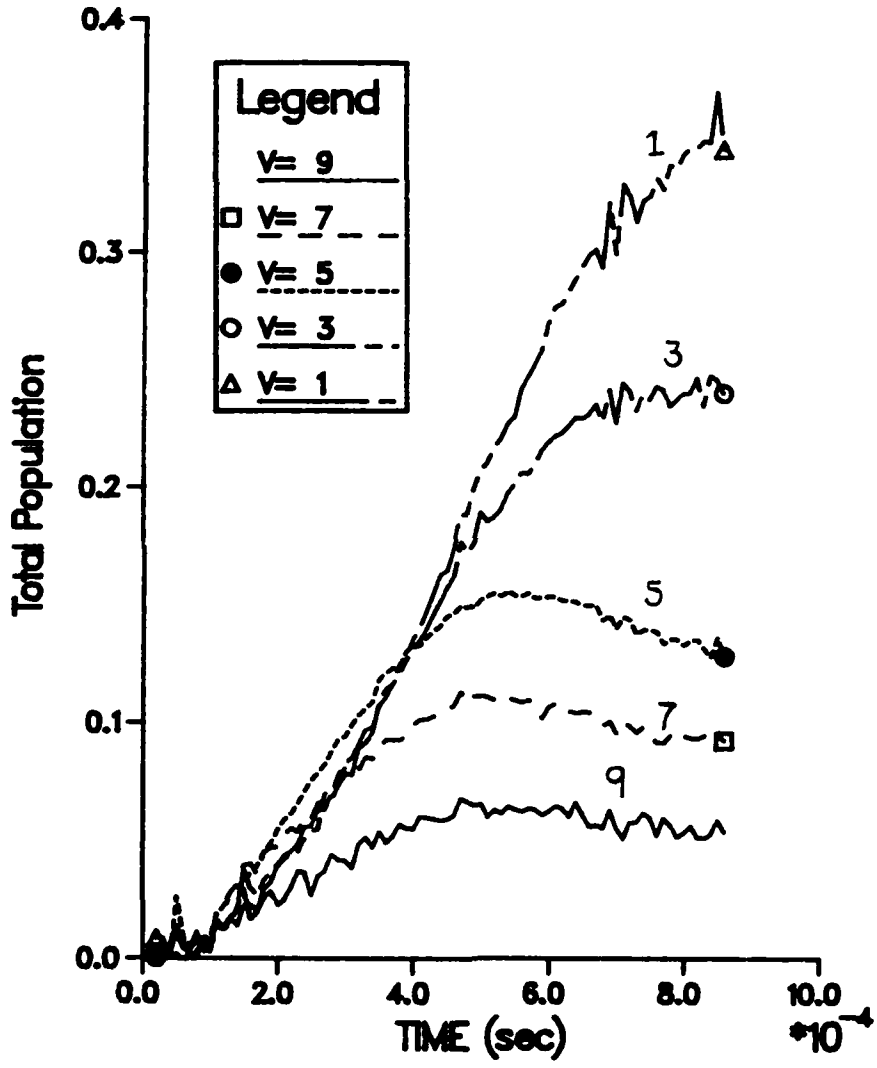

Figure V-9. HF(v) Total Population Versus Time, H + F_2 CM-PP Experiment

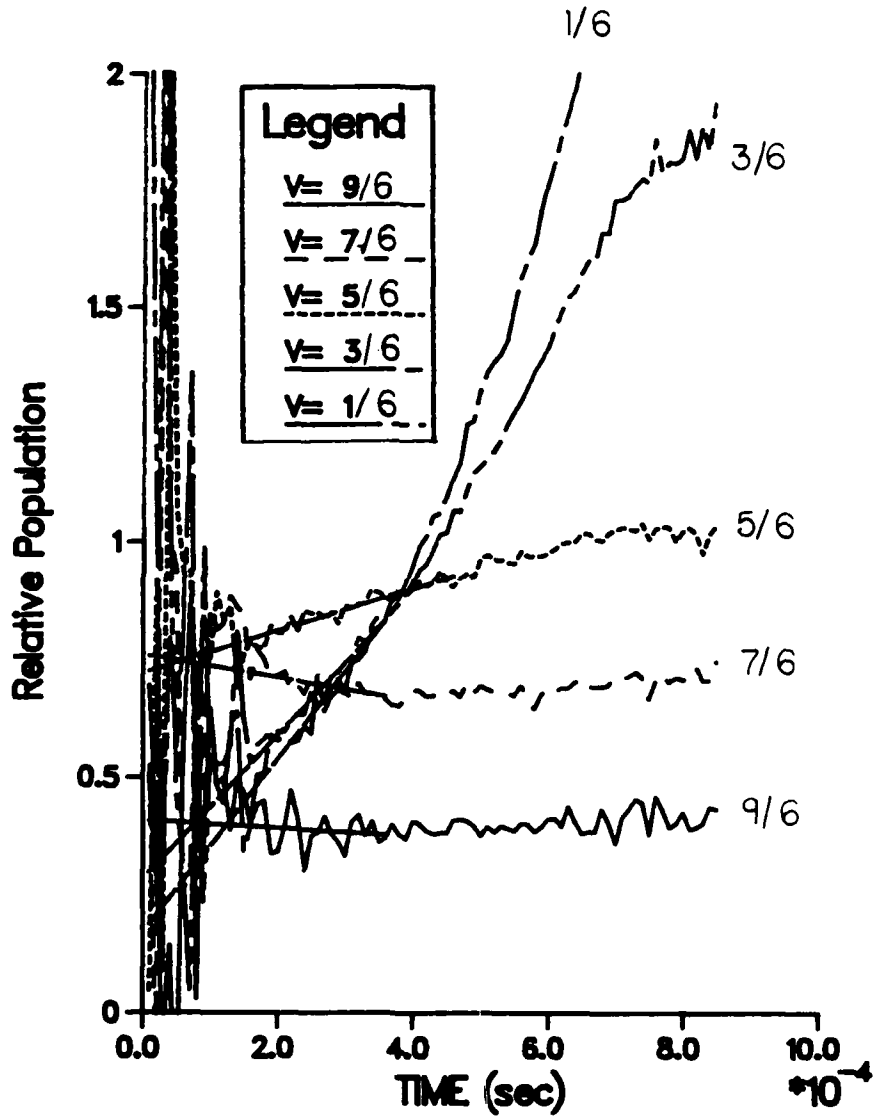

Figure V-10. HF(v) Relative Population Versus Time, H + F_2 CM-PP Experiment

Table V-3

Relative Vibration Distributions for the Reaction $H + F_2 \rightarrow HF(v) + F$

v	MR[a]	AR[b]	FF[c]	FF[d]	CMI[e]	CMII[e]	CM-PP[f]
1	0.09	0.12	0.07	0.06	21.1	0.82	0.15 +/- 0.10
2	0.11	0.13	0.17	0.12	53.2	0.88	0.13 +/- 0.08
3	0.13	0.25	0.28	0.17	22.9	0.46	0.27 +/- 0.06
4	0.45	0.35	0.59	0.37	0.032	0.038	0.41 +/- 0.02
5	0.89	0.78	0.93	0.76	0.026	0.57	0.72 +/- 0.04
6	1.00	1.00	1.00	1.00	1.00	1.00	1.00
7	0.45	0.40	0.52	0.62	0.55	0.62	0.76 +/- 0.08
8	0.20	0.26	----	----	0.20	0.23	0.46 +/- 0.08
9	<0.04	<0.16	----	----	0.19	----	0.41 +/- 0.08
10	<0.04	----	----	----	0.078	----	0.00 +/- 0.10
$\langle f_v \rangle$	0.58	0.53			0.58[g]	0.58[g]	0.57
$\langle f_r \rangle$		0.03					
$\langle f_t \rangle$		0.44					

[a]Measured Relaxation from reference 57.

[b]Arrested Relaxation from reference 11.

[c]Fast Flow from reference 12.

[d]Fast Flow from reference 58.

[e]Chemiluminescence Mapping from reference 26a,
CMI: 4.0 μmole/sec H_2, 44.0 μmole/sec F_2
CMII: 1.9 μmole/sec H_2, 18.0 μmole/sec F_2.

[f]This Work.

[g]Calculated using $v \geq 4$.

distance of the F_2 before the repulsive energy is released. Thus, a larger fraction of the available energy is channeled into relative translation of the separating products.

D + F_2

The available energy for the DF product is 103.2 kcal/mole[55] so that vibrational levels up to 15 (103 kcal/mole[4] above the zero point energy) could be populated. Three previously reported experimental studies of the D + F_2 reaction are not in agreement as to the most populated vibrational level. The initial product vibrational energy distribution from Measured Relaxation experiments[13] peaks at v=10, from Fast Flow experiments[59] at v=9, while the previous CM experiments[14,18,26a] gave a narrow distribution peaking at v=11 with no population observed in v=1-9. The previously reported CM experiments were done with high flows of F_2 (42.6 moles/sec) and a 10 msec observation time; conditions which computer modeling has shown is not conducive to obtaining initial distributions. Therefore, this system was studied again with the modified experimental apparatus.

The results reported are from a CM-PP experiment in which a D_2 flow rate of 5.2 moles/sec and a F_2 flow rate of 14 moles/sec was used. These were the highest flows that could be used without entering the high flow region. As in the H + F_2 system, vibration-rotation populations were obtained from a nonlinear least squares fit to equation IV-2 assuming a Boltzmann distribution. The rotational temperature obtained from this fit was 400 K, the same as for the H + F_2 reaction.

The DF(v) vibrational population-time profiles and DF(v) ratio plots are shown in Figures V-11 and V-12. In order to avoid congestion in these figures, every other vibrational level is shown. The product energy distribution is compared to other measurements in Table V-4.[13] The CM-PP results are in agreement with the Measured Relaxation results[13] peaking at v=10. The results obtained by the fast flow method[59] peak at v=9. Usually when a distribution peaks at a higher vibrational level, it is indicative of the true nascent distribution free of relaxation processes since vibrational energy transfer populates lower levels.

A comparison of the results of the D + F_2 reaction with the H + F_2 reaction shows a higher fraction of the available energy being channeled into vibration for the former reaction. This is in contrast to the F + (H_2/D_2) system where no isotope effect is observed. Jonathon[13] has suggested that the H + F_2 reaction requires more translational energy than the D + F_2 reaction to surmount its slightly greater activation barrier. Thus the hydrogen atom would approach closer to the fluorine molecule than the deuterium atom before the repulsive energy is released. This would result in more energy being channeled into recoil of the products and less into vibrational motion. Another possible explanation could be due to the differences in the masses of H and D. As the repulsive energy between the F_2 is released, more of the available energy is channeled into vibrational motion when the mass of the atom is heavier.

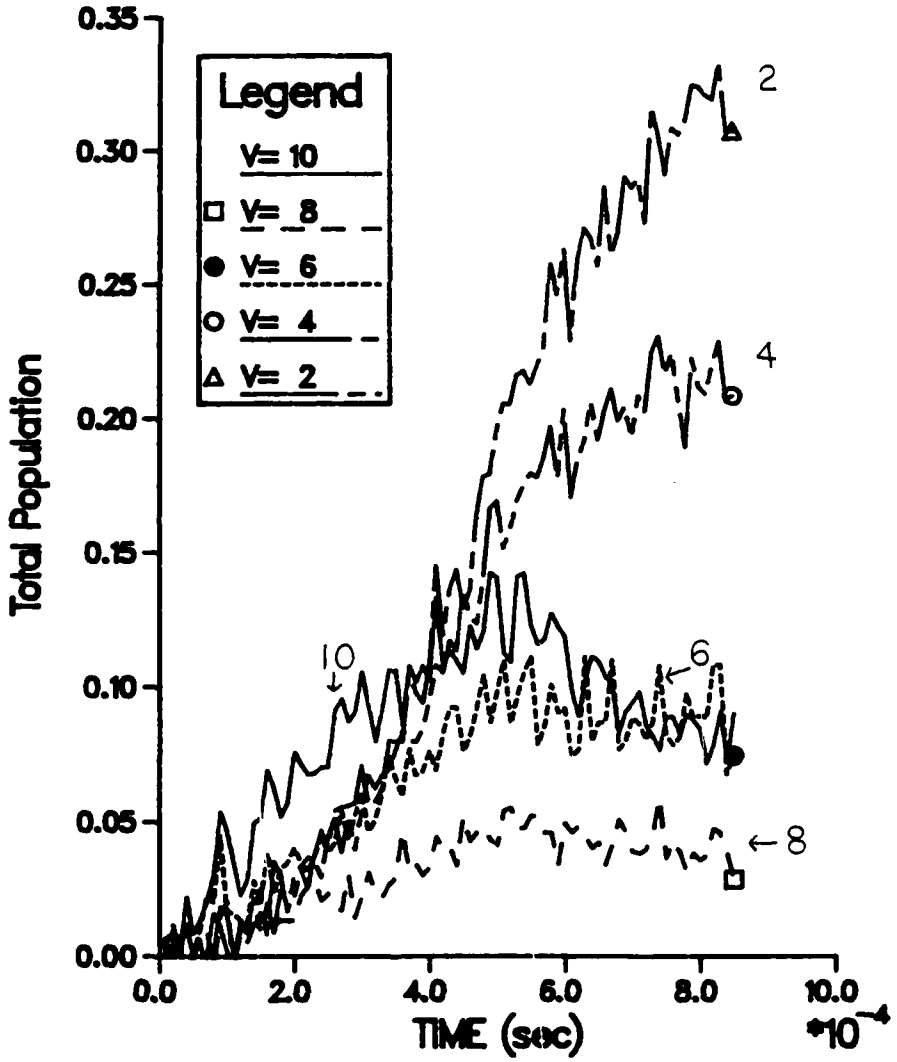

Figure V-11. DF(v) Total Population Versus Time, D + F_2 CM-PP Experiment

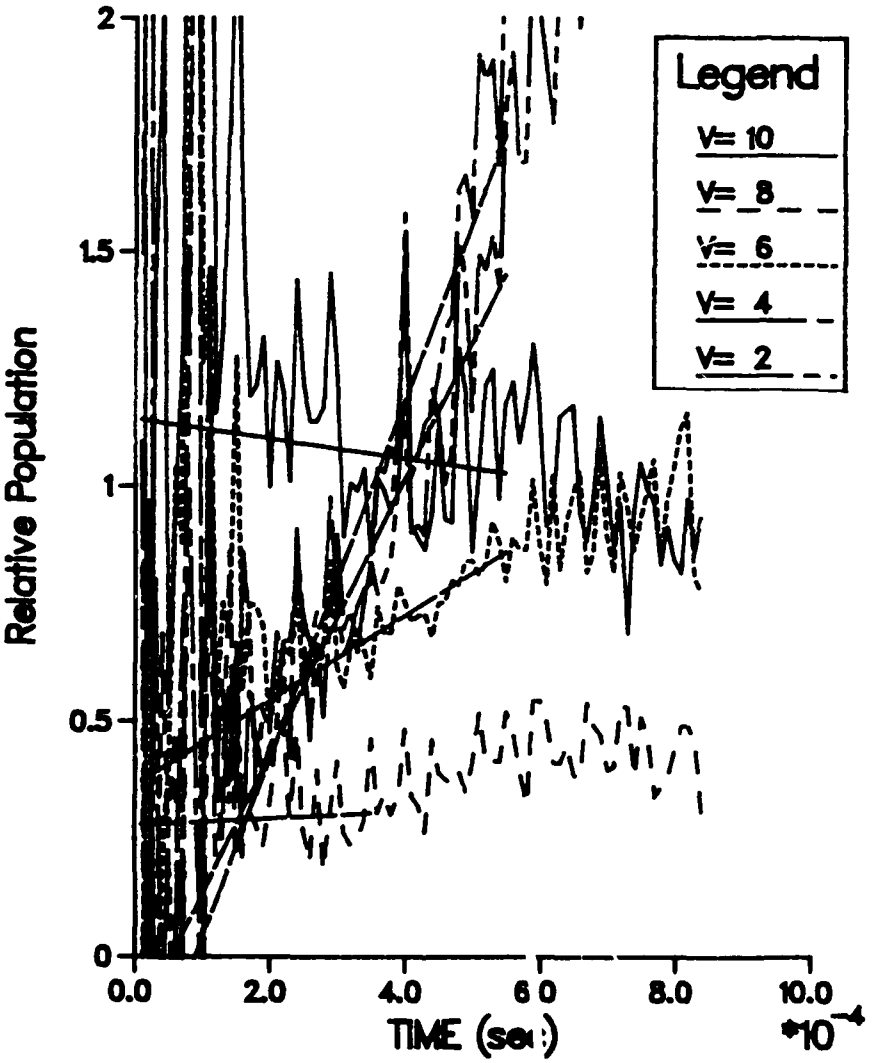

Figure V-12. DF(v) Relative Population Versus Time, D + F_2 CM-PP Experiment

Table V-4

Relative Vibration Distributions for the Reaction D + F_2 ---> DF(v) + F

v	MR[a]	FF[b]	CM-PP[c]
1	----	----	0.00 +/- 0.26
2	0.06	----	0.00 +/- 0.11
3	0.10	0.01	0.00 +/- 0.10
4	0.12	0.03	0.00 +/- 0.10
5	0.18	0.07	0.20 +/- 0.13
6	0.18	0.14	0.36 +/- 0.10
7	0.49	0.22	0.55 +/- 0.21
8	0.70	0.48	0.28 +/- 0.17
9	1.00	1.00	1.00
10	1.19	0.73	1.15 +/- 0.12
11	0.75	0.51	0.66 +/- 0.13
12	0.29	0.15	----
13	<0.10	0.04	----
14	<0.08	----	----
$\langle f_v \rangle$	0.62	0.64	0.62

[a]Measured Relaxation from reference 13.

[b]Fast Flow from reference 59.

[c]This work.

F + HBr

The HF(v) produced from this reaction can populate up to vibrational level 4 (42.4 kcal/mole[55] above the zero point energy) since the available energy is 51 kcal/mole[60]. This reaction is included in this work since there is some disagreement as to the "correct" nascent product vibrational energy distribution.

In 1979, Polanyi's group[61] studied the F + HBr reaction using the Arrested Relaxation technique and observed a dependence on reagent flow. They concluded that a relaxed distribution describes the initially formed products in the F/HBr system and proposed that at high flows preferential deactivation of the low vibration levels cause the distribution to become inverted. They suggested that the deactivation process could be vibration-electronic energy transfer by Br atoms.

Subsequently, Jonathon[62] did an arrested relaxation experiment of the F/HBr system in which he added excess Br_2. Flourine atoms react with Br_2 three times faster than with HBr and produce ground state Br atoms and FBr.[62] He observed no change in the initial distribution with and without the added Br_2, indicating that deactivation by Br atoms was not responsible for the flow dependence. He therefore concluded that the initial distribution was inverted and in agreement with his previous studies of this reaction in which no flow dependence had been observed. Jonathon's Arrested Relaxation technique had a faster pumping system than that used in other Arrested Relaxation techniques, although he did do some experiments in which the pumping speed was reduced with still no change in the observed distributions.

Setser's group[60] obtained results using an Arrested Relaxation technique in which the flow dependence was observed and also a Fast Flow technique in which the flow dependence was absent. The distributions obtained under moderate reagent flow conditions from the Arrested Relaxation experiments were inverted and in agreement with the results of the Fast Flow experiments. He favored these distributions as being the nascent product distributions and suggested that wall effects were important at low flows in the Arrested Relaxation experiments. Excited HF molecules could reenter the observation zone after partial relaxation by the liquid nitrogen cooled walls or the HF molecules could be formed outside the observation zone and then reenter after collisional or radiative relaxation. The existence of some type of wall effect was supported by the fact that the flow dependence was not observed for non-condensibles such as H_2, CH_4, and C_2H_6.

Sloan[63] recently studied the F + HBr reaction using a low pressure infrared chemiluminescence apparatus in which three concentric quartz tubes were used for reagent injection. The innermost tube could be raised or lowered thus enabling the reagent mixing zone to be moved to regions of high or low reagent density without changing reagent flows. Thus reaction could be studied over a range of conditions. For the experimental configuration in which deactivation processes were eliminated, he obtained an inverted vibrational product distribution. He also showed that by changing reagent flows and the mixing geometry that vibrational relaxation by the walls of the vessel or the injector is important when the mean free path in the reaction vessel is unusually

AD-A175 421 STUDIES OF ELEMENTARY PROCESSES AND COUPLING INVOLVED IN THE D2/F2 CHEMICAL LASER(U) IOWA UNIV IOWA CITY DEPT OF CHEMISTRY D C TARDY 01 DEC 86 UI-CHEM-DCT-86 2/2

UNCLASSIFIED N00014-81-K-0207 F/G 20/5 NL

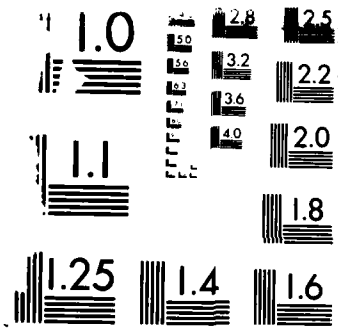
1.0
1.1
1.25
1.4
1.6
1.8
2.0
2.2
2.5
2.8
3.2
3.6
4.0

large as it is for fast reactions such as F + HBr. He pointed out, however, that these conclusions were obtained by operating his apparatus in a way that led to this result; not the normal operating condition.

Table V-5 compares the distributions obtained for the F + HBr reaction from experimental methods in which the flow dependence was not observed. Included in this table are the results obtained from the CM-PP and CM-LP experiments of the present work. The flows used in the CM-PP experiment were CF_4 = 2.6 mole/sec, and HBr = 3.0 and 4.4 mole/sec. These were the limiting flows possible to give measurable intensity and still not to be in the high flow region. The presssures used in the CM-LP experiments were: SF_6 = 60 mtorr, HBr= 10-50 mtorr, and Ar= 3.5 torr. Within experimental error, the distributions obtained from both the CM-PP and CM-LP experiments showed no dependence on reagent flow. The rotational temperatures calculated for the CM-PP experiments were 300 K. The temperatures of the distributions obtained from the CM-LP experiments were 300 K for HF(v=4), 400 K for HF(v=3) and HF(v=2), and 500 K for HF(v=1).

The distributions obtained from the CM-PP and CM-LP experiments are in closer agreement with the inverted distributions than the reported relaxed distributions obtained in experiments where a flow dependence is observed. The CM-LP distribution is slightly broader than the CM-PP distribution lying just within the limits of experimental error. Sloan's group[63] reports the most inverted distribution; by comparison all of the other distributions show some degree of relaxation.

In the present CM-PP and CM-LP experiments, HF(v) collisional relaxation by HBr, HF(v=0) or Ar and HF(v) radiative relaxation can be eliminated as causes of the slightly relaxed distributions. Computer simulations have shown that these processes do not affect the determination of the initial distributions under the conditions used in the present experiments. Relaxation by the walls of the reaction vessel in the CM-PP experiments is unlikely since it would take a minimum of about 0.5 msec for the molecules to travel to the wall and back into the observation volume. Since the extrapolation is performed for data only out to 0.5 msec, the distribution should not be affected.

Table V-6 is a comparison of the reaction and deactivation rate constants (HBr as deactivator) for this system. The reaction rate constant obtained from analysis of the total intensity time profile is in agreement with total intensity measurements reported by Setser[60] and Wurzburg and Houston[64]. The reaction rate constant obtained in this work from the v=4 time profile is slightly outside the error limits of the value reported by Smith and Wrigley[65] who analyzed overtone emission from v=4. Analysis of the experimentally observed HF(v=3) population-time profiles after subtraction of the relaxation contribution from HF(v=4) gives a total reaction rate constant of 2.4 +/- 0.2 x 10^6 $torr^{-1}$ $sec,^{-1}$ in agreement with that obtained from HF(v=4) as expected. As has been shown by modeling in this work, total intensity profiles give low total rate constants when forced to fit the sum of two exponentials, therefore, the result from the fit of the highest vibrational level is preferred. The intercept of the pseudo first order reaction rate constant versus HBr pressure was zero.

Table V-5

Relative Vibration Distributions for the Reaction F + HBr ---> HF(v) + Br

v	FF[a]	FF[b]	IC[c]	AR[d]	CM-PP[e]	CM-LP[e]
1	0.26	0.28	0.35	0.54	0.45 +/- 0.22	0.50 +/- 0.16
2	0.65	0.67	0.58	0.68	0.66 +/- 0.10	0.82 +/- 0.10
3	1.00	1.00	1.00	1.00	1.00	1.00
4	1.03	1.11	1.29	1.05	0.99 +/- 0.18	0.79 +/- 0.06
$\langle f_v \rangle$	0.60		0.63	0.56	0.60	0.57
$\langle f_r \rangle$	0.13		0.08	0.11		
$\langle f_t \rangle$	0.28		0.30	0.33		

[a]From reference 60.

[b]From reference 51.

[c]From reference 63, infrared chemiluminescence experiment.

[d]From reference 62, arrested relaxation.

[e]This work.

Table V-6

Reaction and Deactivation Rate Constants for the Reaction F + HBr ---> HF(v) + Br

Reaction Rate Constants ($\times 10^6$ torr^{-1} sec^{-1})	
k_{tot}	Method
1.45 +/- 0.13	F from Photolysis SF_6 HF(total intensity)[a]
1.5	Fast Flow[b]
2.0 +/- 0.2	F from Photolysis F_2 HF(v=4) Time Resolved IR Chemiluminescence[c]
1.5 +/- 0.6	CM-LP HF(total intensity)[d]
2.6 +/- 0.2	CM-LP HF(v=3)[d]
2.4 +/- 0.2	CM-LP HF(v=2)[d]

Deactivation Rate Constants k_v(HBr) x 10^5 torr^{-1} sec^{-1}			
v = 1	2	3	4
0.27 +/- 0.04[e]			7.2 +/- 0.7[c]
0.27 +/- 0.04[f]		2.3 +/- 0.5[d]	3.2 +/- 0.9[d]

[a] From reference 64.

[b] From reference 60.

[c] From reference 65.

[d] This work.

[e] From reference 71.

[f] From reference 72.

Rate constants for deactivation by HBr are also shown in Table V-6. The rate constant for deactivation of HF(v=4) by HBr obtained in this work is approximately a factor of 2.3 lower than that obtained by Smith and Wrigley[65]. A lower deactivation rate constant usually means that the measurement is free of additional deactivators. Plots of pseudo first order deactivation rate constant versus HBr pressure gave an intercept of 3.3 +/- 0.9 x 10^3 sec^{-1}. As contrasted to the H_2 system, the relative error in the determination of the slope for this system is not significantly affected by the large intercept which is measured.

The relaxation rate constant measured for HF(v=3) deactivation by HBr is 2.3 +/- 0.5 x 10^5 $torr^{-1}$ sec^{-1}. Measurements of this rate constant have not been previously reported. Relaxation rate constants for HF(v=2) relaxation by HBr could not be extracted from the experimental data since the contribution to this population from HF(v=3) relaxation was greater than 70%. When the total intensity-time profile was fit to the sum of two exponentials, a deactivation rate constant of 3.9 +/- 0.3 x 10^4 $torr^{-1}$ sec^{-1} was obtained.

$$F + CH_2Cl_2$$

The total energy available to this system is 44.7 kcal/mole[66] resulting in populated vibrational levels up to v=4 (42.4 kcal/mole[55] above the zero point energy). A study of this system was done since as with the F + HBr reaction, the initial distributions obtained from Arrested Relaxation experiments[66,67] show a dependence on reagent flow. In addition, deactivation of HF by CH_2Cl_2 has not been previously reported.

Polanyi's group[67] observed a flow dependence in the reactions of F atoms with the substituted methane series CH_3Cl, CH_2Cl_2, $CHCl_3$. As in their study of the F/HBr system, they attributed the results at high reagent flows to be due to preferential deactivation of the low vibrational levels and reported a relaxed distribution as being the nascent product energy distribution.

A collaborative[66] effort by Setser's group in Kansas and Heydtmann's group in Frankfurt studied the same methyl chloride series as Polanyi's group[67] in Toronto and a comparison between the results obtained in the three different laboratories was made. Quantitative agreement among the three laboratories for the results from arrested relaxation methods, in which the flow dependence was observed, was poor. For the F/CH_2Cl_2 system, only distributions favoring the v=1 level were observed in Frankfurt. Almost all of the arrested relaxation results showed a minimum at v=2 which suggested the superposition of two distributions; one peaking at v=1 and the other at v=3. When F_2 replaced CF_4 as the source of F atoms in the Frankfurt laboratory, no effect on the distribution was observed. The deviation from the inverted distribution of Fast Flow measurments was found to be greatest for $CHCl_3$ which has the highest number of chlorine substituents and the smallest reaction rate constant of the series. To explain the arrested relaxation results, they hypothesize the existence of two reaction channels. One channel produces vibrationally excited HF(v) while the other forms a metastable complex, CH_2Cl_2*F, that upon dissociating would give a statistical distribution. They suggest that because the arrested relaxation

experiments are done with liquid nitrogen cooled walls, the translational temperature of the reagents may be lower than 300 K so complex formation is favored. They also suggest that for reactions which have small rate constants, the probability that the reagent temperature will be reduced prior to reaction is greater. In addition, complex formation would be more favorable with increasing chlorine substitution.

The flows used in the CM-PP experiments were CF_4 = 3.7 mole/sec and CH_2Cl_2 = 1.9-3.7 mole/sec. The pressures used in the CM-LP experiments were SF_6 = 60 mtorr, CH_2Cl_2 = 33 and 53 mtorr. No flow dependence was observed in either experimental method. The temperature of the rotational distributions from the CM-PP experiments was 300 K. The temperatures of the rotational distributions from the CM-LP experiments were 500 K for the first vibrational level, 400 K for the second vibrational level, and 300 K for the third vibrational level.

Table V-7 gives the nascent product energy distributions. The distributions obtained from both the CM-PP and CM-LP experiments support the inverted distribution obtained from the Fast Flow experiments[68] in which no flow dependence was observed. To test the metastable complex hypothesis, CM-PP and CM-LP experiments could be done in which the translational energy of the reagents is varied.

The reaction rate constants for the CH_2Cl_2 system are given in Table V-8. The plot of the pseudo first order reaction rate constant versus CH_2Cl_2 presssure gave an intercept of zero. The reaction rate constant obtained from the fit of total intensity is 57% - 160% larger than the previously reported reaction rate constants. There could be two causes for this observation. The present result is a measure of F atom depletion so that if some other species present is depleting F atoms, this would result in an apparent faster reaction rate constant. Alternatively, F could be depleted by complexing with CH_2Cl_2 or reacting with $CHCl_2$ as a secondary reaction.

The previously reported reaction rate constants could be low. In the fast flow experiments[68], the reaction rate constant is obtained from the measurement of the formation of HF(v > 0) and so if there is appreciable population in vibrational level 0 then the reaction rate constant would be too small. The other two reported values of the reaction rate constant measure depletion of CH_2Cl_2. If in these experiments, the F atoms are depleted by a source in addition to CH_2Cl_2 then these reported reaction rate constants would also be low.

The deactivation rate constant obtained from the analysis of the total intensity time profile was 5.2 +/- 0.5 x 10^4 $torr^{-1}$ sec^{-1} and the intercept obtained from the pseudo first order relaxation rate constant versus CH_2Cl_2 plot was 1.5 +/- 0.5 x 10^3 sec^{-1}. Unfortunately, because of the small signal/noise ratio of these experiments, no meaningful reaction and deactivation rate constants from the analysis of the individual HF(v) levels could be obtained. The results from analysis of the total intensity time profiles are lower limits of the reaction and deactivation rate constants for this system as shown by the computer simulations and the previous results for the F + H_2 system and the F + HBr system.

Table V-7

Relative Vibration Distributions for the Reaction $F + CH_2Cl_2 \longrightarrow HF(v) + CHCl_2$

v	FF[a]	CM-PP[b]	CM-LP[b]
1	0.17	0.19 +/- 0.14	0.44 +/- 0.42
2	0.31	0.56 +/- 0.12	0.48 +/- 0.26
3	1.00	1.00	1.00
4	0.08	0.09 +/- 0.04	----
$\langle f_v \rangle$	0.66	0.62	0.56

[a]From reference 73.

[b]This work.

Table V-8

Reaction Rate Constants for the Reaction $F + CH_2Cl_2 \rightarrow HF(v) + CHCl_2$

$k_{tot} \times 10^5$ torr^{-1} sec^{-1}	Method
4.6	Fast Flow[a]
4.9 +/- 0.9	Diffusion Cloud[b]
3.0	Mass Spec. of CH_2Cl_2[c]
7.7 +/- 0.2	CM-LP (total intensity)[d]

[a]From reference 73.

[b]From reference 74.

[c]From reference 75.

[d]This work.

VI. CONCLUSIONS

Previously experiments were performed to determine the microscopic rate constants for the formation of DF(v) from the reactions F + D_2 and D + F_2 using a new technique called Chemiluminescence Mapping (CM) which involves both spectral and time resolution. The results of these experiments were questioned. Consequently this project was undertaken to determine the validity of the CM method and to confirm the early CM results.

The work reported here has shown that energy disposal experiments in which a microwave discharge is used for the formation of the atomic reactant is not contaminated with products from ion molecule reactions. Although these results hold specifically for CM-PP systems they are valid for other experiments in which a microwave discharge is used for the formation of atomic species. Using the double floating probe technique the ion content for the CM-PP configuration was found to be less than 1.8×10^{-6} of the gas flowing through the microwave cavity.

Both experiments and computer simulations reported here revealed and evaluated two limiting types of CM experiments: CM-PP in which there is a repetitive pressure pulse of the diatomic species (this corresponds to the early CM system) and CM-LP in which the atomic species are formed repetitively in a constant pressure environment. Both types of CM experiments are capable of producing nascent vibrational energy distributions. CM-LP experiments can also provide detailed information on the rate constants for reaction and relaxation. The advantages of the CM technique over the Arrested Relaxation technique includes a low duty cycle reagent pulse which reduces average molar flow and pumping requirements, the absence of a wavelength dependent baseline, and both spectral and time resolution. Arrested relaxation techniques can provide relative reaction rate constants but do not give relaxation information. Because the CM technique provides both spectral and time resolution, energy transfer information can be obtained as a function of deactivator and vibrational level. Essentially any deactivator may be used, unlike fast flow experiments in which only quenchers that do not react with the atomic reactant can be studied. Direct excitation methods can be used to study any quenchers that do not absorb at the same wavelength as the molecules being excited, but the formation of high vibrational levels via multiquantum absorption has low absorption coefficients and these types of experiments do not give any information on reaction rate constants.

Computer simulations showed that in order to obtain nascent vibrational energy distributions, CM-PP experiments should be performed under low flow conditions (i.e. F >> H_2) and for observation times short enough to resolve the fastest relaxation process. The reaction vessel must be evacuated between pulse cycles to reduce complications (i.e. secondary reactions, collisional and/or radiative relaxation) that can arise from residual reactant and/or product species. Based on these results, improvements were made on the CM-PP experiments which were previously reported. These improvements included:

i) replacement of the 6 channel signal averager by one with 2048 channels, increasing the time resolution from 5 milliseconds to 1

microsecond.

ii) replacement of the diatomic reactant injector with a piezoelectric valve, reducing the pulse length from 10 to 0.5 milliseconds.

iii) reduction of observation volume from 1500 to 10 cc; a concomittant reduction on S/N was experienced.

Analysis of the CM-LP experiments is more direct than the CM-PP experiments because of the pseudo first order experimental conditions. Simulations were used to show that total reaction and microscopic relaxation rate constants could be obtained by fitting total vibrational population-time data to the sum of two exponentials. For vibrational levels below the maximum vibrational level populated, it is necessary to first decouple input due to relaxation of the upper levels from input due to reaction. The simulations revealed that fitting total emission-intensity time profiles to the sum of two exponentials gave reaction and relaxation rate constants that were too small by 20% and 35% respectively.

Experimental results were presented for the F + $H_2(D_2)$, H(D) + F_2, F + HBr and F + CH_2Cl_2 chemical reactions. A comparison of the nascent vibrational distribution and reaction rate constant (analysis of the total intensity-time profiles) for the F + H_2 reaction obtained from the CM-PP and CM-LP experiments with previous values for this system are within experimental error and provide a successful benchmark for the methods. The reaction rate constant obtained from analysis of HF(v=3) is 1.4 +/- 0.3 x 10^6 $torr^{-1}$ sec^{-1}. This value is preferred over the smaller value obtained from total intensity measurements. Microscopic relaxation rate constant measurements obtained in this work were larger than previously determined values. The reason for this discrepancy is believed to be due to the presence of H_2O in the CM-LP experiments.

A comparison of previous CM-PP results with that of the present work for the F + H_2/D_2 systems are within experimental error. Computer modeling has shown, however, that collisional and/or radiative relaxation affects the nascent distributions for the experimental conditions of the previous CM experiments. These effects may have been within the experimental error (> 10%) and thus not apparent in the F + H_2/D_2 experimental results.

The nascent distributions of the present CM-PP experiments for the H/D + F_2 reactions are within experimental error of other results for these systems, but disagree with the previous CM measurements. It is believed that these differences can be reconciled by the double maxima in the HF(v) time profiles (indicating high flow conditions), the large observation times in the earlier experiments and an absorption 'hole' which appears on the liquid nitrogen cooled filter of the detector dewar. Collisional and radiative relaxation effects on the nascent distribution of these reactions were more apparent than in the F + H_2/D_2 systems since the rate of reaction is much slower (factors of 11 and 17 for the D and H reactions respectively).

The initial distributions reported here for the F + HBr and F + CH_2Cl_2 reactions support the previously observed inverted distributions.

No dependence on reagent flow was observed in either the CM-PP or CM-LP experiments. Total reaction rate constants and deactivation rate constants for HF(v=3,4) relaxation by HBr were reported. The HF(v=3) deactivation rate constant has not been measured prior to this work. The HF(v=4) deactivation rate constant is smaller than the previously reported value, indicating that the present measurement is free of additional relaxation processes. Deactivation of HF(v=3,4) by HBr is approximately 10 and 20 times more efficient than deactivation by H_2.

Due to the large errors in the F + CH_2Cl_2 system, microscopic deactivation rate constants could not be obtained. The relaxation rate constant obtained from the total intensity measurement is a lower limit of HF(v) relaxation by CH_2Cl_2.

Future efforts should be focused on improvements in S/N and the elimination of the large intercepts in pseudo-first order rate constant versus HR pressure plots which are apparently due to H_2O contamination in the flow lines, vacuum system and reaction vessel. The analysis of the raw experimental data can be improved. In the present work, a least squares fit of the spectrum for each time slice is made in order to extract vibrational-rotational populations; this involves inversion of up to a 150 by 150 matrix for each time slice. An analysis using fast Fourier Transform filtering and a constrained least squares analysis using the single valued decomposition method is presently being developed. It is anticipated that with these improvements the computer time for data processing will decrease by an order of magnitude.

VII. REFERENCES

1. N. Cohen and J.F. Bott, "Kinetics of Hydrogen Halide Chemical Lasers", in the Handbook of Chemical Lasers, edited by R.W.F. Gross and J.F. Bott, John Wiley, New York (1976)

2. H.L. Chen and R.L. Taylor, J. Chem. Phys., 61, 306 (1974)

3. J.M. Bernard, H.H. Ross, J.G. Coffer, R.A. Chodzko and S.B. Mason, "Temporal Measurement of Spectrally Resolved Output of Multiline HF Lasers", Report SD-TR-83-99, Aerospace Corporation, December 31, 1983

4. R.E. Meredith and F.G. Smith, J. Quan. Specty: Radiat. Transfer, 13, 89 (1973)

5. G.A. Hart, "DF Pulsed Chemical Laser, Rotational Nonequilibrium Computer Model (PULSDF) and Data Base", NRL Memorandum Report 5051, April 8, 1983

6. D.S. Perry and J.C. Polanyi, Chem. Phys., 12, 419 (1976)

7. J.C. Polanyi and K.B. Woodall, J. Chem. Phys., 57, 1574 (1972)

8. M.J. Berry, J. Chem. Phys., 59, 6229 (1973)

9. N. Jonathan, S. Okuda and D. Timlin, Mol. Phys., 24, 1143 (1972)

10. J.C. Polanyi and J.J. Sloan, J. Chem. Phys., 57, 4988 (1972)

11. J.C. Polanyi, J.J. Sloan and J. Wanner, Chem. Phys., 13, 1 (1976)

12. J.P. Sung, R.J. Malins and D.W. Setser, J. Phys. Chem., 83, 1007 (1979)

13. N. Jonathan, J.P. Liddy, P.V. Sellers and A.J. Stace, Mol. Phys., 39, 615 (1980)

14. S. Bittenson, D.C. Tardy and J. Wanna, Chem. Phys., 58, 313 (1981)

15. H. Wang, "On the Nascent Vibrational Population Distribution of D + F_2 (H + F_2) Reactions", Naval Research Laboratory and Sachs/Freeman Associates, Washington, D.C. 20375 (1981)

16. T.S. Zwier, V. Bierbaum, G.B. Ellision and S.R. Leone, J. Chem. Phys., 72, 5426 (1980)

17. G.J. Schulz, Rev. Mod. Phys., 45 423 (1973)

18. D.C. Tardy and J.T. Wanna, S. Bittenson and T. Nelson, "Proceedings of the International Conference on Lasers, 1981", STS Press (1982)

19. A.T. Zander and G.M. Hieftje, Appl. Spectrosc., 35, 357 (1981).

20. R.K. Skogerboe and G.N. Coleman, Anal. Chem., 48, 611A (1976).

21. K.W. Busch and T.J. Vickers, Spectrochimica Acta,Vol. 28B, 85-104 (1973).

22. P. Brassem and F.J.M.J. Maessen, and L. DeGalen, Spectrochimica Acta,Vol. 33B, 753-764 (1978).

23. P. Brassem and F.J.M.J. Maessen, Spectrochimica Acta, Vol. 29B, 203-210 (1974).

24. P. Brassem and F.J.M.J. Maessen, Spectrochimica Acta, Vol. 30B, 547-556 (1975).

25. P. Brassem, F.J.M.J. Maessen, and L. DeGalan, Spectrochimica Acta, Vol. 31B, 537-545 (1976).

26. a) J.T. Wanna, Ph.D. Thesis, University of Iowa (1982).
b) T.O. Nelson, MS. Thesis, University of Iowa (1984).

27. L. Schott (edited by Holtgreven N. Lochte), "Plasma Diagnostics", John Wiley and Sons, Inc. (1968).

28. E.O. Johnson and L. Malter, Phys.Rev., 80, 58-68 (1950).

29. F.C. Fehsenfeld, K.M. Evenson, and H.P. Broida, Rev. Sci. Instrum., 36, 294 (1965).

30. J.D. Swift, and M.J.P. Schwar, "Electrical Probes for Plasma Diagnostics", London ILIFFE Books, New York, American Elsevier Publishing Company, Inc. (1969).

31. G.R. Seemann and J.A. Thornton, AIAA pap. 69-700, AIAA Second Fluid and Plasma Dynamics Conference, San Francisco, California (June, 1969).

32. D. Bohm, E.H.S. Burhop, and H.S.W. Massey (Edited by A. Guthrie and R.K. Wakerling), "The Characteristics of Electrical Discharges in Magnetic Fields", McGraw-Hill Book Co. Inc. (1949).

33. S.R. Goode and D.C. Otto, Spectrochimica Acta, Vol. 35B, 569 (1980).

34. R.F. Wandro and H.B. Friedrich, pap. 860, The Pittsburgh Conference and Exposition on Analytical Chemistry and Applied Spectroscopy, Alantic City, New Jersey (March, 1984).

35. Ira M. Cohen, The Physics of Fluids, Vol. 13, No. 4 (1970).

36. Roger G. Little and John F. Waymouth, The Physics of Fluids, Vol. 9, No. 4, 801 (1966).

37. a) E. Wurzberg, A.J. Grimley and P.L. Houston, Chem. Phys. Lett., 57, 373 (1978).
b) E. Wurzberg and P. L. Houston, J. Chem. Phys., 72, 4811 (1980).

38. R.F. Heidner, J.F. Bott, C.E. Gardner and J.E. Melzer, J. Chem. Phys., 72, 4815 (1980).

39. C. K. Man, D. C. Tardy (unpublished results)

40. James B. Anderson, Adv. Chem. Phys., vol. XLI, (1980).

41. J. F. Bott, R. F. Heidner III, J. Chem. Phys., 68 1708, (1978).

42. P. A. Schulz, Aa. S. Sudbo, E. R. Grant, Y. R. Shen, Y. T. Lee, J. Chem. Phys., 72, 4985, (1980).

43. Stephen R. Leone, J. Phys. Chem. Ref. Data, 11, 975, (1982).

44. Sidney W. Benson, The Foundations of Chemical Kinetics, McGraw-Hill, New York, (1960).

45. Phillip R. Bevington, Data Reduction and Error Analysis for the Physical Sciences, McGraw-Hill, New York, (1969).

46. Abolghassem Sepehrad, Roger M. Marshall, Howard Purnell, Int. J. Chem. Kinet., 11, 411, (1979).

47. William L. Wolfe, George J. Zissis, eds., Infrared Handbook, Environmental Research Institute, Michigan, (1978).

48. G. Herzberg, Electronic Spectra of Polyatomic Molecules, D. Van Nostrand Co., New York, (1966).

49. J. R. Airey, Ph.D. Thesis, Univ. of Toronto, (1964).

50. K. Tamagake, D. W. Setser, J. Phys. Chem., 83, 1000, (1979).

51. L. S. Dzelzkalns, F. Kaufman, J. Chem. Phys., 79, 3836, (1983).

52. H. W. Chang, D. W. Setser, J. Chem. Phys., 58, 2298, (1973).

53. J. G. Moehlmann, J. D. McDonald, J. Chem. Phys., 62, 3061, (1975).

54. P. Beadle, M. R. Dunn, N. B. H. Jonathon, J. P. Liddy, J. C. Naylor, S. Okuda, J. Chem. Soc. Faraday Trans. II, 74, 2158, (1978).

55. N. Cohen and J. F. Bott, "Kinetics of Hydrogen Halide Chemical Lasers", in Handbook of Chemical Lasers, edited by R. W. F. Gross and J. F. Bott, John Wiley, New York, (1976).

56. J. C. Polanyi, Acc. Chem. Res., 5, 161, (1972).

57. N. Jonathon, S. Okuda, D. Timlin, Mol. Phys., 24, 1143, (1972).

58. L. S. Dzelzkalns, F. Kaufman, J. Chem. Phys., 77, 3508, (1982).

59. L. S. Dzelzkalns, F. Kaufman, J. Chem. Phys., 80, 6114, (1984).

60. K. Tamagake, D. W. Setser, J. P. Sung, J. Chem. Phys., 73, 2203, (1980).

61. D. Brandt, L. W. Dickson, L. N. Y. Kwan, J. C. Polanyi, Chem. Phys., 39, 189, (1979).

62. N. Jonathon, P. V. Sellers, A. J. Stace, Mol. Phys., 43, 215, (1981).

63. P. M. Aker, D. J. Donaldson, J. J. Sloan, J. Phys. Chem., 90, 3110, (1986).

64. E. Wurzberg, P. L. Houston, J. Chem. Phys., 72, 5915, (1980).

65. Ian W. M. Smith, David J. Wrigley, Chem. Phys., 63, 321, (1981).

66. M. A. Wickramaaratchi, D. W. Setser, H. Hildebrandt, B. Korbitzer, H. Heydtmann, Chem. Phys., 94, 109, (1985).

67. M. A. Nazar, J. C. Polanyi, Chem. Phys., 55, 299, (1981).

68. J. F. Bott, J. Chem. Phys., 65, 4239, (1976).

69. G. M. Jurisch, D. R. Ritter, F. F. Crim, J. Chem. Phys., 80, 4097, (1984).

70. D. J. Douglas, C. Bradley Moore, Chem. Phys. Lett., 57, 485, (1978).

71. J. F. Bott, N. Cohen, J. Chem. Phys., 58. 4539, (1973).

72. J. L. Ahl, T. A. Cool, J. Chem. Phys., 58, 5540, (1973).

73. A. S. Manocha, D. W. Setser, M. A. Wickramaaratcchi, Chem. Phys., 76, 129, (1983).

74. G. Lebras, J. I. Butkovskaya, I.I. Morozov, V. L. Talrose, Chem. Phys., 50, 63, (1980).

75. M. A. A. Clyne, D. J. McKenney, R. F. Walker, Can. J. Chem., 51, 3596, (1973).

END

2-87

DTIC